Evaluating the Effects of Spalling on the Capacity of Reinforced Concrete Bridge Girders

by

Jeffrey Luckai

A thesis
presented to the University of Waterloo
in fulfillment of the
thesis requirement for the degree of
Master of Applied Science
in
Civil Engineering

Waterloo, Ontario, Canada, 2011

Author's Declaration

I hereby declare that I am the sole author of this thesis. This is a true copy of the thesis, including any required final revisions, as accepted by my examiners. I understand that my thesis may be made electronically available to the public.

Abstract

Corrosion of the reinforcing steel is a primary deterioration mechanism for reinforced concrete bridges. Heavy use of de-icing salts is believed to be a major contributor in Ontario to severe girder soffit spalling in certain cases. This thesis develops an assessment methodology to evaluate spalled bridges based on ultimate limit states. Specifically, a deterministic program is developed for assessment. It is subsequently compared to laboratory test results and used as a basis for a probabilistic reliability study.

A modified area concept is proposed in this thesis to consider the effects of exposing reinforcement at various locations along the girder length. A multipoint analysis program, BEST (Bridge Evaluation Strength Tool), is developed that employs this concept, along with graphical spalling surveys and structural drawings, to evaluate reinforced concrete bridge girders. The program is adapted for a full bridge analysis and to consider the other effects of corrosion, such as bar section loss and bond deterioration.

A case study bridge is evaluated to show that the BEST program offers a viable tool for the rapid assessment of spalled bridge girders and to facilitate the prioritization of rehabilitation projects. This evaluation indicates that the spatial distribution of the spalling along a girder, relative to bar splices and laps, has the most significant influence on structural capacity. Single girders show strength deficiencies in flexure and shear due to spalling. In general, the consideration of system effects improves the predicted bridge condition, while considering section loss and bond deterioration has the opposite effect.

Laboratory work is used to validate the proposed model and identify a number of areas for future research. The laboratory test results also suggest that the current repair methods are effective in restoring bond and strength.

In order to further explore potential uses for the BEST program, modifications are made so that it can be used to perform reliability analyses using Monte-Carlo simulation techniques.

A simplified approach for estimating the reliability index as a function of the deterministic resistance ratio is proposed based on the reliability analysis results.

Acknowledgements

I would like to thank the following parties for their contributions to this work:

- Dr. Scott Walbridge and Dr. Maria Anna Polak, co-supervisors of this thesis,
- Wade Young, Randy Yu and Andy Turnbull of the Ministry of Transportation of Ontario for their feedback and support,
- Lindsay, Nneka, Nizar, and Lawrence, as well as, Doug Hirst, Robert Sluban and Richard Morrison for the laboratory assistance,
- Sika Canada and HOGG Fuel & Supply Ltd. for material donations, and
- my family, friends and colleagues at UW for their support.

Dedication

To My Parents

Table of Contents

List of Figures

List of Tables

Chapter 1
Introduction

1.1 General

In the Province of Ontario, as in the rest of North America, the assessment and maintenance of existing highway bridges is currently an area of significant concern (Council of the Federation 2005). It is widely agreed that the condition of these structures is deteriorating over time. The following paragraphs discuss the current state of Ontario's highway bridge infrastructure.

Ontario's Highway Bridges

Ontario has approximately 14800 road bridges in total. Approximately 12000 of these are located within municipalities, while 2800 are owned and maintained by the province (Aud. 2009). Of the provincially managed bridges, more than 70% were built between 1950 and 1980 with an average age of approximately 40 years. The majority of municipal bridges in Ontario are slightly older with an average age of 43 years (Aud. 2009).

Many of the bridges requiring repair and rehabilitation in Ontario are located along major highways. In the Greater Toronto Area there are over 660 bridges on 400 series highways, some of which span over up to 16 lanes of traffic (Aud. 2009).

Work Backlog

A number of sources have indicated that there currently is a backlog in bridge maintenance and repair in Ontario. According to the Ontario Ministry of Transportation (MTO) current assessment methodology, more than 180 or 7% of provincial bridges were in poor condition, which is defined by MTO as requiring repair or rehabilitation work within one year of the inspection, and 17% (or 471 bridges) were in fair condition (Aud. 2009). A 2009 review by the Ontario Auditor General (Aud. 2009) found that around 60% of the bridges rated in fair or poor condition by MTO were not on the Ministry's five-year capital work plan. The same

report found that approximately 85% of the municipalities responding to the survey confirmed that they had a backlog of rehabilitation work. Of those, 45% had 1-5 year backlogs, 25% had 6-10 year backlogs, and 10% had work backlogs of over 10 years.

Funding

Economic conditions have greatly influenced infrastructure spending in Canada and Ontario. Infrastructure spending in Ontario has annually increased over the past three years. In 2010-2011 the Renew Canada program (Renew 2009) boasted $4.53 billion in funding for transportation investments. Of this amount, 44% was dedicated for provincial highways. An increase in funding for transportation and transit to $5.40 billion is expected for 2011-2012 (39% will be dedicated to provincial highways).

In 2009, MTO estimated that the cost of repair and rehabilitation of its structures in either fair or poor condition over the next five year period (from 2009) to be approximately $2.2 billion, yet the Ministry budget for bridge work over the same period was only $1.4 billion.

Industry Challenges

Aging infrastructure is the primary challenge currently facing Ontario bridge managers, including MTO. It is expected that there will be a spike in the need for major repair and rehabilitation work over the next 6-10 years (based the average structure age).

Due to the quantity of work in Ontario, a shortage of available specialized contractors has developed. Project costs have also escalated due to a lack of competition created in part by the consolidation of the consulting industry, and the result of a market that is flooded by local government spending (Aud. 2009).

In urban areas, a steady increase in congestion has increased the need for highway expansion. When roadway expansion is anticipated, as it currently is in the foreseeable future, bridge

replacement is delayed and the need for structural assessment and repair increases. To complicate matters, structural repair and replacement by conventional means often requires expensive highway closures, and work of this nature is difficult and time consuming (personal correspondence, R. Yu 2010).

As a result, there is currently an emphasis on the need to develop better assessment and repair methods for bridge structures. At this time, many reports indicate that bridge inspectors are unable to distinguish between many visible deterioration effects and those that actually have a significant impact of the safety of the public (Aud. 2009). In particular, surface spalling of reinforced concrete (RC) bridge girders, at this time, due to the uncertainty of its impact on structural capacity, often falls within the realm of "routine maintenance" work, when in fact it should first be evaluated based on the estimated residual strength and safety of the structure.

1.2 Research Objectives

Based on the discussion in the previous section, the objectives of the research project summarized in the current thesis are as follows:

1) execution of a field survey of RC bridges with varying levels of deterioration, to assess the significance of the problem and determine what information bridge inspectors have at their disposal when carrying out a bridge assessment,

2) development of deterministic and probabilistic prediction models for evaluating the safety of RC flexural members with exposed reinforcement, and

3) initial study and evaluation of a number of alternative simple, rapid, and cost effective rehabilitation methods for RC bridges with spalled concrete.

1.3 Scope

The scope of the current thesis is limited to the assessment and rehabilitation of multi-girder RC highway bridges without prestressing. The studied deterioration is limited to soffit spalling of primary girder elements. Shear and moment resistance models for beams are used in the developed assessment program, meaning that the beneficial effects of arch action are not considered. The presented assessment program research focuses on the development of a simple, rapid assessment tool, employing code-like models and modified design formulas that are already familiar to structural engineers. The developed assessment program is verified by comparison with results of a small-scale laboratory study. Extension of the developed assessment program for applications involving prestressed girders or two-way structural systems (e.g. deck slabs) is beyond the scope of the current thesis.

1.4 Thesis Organization

This thesis is organized into seven chapters, as follows:

- In Chapter 2, relevant background information and a state-of-the art literature review are presented, to introduce important concepts related to the research.

- Next, in Chapter 3, a field survey is used to develop the concepts employed in the current thesis for the strength assessment of deteriorated RC bridge structures.

- In Chapter 4, the implementation of these concepts in a computer assessment program is discussed and the program application is demonstrated using a case study structure.

- In Chapter 5 a pilot laboratory study is presented, wherein several spalling configurations and rehabilitation approaches are tested.

- In Chapter 6, the program is modified to facilitate the full reliability (i.e. probabilistic) analysis of single girders in spalled RC bridge structures.

- Finally, conclusions and recommendations are presented in Chapter 7.

Chapter 2

Background and Literature Review

2.1 Deterioration of Concrete Bridges

2.1.1 Corrosion

In general, the corrosion of steel reinforcement is primarily responsible for surface spalling and is highly detrimental to our infrastructure. To understand the effects of corrosion on the residual capacity of a reinforced concrete member, it is prudent to first understand the cause. This section presents a brief background of steel corrosion and describes the main causes of concrete deterioration.

2.1.1.1 Corrosion Reaction

Concrete is naturally a non-corrosive environment for steel due to its high alkalinity (ph > 13). Initially, the concrete creates a passive layer around the embedded reinforcement that is capable of effectively protecting the steel reinforcing bars. However, from the time of casting, corrosion accelerators, such as chlorides or carbon dioxide, start to penetrate the concrete cover and act to lower the ph of the concrete surrounding the reinforcement, thus triggering corrosion.

The corrosion of steel reinforcement coincides with the formation of a rust layer on the steel surface. The formation of rust can be characterized by the following reactions (Hansson et al. 2007):

$$Fe^{2+} + 2OH^{-} \rightarrow Fe(OH)_2 \qquad (3.1)$$

$$4Fe(OH)_2 + O_2 + 2H_2O \rightarrow 4Fe(OH)_3 \qquad (3.2)$$

$$2Fe(OH)_3 \rightarrow Fe_2O_3 \cdot H_2O + 2H_2O \qquad (3.3)$$

In the corrosion reactions, iron ions react with hydroxide ions and dissolved oxygen to form iron oxides and hydroxides. Hydration of the ferric hydroxide compounds forms ferric oxide or red rust. If the passive layer is uniform, continuous and dense, then corrosion may be stifled or negated under natural conditions. In a concrete member, according to Hansson et al. (2006), corrosion occurs either on a micro or macro cell level.

Micro cell corrosion is classified as active corrosion that occurs on adjacent parts of the same piece of metal. This type of corrosion is illustrated in Figure 2-1. On a single piece of metal, potential differences occur between anodic and cathodic sections due to non-uniformities of the metal, electrolyte or variations in physical conditions. In Figure 2-1, the pit location is the anode and subsequently the site for oxidation.

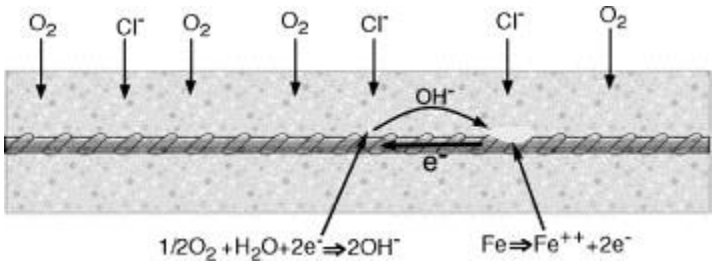

Figure 2-1: Schematic of micro-cell corrosion (Hansson et al. 2006).

Macro cell corrosion occurs when different levels of active corrosion interact through coupling of reinforcement steel as shown in Figure 2-2. When concrete surface conditions vary, as is the case for the member shown in Figure 2-2, a potential difference occurs between the coupled cathodic bottom steel and anodic top steel. This difference facilitates oxidation and corrosion occurs on the upper bars.

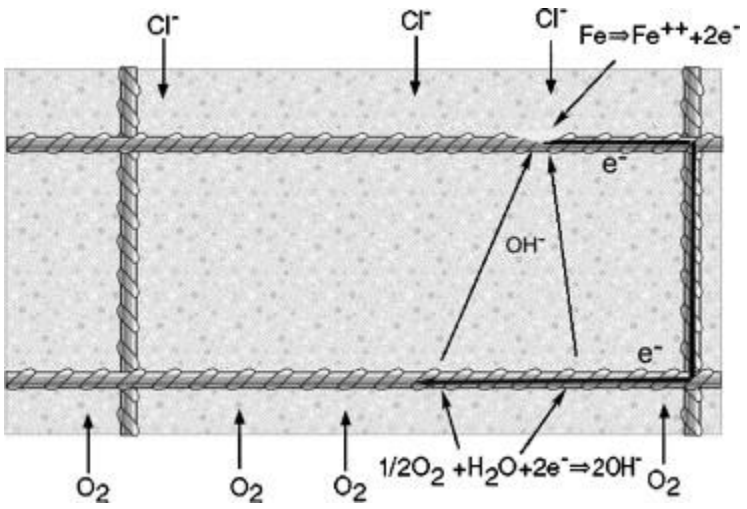

Figure 2-2: Schematic of macro-cell corrosion (Hansson et al. 2006).

2.1.2 Corrosion Accelerators/Instigators

A structure's exposure to the surrounding environment instigates and accelerates corrosion and corrosion induced damage. The main accelerating mechanisms that act on a typical reinforced concrete structure in Ontario are: chloride ingress, carbonation, and freeze-thaw cycles.

2.1.2.1 Chloride Attack

Concrete structures are exposed to chlorides in a number of ways. In northern climates calcium chlorides are present in the de-icing salts applied to roadways during winter months. In coastal or offshore structures, direct exposure to sea-water results in chloride ingress. Finally, chlorides can also be cast-in; in mix-water or in some accelerating admixtures commonly used in mid-1970's (ACI 222 1988). Chloride ion solutions permeate the concrete cover and reach the passive steel layer, where they act to dissolve and break down the passive film. Due to the alkalinity of the concrete, the passive film can repair itself if chloride levels are low.

If chloride levels are greater than a threshold of 0.4% chlorides by weight of concrete (internal-cast-in) or 0.2% (external-diffused), then the passive film will be unable to repair

itself (Hope and Ip 1987). Once they reach the steel, chlorides are not consumed in the reaction; rather they act as a catalyst for the cathode reaction (oxygen consumption). Since the chloride ion concentration that reaches the steel and the subsequent breakdown of the passive layer is not uniform, chloride induced corrosion is highly localized and leads to pitting.

2.1.2.2 Carbonation

Carbon dioxide, found in air, can dissolve in concrete pore water to form carbonic acid. This carbonic acid can react with cement hydration products, i.e. calcium hydroxide, and reduce the alkalinity of the concrete according to the following reaction (Hansson et al. 2007):

$$CO_2 + H_2O + Ca(OH)_2 \rightarrow CaCO_3 + 2H_2O \qquad (3.4)$$

At the reinforcement, depassivation occurs due to the imposed acidity, and corrosion can begin with the presence of moisture and oxygen. It should be noted that the process is relatively slow compared to chloride induced corrosion and occurs uniformly over the bar length. Therefore, corrosion by carbonation is often referred to as homogeneous corrosion.

2.1.2.3 Freeze-Thaw

Persistent cycles of freeze-thaw can be devastating to concrete structures in northern climates. During mild cycles, a water chloride solution enters the concrete pores, freezing when temperatures drop below zero. The change of state attacks both the concrete paste and aggregate. The scientific explanation of the cracking and spalling caused by freeze-thaw varies significantly.

Powers (1945) hypothesized that freeze-thaw damage was caused by hydraulic pressure (internal stresses) created by the volumetric increase of water freezing to ice within concrete pores and considered the role of chlorides with the osmotic potential concept (Powers 1975). Litvan (1972) suggested that water absorbed within small pores cannot freeze in-situ due to surface/water interactions (Van der Waals forces) and thus a vapour pressure deference exists.

Mindless and Young (1981) and Pigeon and Pleau (1995) suggest that the solution saturating the pores, within the concrete, immediately below the surface, has a high chloride concentration. On the surface the water is pure, resulting in a difference in freezing points and vapour pressures, creating surface scaling. Other researchers believe the opposite occurs and the solution is highly concentrated outside the pores. Throughout the chloride application and freeze-thaw cycles experienced over a structure's lifetime it is likely that several deterioration mechanisms exist.

2.1.3 Damage Manifestation

The effects of corrosion of the reinforcing steel (rebar) on the deterioration of reinforced concrete structures are: steel section loss, concrete cracking and spalling or delamination (Cairns et al. 2008).

Concrete Cracking

When reinforcing steel corrodes, the resulting corrosion products can have a volume of up to six times that of the original material (Herholdt et al. 1985). This volume increase causes radial tensile stresses on the surrounding concrete as shown in Figure 2-3. When these stresses exceed the concrete tensile strength, cracking occurs. The most common form of cracking consists of longitudinal cracks at the height of the reinforcement layer as shown in Figure 2-4.

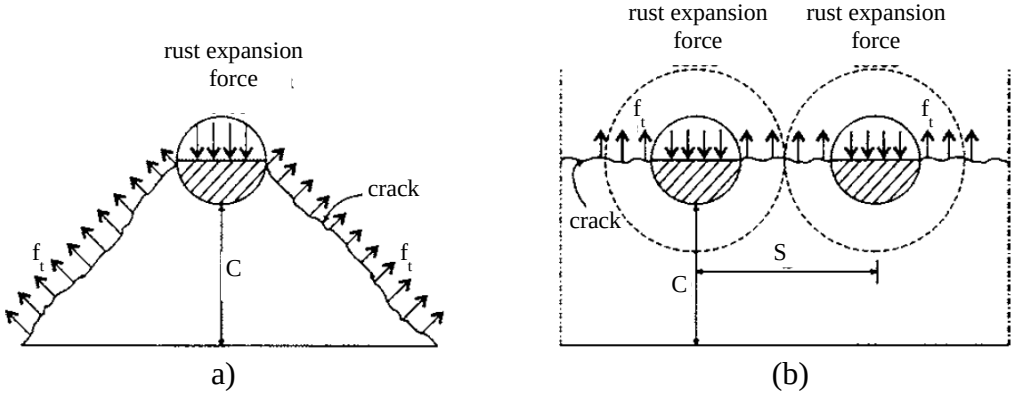

Figure 2-3: Rust expansion and resulting: (a) Inclined fracture plane; (b) Parallel fracture plane (Li et al. 2007).

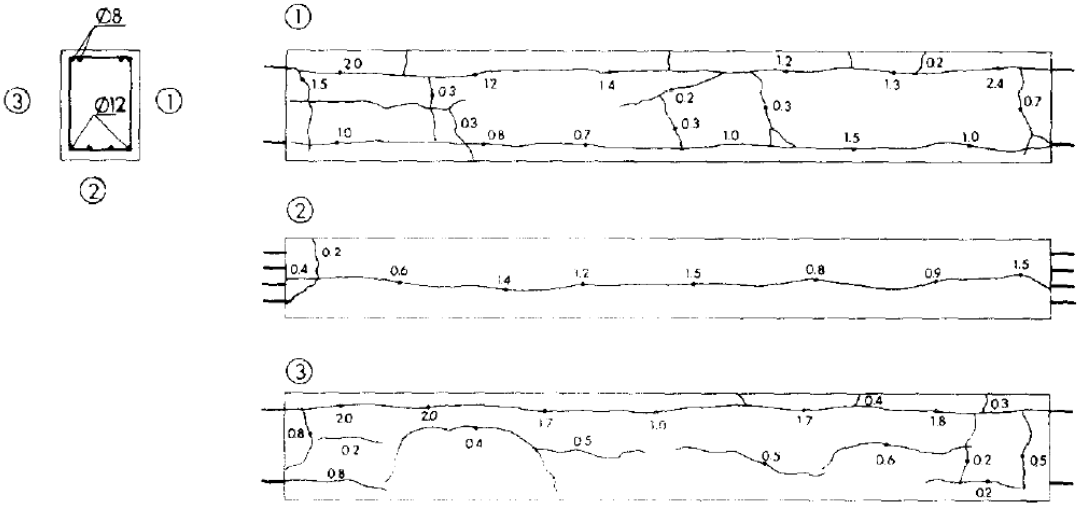

Figure 2-4: Mapping of corrosion cracking on specimens by Rodriguez et al. (1997).

Spalling

When longitudinal cracks occur on both sides of a girder, a failure plane is created and full sections of concrete can break off, revealing the underlying reinforcement. Spalling is the localized occurrence of this phenomenon, while delamination generally refers to large sections of exposed reinforcement as shown in Figure 2-5.

Figure 2-5: Bridge girder spalling and delamination (MTO).

Steel Section Loss

In the corrosion reaction, steel is consumed. Chloride induced corrosion tends to result in pitting or localized steel consumption, while carbonation tends to produce a generalized deterioration as shown in Figure 2-6.

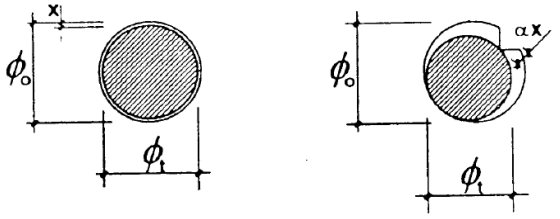

(a) (b)

Figure 2-6: Residual section loss for the (a) Uniform and (b) Localized corrosion (CONTECVET 2001).

2.1.4 Phases of Corrosion in Concrete Structures

The corrosion process is divided into a two phase process by Tuutti (1982): initiation and propagation. These two phases are depicted graphically in Figure 2-7.

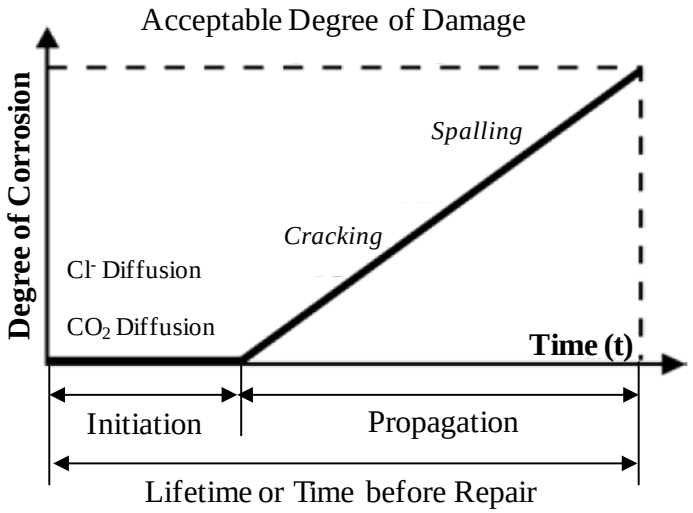

Figure 2-7: Phases of corrosion in concrete structures (CONTECVET 2001).

2.1.4.1 Initiation

The initiation phase represents the time for either chlorides or carbonation (or both) to permeate the concrete cover, reach the steel, and overcome the threshold levels. It extends from the time of construction to the time T_1, which is generally approximated by modelling the diffusion of contaminants through the concrete cover.

Chloride Diffusion

For chloride diffusion in concrete, Fick's second law of diffusion is commonly adopted (Andrade 1993):

$$C_x = C_s(1 - \text{erf}\left[\frac{x}{2\sqrt{D_c t}}\right]) \tag{3.5}$$

where:

t = time in seconds

D_c = diffusion coefficient ($0.1 - 3.0 \cdot 10^{-12}$ m^2/s)

x = depth of Cl^- level

C_S = Cl^- content @ surface

C_x = Cl^- content @ depth x

erf = Gauss error function

Theoretically, the initiation time depends on:

- chloride or carbon dioxide concentration in contact with concrete,
- permeability, w/c ratio, and quality of the concrete,
- amount of moisture present,
- concrete alkalinity (ph, passive layer),
- concrete cover, and
- quantity and severity of flexural cracks.

Carbonation

A simple model for carbonation diffusion is the square root method (CONTECVET 2001), where:

$$x = V \cdot \sqrt{t} \tag{3.6}$$

where,

t = time in seconds

x = penetration depth of carbonation

V = velocity of advance = $72 \cdot \left(\frac{1}{\sqrt{f_c'}} - 0.126 \right)$ for RH = 50%

Linear reductions may be used for RH greater or less than 50%. Four other models are suggested in (CONTECVET 2001).

2.1.4.2 Propagation

The propagation or active corrosion stage, T_{corr}, extends from the time of first formation of corrosion products, depassivation, or the end of initiation to a difficult to define state generally referred to as the end of service life. The following are some examples of the different definitions for the end of propagation:

- the time when corrosion generates sufficient stress to crack or spall the concrete cover, or the local attack on the reinforcement becomes sufficiently severe as to impair its load carrying capacity (Liang et al. 2002),
- the end of a structure's useful life. This may include longitudinal cracking (that exceeds 0.3 mm in width), spalling (cracking that exceeds 2.0 mm) or bar section loss exceeding 10% of the bars cross-sectional area (Cairns et al. 2008),
- an absolute period of 6 years (Thomas and Bentz 2000), or
- first corrosion cracking (El-Maadawy and Soudki 2007).

The definition of the end of the propagation stage is clearly open to debate. Conservatively, many base the end of propagation on the initiation of corrosion cracking (i.e. the last definition given above). With the exception of very localized pitting corrosion, it is assumed that cracking precedes rebar-governed strength loss, as further discussed in Section 2.2.1. This is actually not the end of the service life, however, and structures continue to function and are relied upon well beyond this point. Thus, there is a need for improved methods of predicting the remaining capacities and service lives of concrete structures that have already exceeded this limit.

2.1.4.3 Service Life Predictions

A practical tool for evaluation engineers may be one that allows the bridge owner to simply deduce a remaining service life based on chloride levels and the construction date.

Liang et al. (2002) provides an extensive review of research on service life estimations; most of which, work to combine estimates of initiation and propagation times. Therefore, a further review is not repeated here. The influence of seasons, climate change, chloride exposure, and environment may be too difficult to predict over the long term. Liang et al. (2002) confirms that the parameters involved should be further verified by experimental work before the models available are adopted to other structures. The authors compared the life estimates for various components of a 72 year old structure and suggest the models by Bazant (1979) and a modified model by Amey el al. (1998) be used, based on what they feel is a preferable ratio of $T_1 \approx (4 \text{ to } 5) \cdot T_{corr}$.

Again, although service life predictions may be useful for assessment and maintenance planning, in reality, many of the structures of primary concern are outside of the realm of the existing studies. Simply put, the onset of corrosion cracking may be estimated, but spalled structures continue to function and are relied upon by society well past this point.

2.2 Impacts of Deterioration on Structural Performance

Less is known about the 'effects' of concrete deterioration than the 'causes'. Many heavily deteriorated concrete structures remain in service, and the effects of deterioration on structural capacity and service are therefore a primary concern for evaluation engineers. Research by Cairns et al. (2008), suggests the effects of reinforcement on the residual structural capacity of a concrete member can be summarized by Figure 2-8.

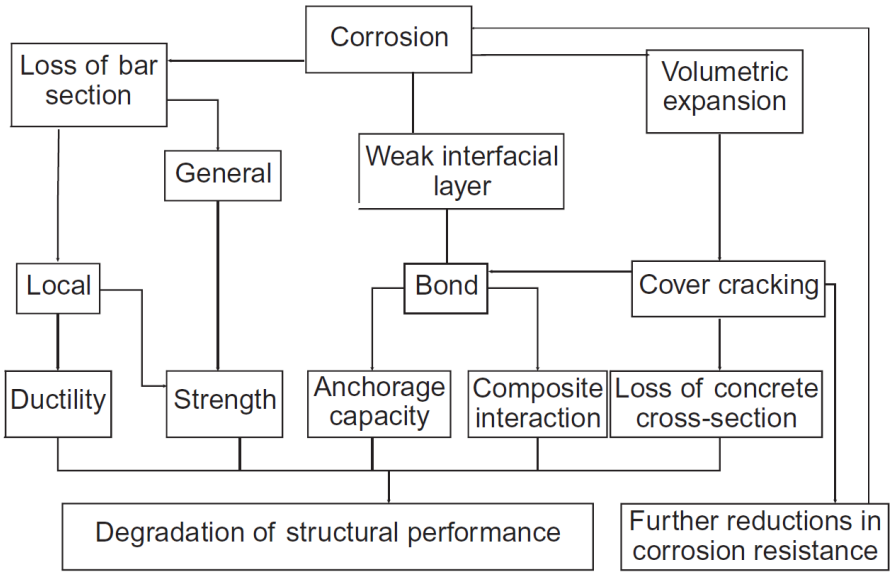

Figure 2-8: Effects of reinforcement corrosion on residual structural capacity (Cairns et al. 2005a).

Ultimately, the effects of reinforcement corrosion on structural performance are: 1) a reduction in the capacity of the rebar itself due to section loss, 2) a loss of bond between reinforcement steel and concrete that results in a loss of anchorage, and 3) a change in a member's behaviour due to loss of steel/concrete composite interaction. Additionally, the reinforcement strength and ductility changes may compromise the overall member strength. Each of these effects is discussed in the following subsections.

2.2.1 Reinforcing Steel Deterioration

The loss of bar section is the most obvious effect of corrosion on a member's capacity. Corrosion attack is broadly defined as either, localized (also known as pitting corrosion) or

uniform. Of the two, the effect of pitting corrosion has the most severe consequence. For pitting corrosion, there is both a loss of load carrying capacity and ductility.

2.2.1.1 Loss of Capacity

For uniform corrosion the residual strength computation is directly related to the reduced cross section and the average residual cross section can be determined at any exposed section of the bar. This is not the case for pitting corrosion, in which an overall minimum cross section (experienced along the bar's length) likely governs its strength. To complicate matters, Cairns et al. (2005b) suggests that localized corrosion creates less expansive forms of oxidation products that allow for substantial section losses prior to warning signs in the concrete such as longitudinal cracking. Therefore, the minimum cross section is difficult to determine. Cairns et al. (2005b) suggests that the distribution of pits may have the following form:

$$A_{res} = UF \cdot A_0 \cdot (1 - PF \cdot A_{los}) \tag{3.7}$$

where:

A_0 = original cross-sectional area

A_{res} = residual cross-sectional area

UF,PF = coefficients to represent mean and local section loss

A_{los} = normally distributed random variable representing the cross-sectional area lost to corrosion

Equation 2.7 can be used to predict both minimum and average cross-sectional areas. To simplify matters, researchers have suggested using an average cross section loss and reducing the steel yield strength with empirical relationships accordingly. The following general form has been adopted (Cairns et al. 2005b):

$$f_y = \left(1.0 - a_y \cdot Q_{corr}\right) \cdot f_{y0} \tag{3.8}$$

where:

f_y = yield strength after time t

f_{yo} = yield strength of noncorroded bars

Q_{corr} = average section loss (% of the original cross section)

α_y = empirical coefficient

A range of values for the empirical coefficient, α_y, have been proposed by various researchers. Cairns et al. (2005b) summarizes of the results of a number of available studies on α_y. Figure 2-9 compares several available empirical models.

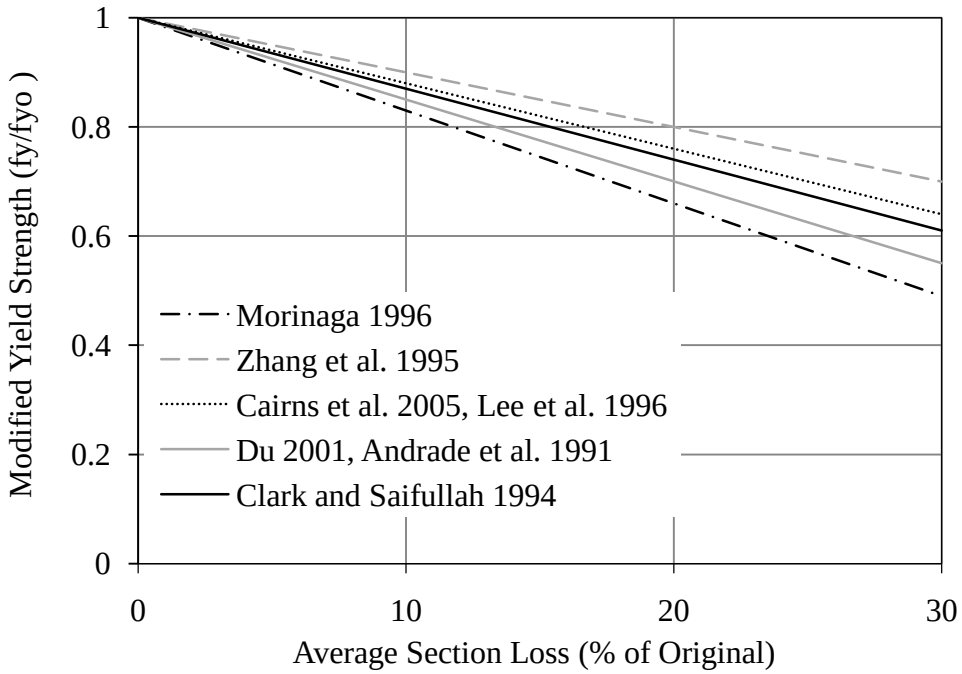

Figure 2-9: Empirical models for residual yield strength of corroded bars.

2.2.1.2 Loss of Ductility

Researchers have found that there may also be a significant loss in bar ductility due to corrosion. A change in ductility may result from the following:

1) Stress concentrations that form at pits due to abrupt geometric changes along short sections relative to the length of the bar (Cairns et al. 2005b; Palsson and Mirza, 2002; Lee and Cho, 2009).

2) Changes in the metal properties that result in a change in ductility. Palsson and Mirza (2002), for example, found significant impurities in a spectrochemical analysis of metal taken from an abandoned structure originally constructed in 1959.

In ageing structures, impurities are to be expected but the extent of their impact on ductility is still unclear (Palsson and Mirza 2002) and often ignored (Cairns et al. 2005b). To consider the change in bar ductility the following empirical relationships may be used:

$$f_u = \left(1.0 - \alpha_u \cdot Q_{corr}\right) \cdot f_{u0} \tag{3.9}$$

$$\varepsilon_u = \left(1.0 - \alpha_1 \cdot Q_{corr}\right) \cdot \varepsilon_0 \tag{3.10}$$

where:

f_u	= ultimate tensile strength and elongation at time *t*
ε_u	= elongation corresponding to the ultimate strength at time *t*
f_{uo}, ε_{uo}	= ultimate tensile strength and elongation of new bars
Q_{corr}	= average section loss (% of the original cross section)
α_u, α_1	= empirical coefficients

Figure 2-10 and Figure 2-11 present curves of Q_{corr} versus f_u and ε_u from several studies.

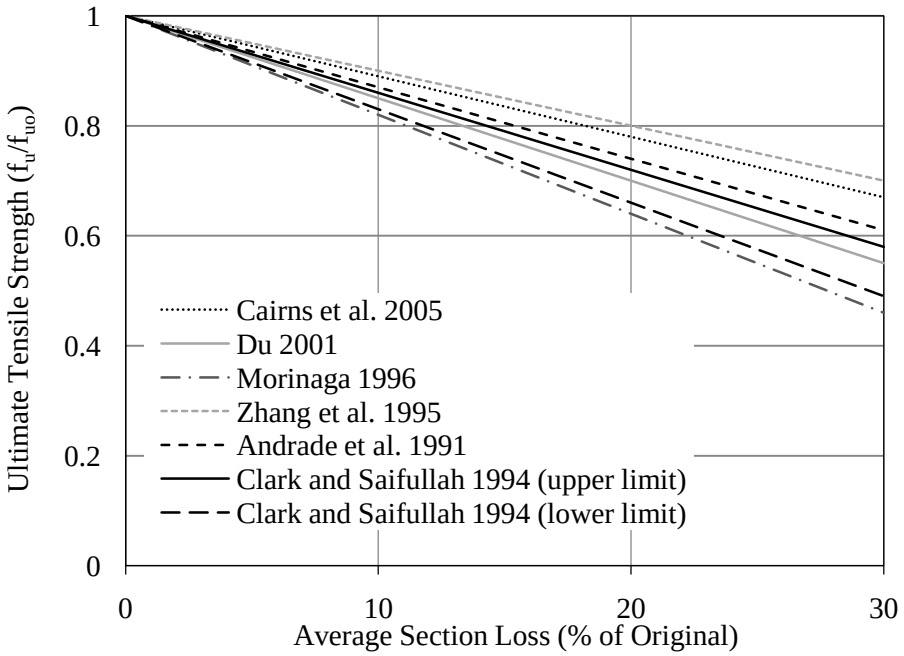

Figure 2-10: Empirical models for residual ultimate strength of corroded bars.

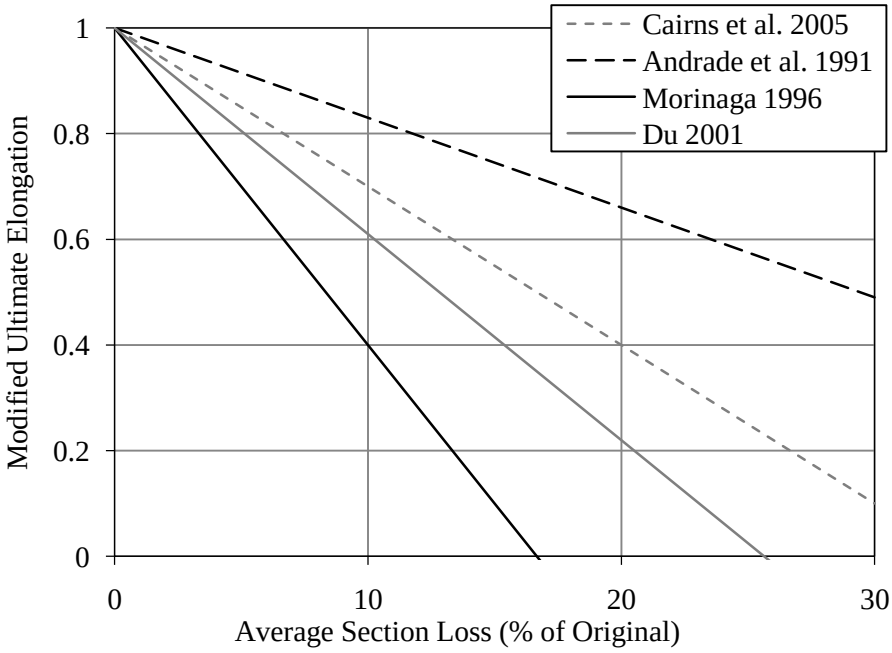

Figure 2-11: Empirical models for residual ultimate elongation of corroded bars.

Design rules in most national standards specify a minimum ductility that should be met. The residual ductility computed by Equations 2.9 and 2.10 must continue to satisfy these requirements, in order to ensure adequate structural performance. On this basis, a simple ductility check could be implemented for the evaluation of corroded structures.

2.2.2 Concrete/Steel Bond Loss

Generally, it is assumed that there are two stages of bond between concrete and steel when an axial force is applied to a reinforcing bar cast and developed in concrete. A report on bond (CEB 2000) describes these stages as follows: First, there exists a chemical bond between the hardened cement and steel. This condition is generally weak and broken at low stresses. Slip starts to occur at Stage 2; in which friction provides the bond. Where ribbed bars are used, bearing and mechanical interlock between the ribs and surrounding concrete resists pullout. Given that the ribs are strong, failure eventually occurs by bursting or splitting of the surrounding concrete.

2.2.2.1 Effect of Corrosion on Bond

The effect of corrosion on bond is summarized as follows (CEB 2000):

- Increased bar diameter, due to the creation of corrosion products, initially increases radial stresses and the frictional component of bond. Bond strength increases as a result.
- When radial stresses (due to further corrosion) exceed the threshold (determined by concrete strength and cover) bursting and splitting of the concrete cover occurs, resulting in longitudinal cracking and a reduction in confinement and bond strength.

However, the following has also been hypothesized;

- Corrosion products at the bar/concrete interface under low corrosion levels may have a roughening effect, increasing friction and bond (Al-Sulaimani et al. 1990).
- As corrosion increases, the weak corrosion product acts as a lubricant to reduce friction and bond strength (Cabrera and Ghoddoussi 1992).

- Under severe corrosion, bar ribs may reduce in height or fracture; reducing bearing area and bond strength (Al-Sulaimani et al. 1990).
- The layer of corrosion product may force the concrete away from the bar core and subsequently reduce the effective rib height and bearing area; reducing bond strength. This phenomenon is often referred to as "disengagement of ribs" (CEB 2000).

2.2.2.2 Corroded Bond Tests

The residual bond strength of corroded reinforcing bars embedded in concrete has been extensively tested in the laboratory. The types of tests conducted by others to date include concentric pullout tests, tension pullout tests, bond beam tests, bureau of standards beam tests, cantilever bond tests, and the University of Texas beam tests. These can be divided into two broad categories: pullout and beam tests. In all cases, corrosion was accelerated in the laboratory using electrochemical techniques. In a review by Bhargava et al. (2007) the results of a number of experiments were summarized as shown in Figure 2-12(b).

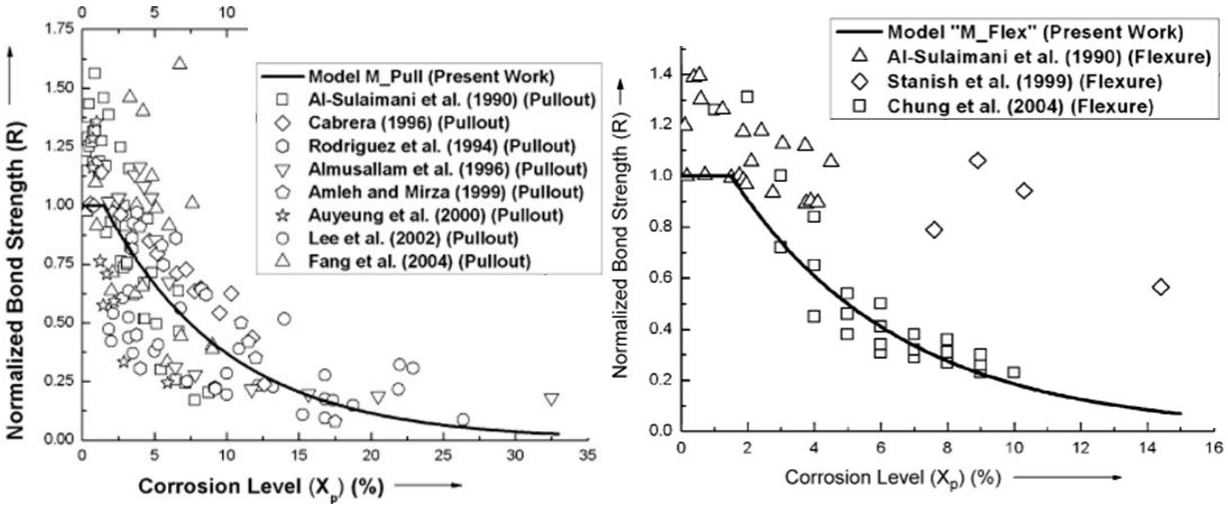

(a) (b)

Figure 2-12: Bond strength with corrosion. (a) Pullout and (b) Flexure test results (Bhargava et al. 2007).

The scatter in results is obvious. Bhargava et al. (2007) attributes this variation to both the wide-range of bond specimens and bar types tested and the variation in conditioning techniques. The CEB/FIB report (CEB 2000) agrees that there are distinct variations in the applied current density, methods of weight loss measurement and specimen detailing and that "developing an appropriate measure of damage is clearly a priority in reconciling test data and development of assessment guidelines for bond".

Electrochemical corrosion has limitations when compared to corrosion on real structures. Poursee and Hansson (2009) recommend against applied anodic current corrosion techniques, as used by the majority of researchers highlighted here, due to significant differences between corrosion products developed artificially to those on real structures. They suggest that the resulting corrosion is overly uniform, many tests neglect differentiating between micro and macro cell corrosion, and specimen detailing such as steel grade and surface finishing has variable impacts. Ballim and Reid (2002) highlight the importance of applying the selected technique under service load levels.

2.2.2.3 Predictive models

The development of predictive models for the degradation of bond strength with corrosion is a challenging task currently facing researchers. The influence and interaction of each of the proposed mechanisms listed in Section 2.2.2.1 is very difficult to predict. As a result, simple empirical and analytical relations remain as the best representations available.

Analytical Models

Cairns and Abdullah (1996) suggested analytical formulas to represent splitting modes of noncorroded bar bond failure. They predicted bond strength based on the resolution of forces acting on the ribs into radial bursting forces as shown in Figure 2-13 for failure modes 2 and 3 shown in Figure 2-14 within good agreement to laboratory test.

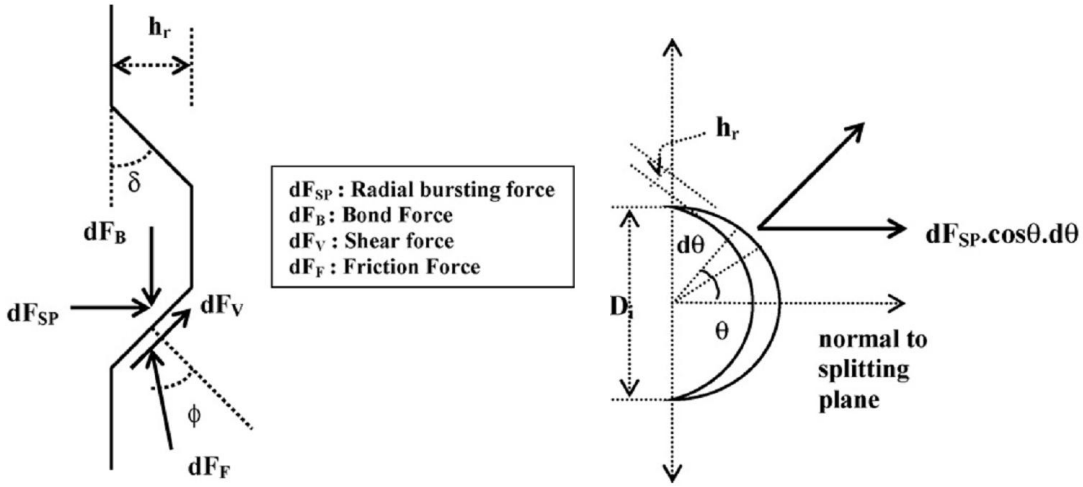

(a) (b)

Figure 2-13: (a) Forces acting on rib and (b) Resolution of radial bursting forces (Cairns and Abdullah 1996 as cited by Bhargava et al. 2007).

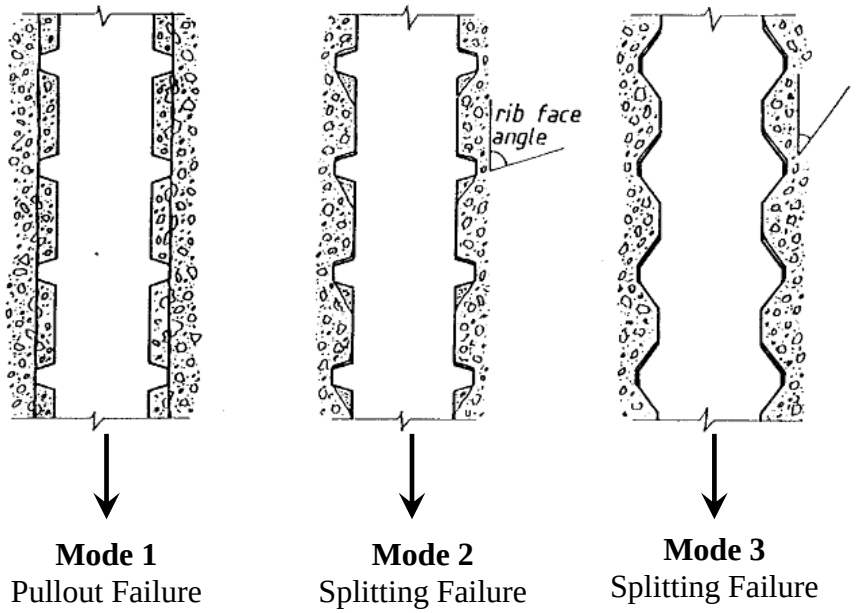

Figure 2-14: Bond failure modes of ribbed reinforcing bars by Cairns and Abdullah (1996).

The first mode is the standard pullout associated with concrete shear and thick cover, while the second occurs when concrete wedges shear and no slip between rib and bearing surface occurs. The third mode is the conventional bursting failure in which an inclined failure surface is developed along the rib/bearing surface interface.

Coronelli (2002) expanded the model described in Figure 2-13 and Figure 2-14 to consider corroded bars. The primary changes due to corrosion resulted in:

- modified cohesion, f_{coh}, and angle of cohesion, φ, values,
- reduced rib height, h_r, values and resulting modified rib area, A_r, and
- an additional pressure term, $p(X)$, to represent the stress distribution at the bar/concrete interface between ribs resulting from rust. The pressure is based on a coefficient of friction for rusted steel of $\mu(X)$.

The model, correlated well with the experimental work by Rodriguez et al. (1994).

In their study, Bhargava et al. (2007) continued to modify the model by estimating parameters such as corrosion pressure, confining action of cracked concrete and shear stirrups after incorporating the effect of corrosion products and adhesion on friction between steel and concrete. The modified version appears to be better for predicting, pre-cracking behaviour but appears to add complexity.

Empirical Models

Several researchers have suggested empirical formulations to quantify bond deterioration. Table 2.1 defines a set of conditions established (based on the case study structure) to facilitate a comparison of the different empirical models. The comparison of available models is shown in Figure 2-15.

Table 2.1: Input for bond degradation model comparison.

Input Parameter	Assumed Value	*Required for:*
Longitudinal Bar Diameter	31.8 mm	Rodriguez et al. 1994
Concrete Cover	50.8 mm	Rodriguez et al. 1994
Development Length, (l_d)	36.2 mm	
Concrete Strength, (f_c')	20 MPa	Rodriguez et al. 1994, Chung et al. 2004
Stirrup Strength, (f_y)	230 MPa	Rodriguez et al. 1994
Stirrup Spacing	304.8 mm	Rodriguez et al. 1994
Stirrup Area	125.7 mm^2	Rodriguez et al. 1994

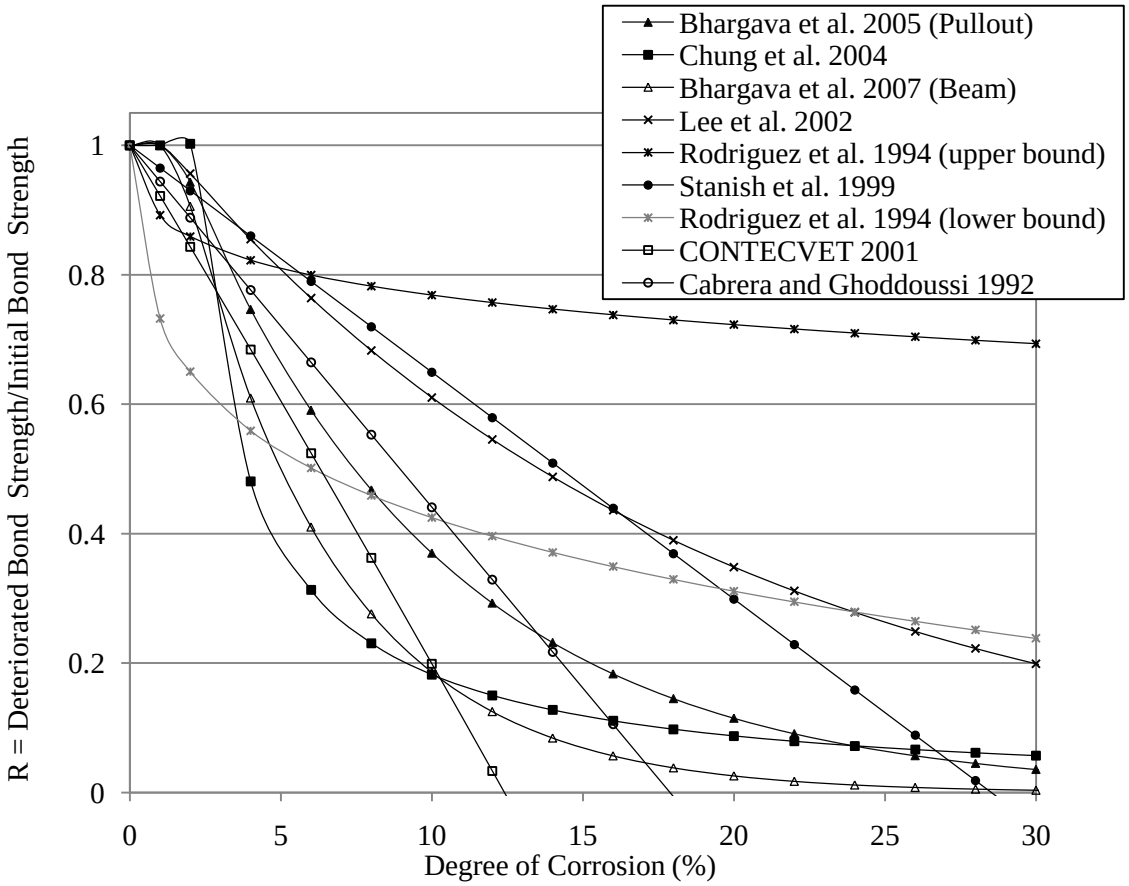

Figure 2-15: Empirical models for steel-concrete bond deterioration.

There is significant evidence in literature to suggest that a small increase or no change in bond strength occurs at low levels of corrosion due to a slight roughening effect by the corrosion products (Bhargava et al. 2007, Lee et al. 2002, Chung et al. 2004).

With increasing corrosion, longitudinal cracks and slip occurs and bond strength decreases rapidly. The strength plateaus at minimal strength once confinement is lost. Simple linear models, such as those by Stanish et al. (1999), Cabrera (1996), and the Contecvet manual (2001), neglect these effects and appear to underestimate the bond strength at low levels of corrosion and overestimate the strength at higher levels.

2.2.3 Composite Action

Traditional concrete design assumes that the steel is bonded perfectly to the concrete. Tension stiffening occurs as the steel transfers tensional forces to the concrete through this bond. Even after flexural cracking, tension stiffening continues to occur between cracks. However, when this bond is completely compromised by corrosion, the tension stiffening contribution of the steel is reduced or eliminated. The result is the reinforced concrete member globally acts like a tied arch. Both flexural and shear behaviour of the member can change. Several researchers have attempted to describe and model the change in behaviour of beams when reinforcement is exposed. This section first develops the theory, and then discusses the effect of a loss in composite action on flexural strength, shear strength, and ductility.

2.2.3.1 Concept

The theoretical change in beam behaviour can be described in two stages. Stage 1 re-equilibrates forces, while Stage 2 maintains deformation compatibility. To illustrate these changes, first consider the normal, un-exposed beam. Equilibrium of forces is met and deformations of the concrete and the steel are compatible. The tensile stress in the reinforcement varies proportionally to the applied moment along the member. In the case of symmetric point loads, as the section of interest moves towards the supports, the tensile stress

in the rebar and the maximum compressive stress in the concrete decrease proportional to each other and the applied moment as shown in Figure 2-16.

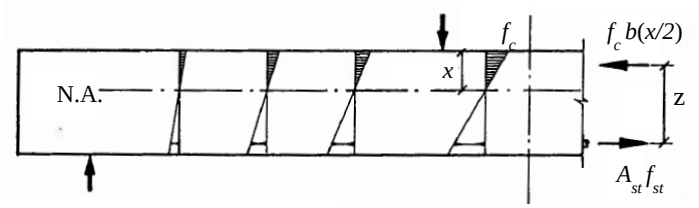

Figure 2-16: Noncorroded beam subject to symmetric point loads (Cairns and Zhao 1993).

However, when bond is broken over a certain length, the tensile stress in the rebar becomes constant along this length and equal in magnitude to the maximum experienced along this section. To maintain equilibrium, as the applied bending moment decreases (towards the supports) and tensile rebar stress remains constant, the lever arm must decrease. This in turn causes the neutral axis to drop. The maximum concrete stress decreases with increased neutral axis depth. It is possible for the neutral axis to drop to the bottom edge of the beam, putting the entire section in compression. At very low moment sections (towards the supports), it is even possible for a stress reversal to occur and the top fibre to be subject to tension and the bottom fibre compression a shown in Figure 2-17.

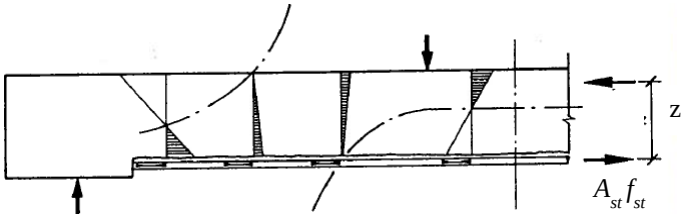

Figure 2-17: Corroded beam after Stage 1 (Cairns and Zhao 1993).

However, in Stage 2, deformation compatibility is not satisfied. It is apparent that the elongation in the steel reinforcement will be greater in the unbonded reinforcement due to the constant bar strain. The extension of the bottom concrete fibre is reduced in this case. To maintain deformation compatibility, the neutral axis depth at the midspan must be reduced as shown in Figure 2-18. The result is higher midspan concrete compressive strains and increased midspan curvature. Also, with a decreased depth of neutral axis, the lever arm

increases, resulting in a slight decrease in the reinforcement stress. Stage 2 ends with this stress adjustment (Cairns and Zhao 1993).

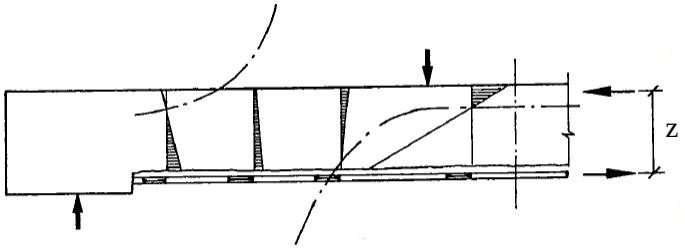

Figure 2-18: Corroded beam after Stage 2 (Cairns and Zhao 1993).

As the exposed rebar length increases, the compressive strains in the concrete also increase. It is therefore logical that a conventionally balanced beam will become overreinforced due to concrete crushed under reduced loads. Likewise, an underreinforced beam could fail by concrete crushing or yielding depending on the reinforcement ratio and the length of exposed region. Initially overreinforced members will show the most significant strength reduction, again, due to concrete crushing occurring under reduced loads. Crushing failure is less ductile and can occur suddenly.

2.2.3.2 Effect on Flexural Capacity

Researchers have used the following experimental research to support their hypotheses and to verify their numerical models for predicting the effects of loss of composite action on the behaviour of concrete beams with corroding reinforcing bars.

Laboratory Testing

Cairns and Zhao (1993) mechanically delaminated 19 test beams, to test the influence of each of the following parameters: exposed length/span ratio, form of loading, reinforcement ratio, and effective depth. They found underreinforced specimens, with up to 95% of the span exposed, had no loss in strength and failure was still governed by reinforcement yielding when anchorage was provided. On the other hand, heavily reinforced specimens, with up to 95% of their span debonded, had strengths reductions up to 50%.

To better replicate bridge girders, Bartlett (Unpublished) tested two T-beams under four point loading, designed to fail in flexure (steel yielding). The deteriorated girder, with 50% of its span symmetrically debonded mechanically, again attained full yield flexural strength.

Analytical Modelling

Compatibility theory and the concept discussed in Section 2.2.3.1 can be used to estimate the flexural capacity. Cairns and Zhao (1993) proposed the method, and confirmed its validity with a test: predicted ratio of 1.01 and a standard deviation of 0.06. They also found that the method estimated the failure mode reasonable well and that the strains could be used to estimate ductility. Bartlett (Unpublished) later adapted the model for application to T-beams using CSA Standards. They reported a test to predicted ratio (test:predicted) of 1.08.

2.2.3.3 Effect on Shear Capacity

Laboratory Testing

Azam (2010) tested ten deep and ten slender shear critical beams at the University of Waterloo, electrochemically corroding 60% and 80% of their spans respectively. They found that the deep beams had an increase in ultimate capacity due to arch action. In these specimens, corrosion shifted the failure from shear-compression failure to splitting of the compression strut. The slender beams also experienced arch action, but failure shifted from diagonal tension failure to flexure or anchorage. Similarly, Cairns and Zhao (1993) found that shear failures did not occur in their tests, even in specimens detailed for this type of failure. They concluded that shear strengths increased as a result of arch action and diagonal compression fields acting as struts transfer shear stresses directly to the supports.

Analytical Modelling

Azam (2010) proposes a modified strut-and-tie model to describe the shear strength of corroded test specimens within 15% error. For deep beams, the model checks splitting of the struts and yielding of the tie. For slender members, they suggest that the direct strut be replaced by an arch band.

2.2.3.4 Effect on Serviceability

The effects on serviceability appear to be the most significant impact due to a loss in composite interaction. This section discusses changes in ductility and issues regarding cracking.

Ductility

Cairns and Zhao (1993) found, as expected, that reinforcement strains at failure do indicate an overall loss of ductility due to the loss of composite action. Bartlett (Unpublished) noted that their test specimen had an 80% reduction in ultimate moment capacity and flexural stiffness. The analytical model suggested in Section 2.2.3.2 is capable of determining ductility changes. As expected, Azam (2010) found that shear sensitive beams also experienced a reduction in ductility and increased deflections.

Cracking

Deflections and cracking becomes more severe with the loss of composite interaction. Cairns and Zhao (1993) noted that in members where concrete crushing governed, large cracks at a wide spacing appeared under low loads in the constant moment zones. These cracks extended to the level of the neutral axis, often propagating outwards under increased loading. Near the supports, cracks developed in the top flange, where it was evident that tension was present, as anticipated, and curvature was significant. They also found that crushing of concrete at the ends of the exposed regions on the tension face occurred if they intersected the inclined compressive struts.

2.3 Summary

The majority of the existing research on each of the effects of corrosion on the remaining structural capacity of reinforced concrete flexural members has focused on exclusively considering one or several of the effects in isolation. In the case of the laboratory tests, none of the cited studies have modelled the effects of spalling in the vicinity of lap splices or bar

ends. In all cases bars are fully developed into supports. As a result, there currently exists little in the way of previous research examining the interactions of these corrosion effects and how they may influence the remaining structural capacities of real, heavily spalled bridge girders. On this basis, a “modified area concept”, which offers a practical way of considering these affects, is proposed, developed, and then demonstrated on a case study bridge in the following chapters.

Chapter 3

Structural Strength Assessment

3.1 Introduction

It is apparent that reinforced concrete structures retain their structural capacity and function after significant spalling has occurred. In fact, aging bridge infrastructure in Canada remains in service and appears to be performing adequately despite obvious extensive deterioration. The commonly adopted explanation is arch action and the development of inclined compressive struts as discussed in Section 2.2.3. Bar development, however, becomes critical when tension ties form and many studies assume that bars are sufficiently developed and development regions are completely undeteriorated. In reality, this is not the case. Spalling may occur randomly along the span of a bridge, and reinforcing splices are common in structures of aging vintage. The potential bond failure is brittle, sudden, and potentially catastrophic. The concepts developed in this chapter provide a simple structural analysis tool, capable of evaluating a structure's capacity and reliability given any spalling pattern and severity and the positioning of reinforcement curtailment. This chapter uses a case study structure presented in Section 3.2, to develop the modified area concept introduced in Section 3.3. The concept is applied to proportionally reduce flexural and shear capacities in Sections 3.4 and 3.5 respectively. Finally, Section 3.5 presents a simple reliability study based on the CAN/CSA S6-06 bridge evaluation procedures to provide early indications of individual girder and overall bridge deficiencies created by exposed reinforcement.

3.2 Case Study Structure

The case study structure provided by the MTO represents a typical structure of concern. It was indicated by Ministry engineers that there are currently a large number of structures of the same design and vintage currently in service in Ontario along 400 series highways. Therefore, this structure was used to develop the concept and analysis program. This section discusses the background, deterioration, and the available resources for this structure.

3.2.1 Background

The case study structure crosses a major highway with an annual average daily traffic (AADT) of more than 425,000 vehicles. Originally designed in May 1954, the structure is a single span, conventionally reinforced slab on girder rigid frame as shown in Figure 3-1. Although it is shaped as an arch, design details indicate that this feature is simply for aesthetics and an increased shear capacity at critical locations. In service, the structure supports two lanes of traffic while spanning six lanes of highway at a skew angle of 107°. Ministry engineers have indicated that the narrow shoulders would not be sufficient for future highway expansions that may be inevitable. When these occur, a full bridge replacement will be necessary.

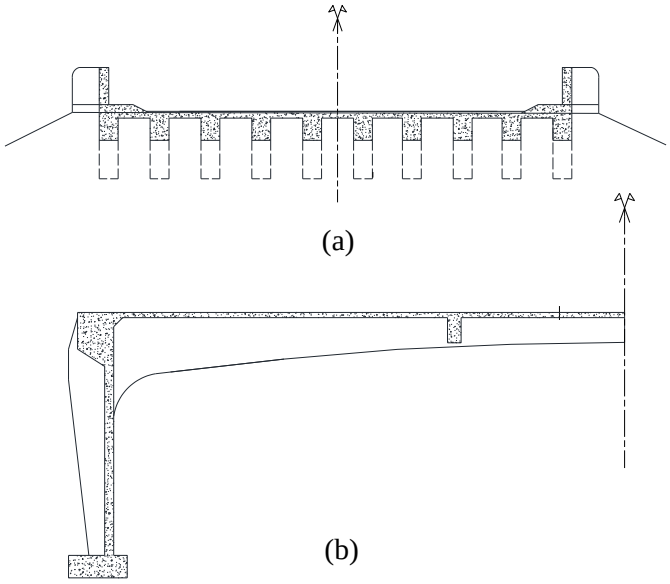

Figure 3-1: Case study structure (a) Cross section, and (b) Elevation.

The flexural reinforcing consists of a bottom lower level with bottom upper reinforcement in the maximum positive moment regions. Negative moment top steel spans the length of the structure, with a second (lower) layer in the maximum negative moment regions. The flexural reinforcing bars are spliced with butt or lap splices as shown in Appendix A-1.

3.2.2 Deterioration

The structure has been under investigation by the Ministry for several years. In 1991, Shotcrete repairs were performed to address concerns of spalling and delamination on the girder soffits. Drawings specifying the details of these repairs were provided by the Ministry. To gauge the success of the repairs, the current spalling pattern was superimposed on the drawing specifying the repair details as shown in Appendix A-3. It was concluded from this qualitative analysis that the current spalling is randomly distributed with little or no correlation to the previous repairs. Significant deterioration of the structure is evident by site inspection and photographs. The visible deterioration includes:

- hand rail corrosion, rust holes and staining of adjacent concrete,
- exposure of rail support bolts and sidewalk deterioration,
- leakage and staining below expansion joints,
- girder soffit spalling and delamination exposing the bottom layer of reinforcing steel,
- staining and spalling below stirrups on girder soffits, and
- minor slab soffit spalling.

Of these deterioration effects, the severe spalling and delamination of the girder soffits as shown in Figure 3-2, poses the greatest threat to the ultimate strength of the structure and therefore is the primary concern of the current investigation and research.

Figure 3-2: Girder spalling and delamination.

3.2.3 Available Resources

To document the extent of the deterioration, MTO engineers have created spalling maps of the bridge underside. A sample is shown in Figure 3-3. Two different spalling maps were created for this structure. The first map was completed in July 2009 from images taken of the structure from the road shoulders during live traffic. From these images, it was concluded that scaling was required to remove chunks of loose concrete that pose a danger to highway traffic. Under lane closures, Ministry employees used hammers to remove loose concrete as shown in Figure 3-4. A second spalling survey was completed during these lane closures in August of the same year. It should be noted that there are significant deviations between these two representations, which are both included in their entirety in Appendix A-2. The ultimate accuracy of the analysis presented herein is dependent of the accuracy of the spalling survey.

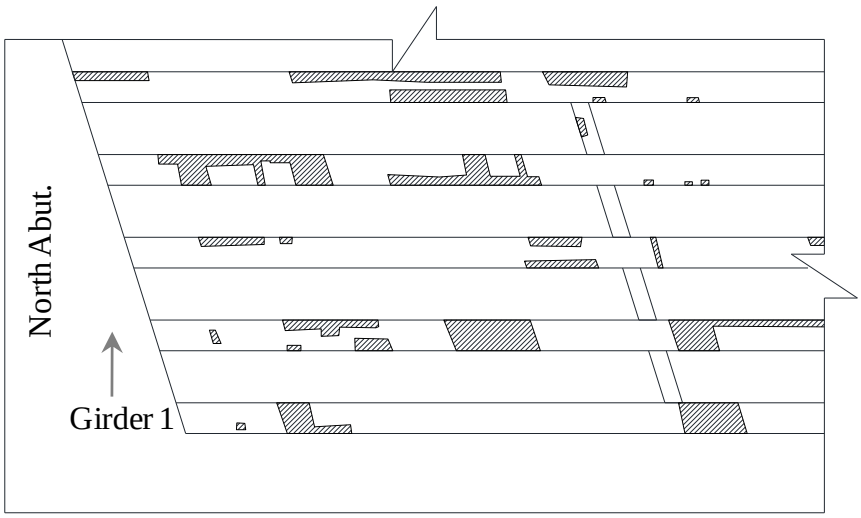

Figure 3-3: Spalling survey sample (August 2009).

Figure 3-4: Scaling operation (MTO).

The Ministry also maintains a library of original design drawings for the structure (see Appendix A-1). From these drawings a typical girder reinforcement layout is shown. Spalling primarily impacts the bottom lower layer of the positive flexural reinforcing. Therefore, the analysis begins by superimposing this reinforcement on the most current spalling survey. If the original bottom reinforcement drawing is superimposed on the spalling survey, a representation, such as the one illustrated in Figure 3-5, can be generated. The complete superposition for each girder is provided in Appendix A-4.

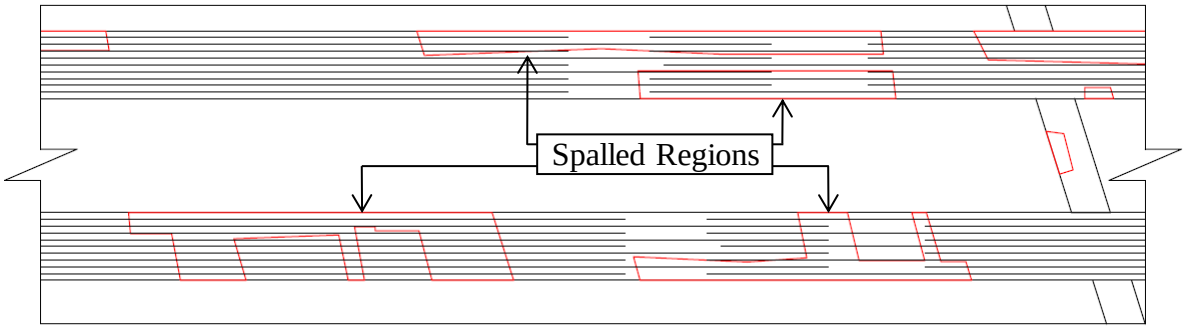

Figure 3-5: Spalling/reinforcement superposition.

3.2.4 Structural Analysis

A simple structural analysis was conducted to determine the load effects on the structure. Since the structure is statically indeterminate, the load effects were determined using a simple Finite Elements Analysis (FEA), as outlined in Section 3.2.4.1. The transverse distribution of load effects between girders was determined using CAN/CSA S6-06, as discussed in Section 3.2.4.2.

3.2.4.1 FEA Analysis

For the case study structure, the girder end fixity is a function of its rigidity relative to that of the legs and joints. To determine the load effects, the SAP2000 commercial structural analysis software was utilized. For simplicity, the structure was approximated by a 2-D single girder model as shown in Figure 3-6. Both the CAN/CSA S6-06 CL-625 truck, and truck plus CLW lane load shown in Appendix A-5 were applied in SAP using the built in bridge module. The slab self weight was added as a uniform load. Results were obtained as unfactored load envelopes. Slab and girder self weight moments and shears are provided in Appendix A-5.

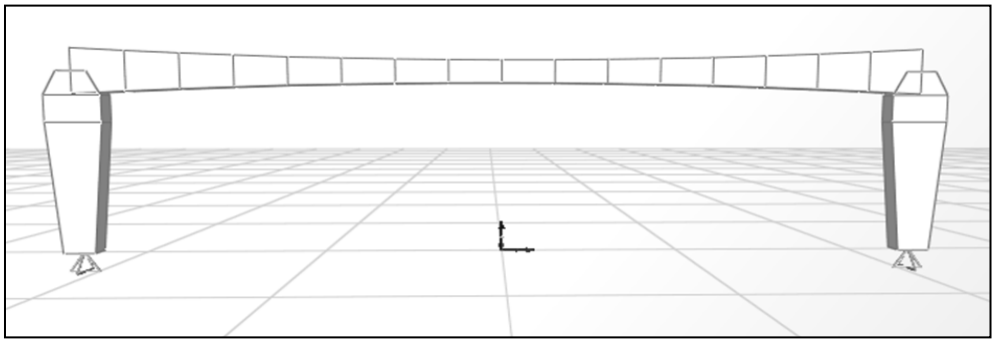

Figure 3-6: SAP2000 model.

For a bridge structure, the vehicular load envelope represents the bounds for moment and shear for each truck position along the bridge. That is, each point along the envelope represents the worst case moment or shear. It was found that the CL-625 truck plus CLW lane load case governed. The corresponding live unfactored moment and shear envelopes are shown in Figure 3-7 and Figure 3-8.

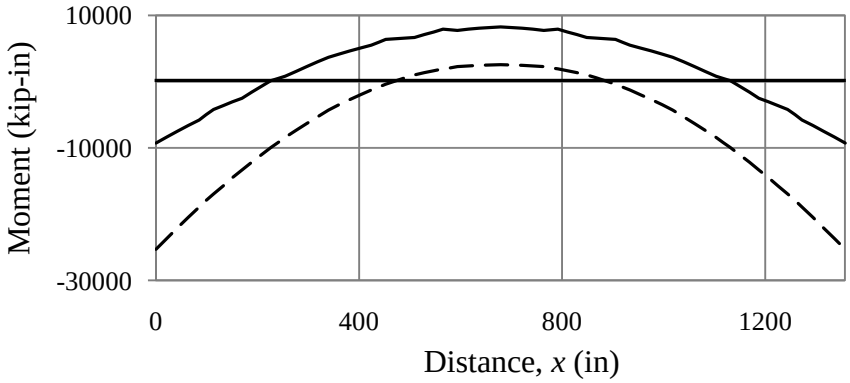

Figure 3-7: Live load (unfactored) moment envelope.

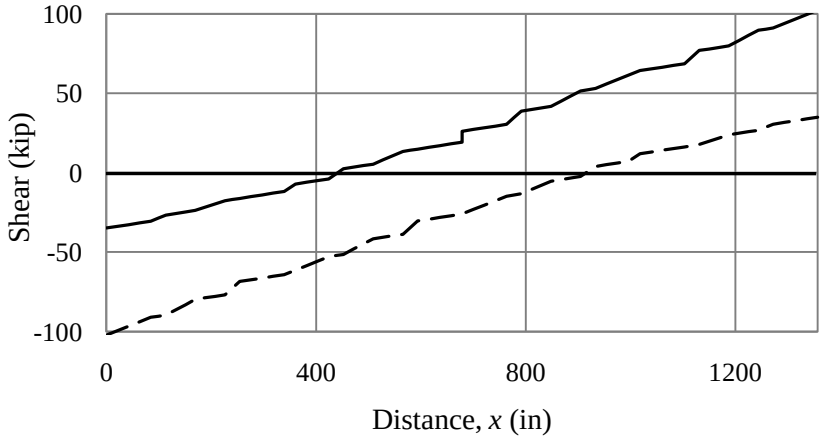

Figure 3-8: Live load (unfactored) shear envelope.

3.2.4.2 Transverse Distribution

In lieu of a time consuming 3-D analysis, the CAN/CSA S6-06 simplified transverse distribution model was used. Simplified live load analysis may be used if all the criteria of Cl. 5.7.1.1 of this standard are met. The approach provides amplification factors for the (2-D) beam analogy method. These transverse distribution factors are computed in Appendix A-7.

3.3 Modified Strength Concept

For the investigated bridge, a typical longitudinal reinforcing bar is spliced 3-4 times along the length of the girder. At each splice location, development can be compromised by the spalling. Upon examination of the spalling surveys in Appendix A-4, it was noted that several longitudinal bars end in spalled regions or have significant spalling along their length. Therefore, the proposed concept evaluates the residual strength due to development deficiencies resulting from spalling. The modified area concept is founded on the following basic assumptions:

1) The spalled areas are fully de-bonded with no remaining force transfer.

2) Full concrete and bond strength is assumed in the unspalled areas.

3) The reinforcing steel is at full strength and has no change in strength or ductility due to corrosion.

4) The bond strength is linearly proportional to the available development length.

Each of these assumptions is addressed later in this thesis in subsequent refinements of the model. The following sections introduce CAN/CSA A23.3-04 development, moment and shear design concepts and use each to determine modified moment and shear capacities for any member with exposed reinforcement.

3.3.1 CSA Development Length

CAN/CSA A23.3-04 considers development secondary to flexural design. Bars are simply designed to ensure that development and splice lengths are "sufficiently over-strengthened to decrease the probability of a bond related failure before failure occurs in a more ductile flexure mode". For bars in tension, CAN/CSA S6-06 defines the required development length, l_d , as follows,

S6-06, Cl. 8.15.2.2

$$l_d = 0.45 \frac{k_1 k_2 k_3}{(k_{tr} + d_{cs})} \left[\frac{f_y}{f_{cr}} \right] A_b \qquad (3.11)$$

S6-06, Cl. 8.15.2.2

$$k_{tr} = 0.45 \frac{A_{tr} f_y}{10.5 s n} \qquad (3.12)$$

where:

$k_1 k_2 k_3$ = modification factors for the effects of casting position, epoxy coating and bar size

d_{cs} = the lesser of 2/3 bar diameter or distance from bar to closest concrete surface

A_b = x-sectional area of the bar being developed

If the minimum cover, spacing and/or transverse reinforcement is provided, then the equation can be simplified to the following:

S6-06, Cl. 8.15.2.3

$$l_d = 0.18 k_1 k_2 k_3 \left[\frac{f_y}{f_{cr}} \right] d_b \qquad (3.13)$$

S6-06, Cl. 8.15.2.3

$$l_d = 0.24 k_1 k_2 k_3 \left[\frac{f_y}{f_{cr}} \right] d_b \qquad (3.14)$$

3.3.2 Modified Area Concept

The proposed method for assessing spalled bridge girders with exposed reinforcement proportionally modifies a reinforcing bar's cross-sectional area to accommodate for the reduced strength if the code specified development length is compromised by spalling as shown below. First, consider a discrete location, 'A', at a distance greater than the required development length, l_d, from the end of the reinforcing bar as shown in Figure 3-9.

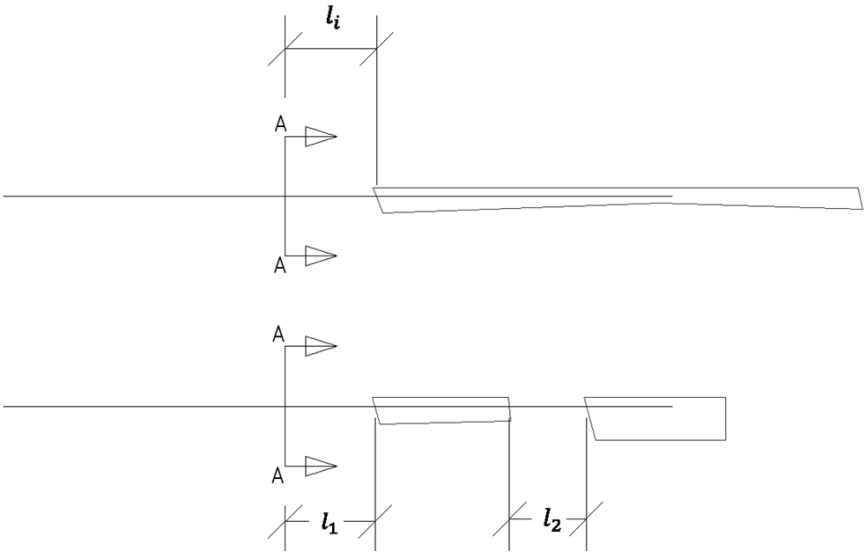

Figure 3-9: Modified area concept.

At Section 'A' the remaining intact length available for development is l_i. If multiple spalled regions are present, then the intact length is simply taken as the sum of each intact section, i.e.:

$$l_i = \sum_{k=1}^{n} l_k \tag{3.15}$$

If the intact length is less than the required development length (i.e. $l_i < l_d$), then the proposed method proportionally modifies the bar's cross-sectional area as follows:

$$A_d' = A_d \left(\frac{l_i}{l_d} \right) \tag{3.16}$$

where:

l_i = intact (remaining) length

A_d = actual (unspalled) bar cross sectional area

A_d' = modified bar cross sectional area

If the intact length is greater than the required development length (i.e. $l_i > l_d$), then the bar area is not modified.

3.4 Modified Moment Resistance

The flexural capacity of a reinforced concrete member is a function of:

1. concrete strength
2. steel strength
3. sectional geometry
4. development length

If the development length is compromised, then the flexural capacity is reduced. This section describes this concept, after introducing the CAN/CSA A23.3-04 provisions for moment capacity.

3.4.1 CSA Moment Capacity

The CAN/CSA A23.3-04 flexural design provisions are based on strain compatibility and the following general principles:

1. Plane sections remain plane: the strain in the reinforcement and concrete is assumed to be directly proportional to the distance from the neutral axis (Cl. 10.1.2).
2. The maximum strain at the extreme concrete compression fibre is assumed to be 0.0035 (Cl. 10.1.3).
3. A balanced strain condition is assumed to exist at a cross-section, where the tension reinforcement reaches its yield strain just as the concrete in compression reaches its maximum strain of 0.0035 (Cl. 10.1.4).
4. The tensile strength of the concrete is neglected in the calculation of the factored flexural resistance of reinforced concrete members.

The design procedure relies on the assumption of an equivalent rectangular stress block as explained in Figure 3-10.

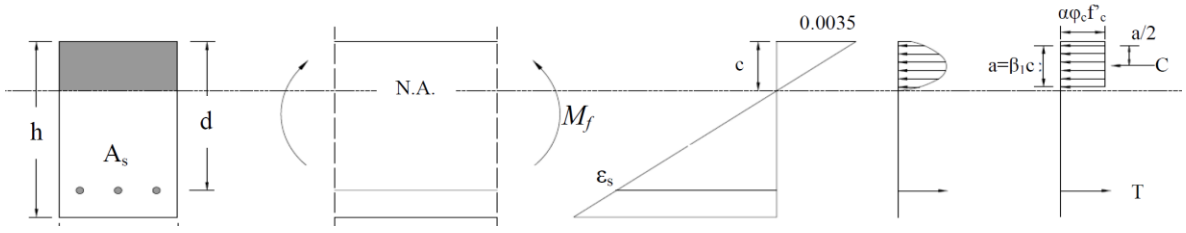

Figure 3-10: Rectangular stress block theory for flexural design of an RC member.

CAN/CSA A23.3-04 considers flexural capacity in two phases. The first phase consists of the section design while the second evaluates the member design, including bar lengths and cutoffs. Bars are simply designed to ensure that development and splice lengths are "sufficiently over-strengthened to decrease the probability of a bond related failure before failure occurs in a more ductile flexure mode".

3.4.2 Modified Moment Capacity

For a conventionally reinforced rectangular cross section, as shown in Figure 3.9, the moment resistance is:

CAN/CSA A23.3-04

$$M_r = A_s \phi_s f_y (d - \frac{a}{2}). \quad (3.7)$$

where:

A_s = total longitudinal steel in x-section

f_y = steel yield strength

ϕ_s = resistance factor for concrete

d = distance from extreme compression fibre to centroid of tensile reinforcement

a = depth of equivalent rectangular stress block

When longitudinal reinforcement is exposed, and development is compromised, the modified moment capacity becomes, M_r',

$$M_r' = A_s' \phi_s f_y (d - \frac{a}{2}) \quad (3.8)$$

where:

A'_s = is the total modified longitudinal steel in the cross-section

To illustrate this concept, a single bar is considered. The moment capacity along the bar is shown in Figure 3-11. Once spalling occurs, if the spalled region is within l_d the capacity plateaus and is reduced at locations outside l_d. The concept is easily extended to include all the bars in the cross section, in order to determine a total capacity at a given location along the member, as will be seen in Chapter 4.

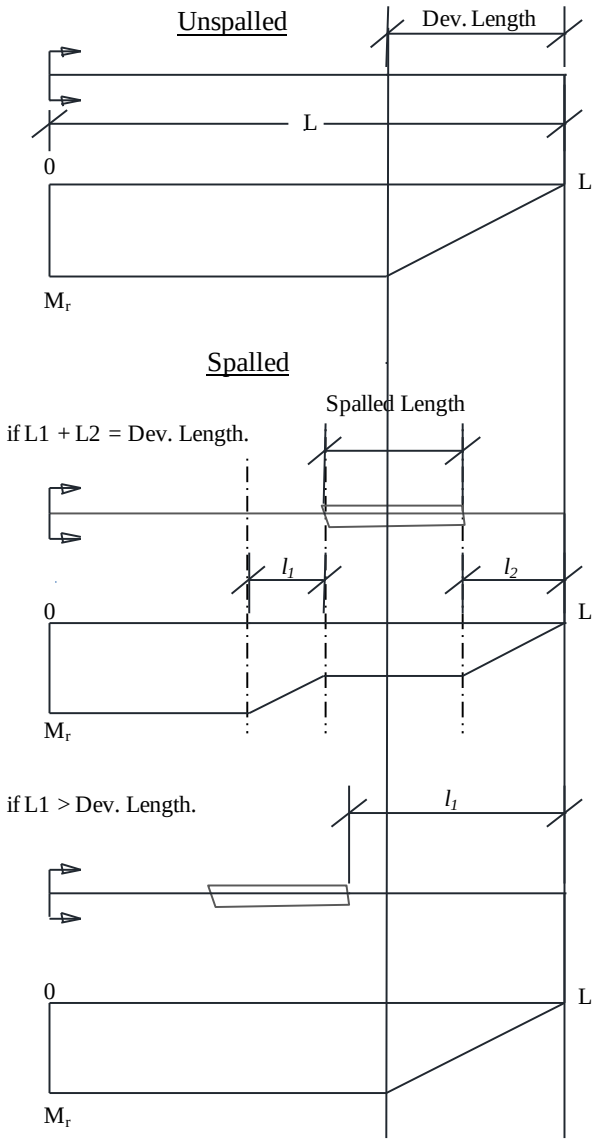

Figure 3-11: Moment resistance of unspalled and spalled bars.

3.5 Modified Shear Resistance

Exposing longitudinal reinforcement (spalling), also has an adverse effect on the shear capacity of a reinforced concrete member, if the development of longitudinal reinforcement is compromised. Although longitudinal reinforcing is primarily specified for moment and axial loads, the shear force on an inclined shear crack has both vertical and horizontal components as shown in Figure 3-12. The horizontal component must be resisted by the longitudinal reinforcement, and subsequently the longitudinal reinforcement anchorage.

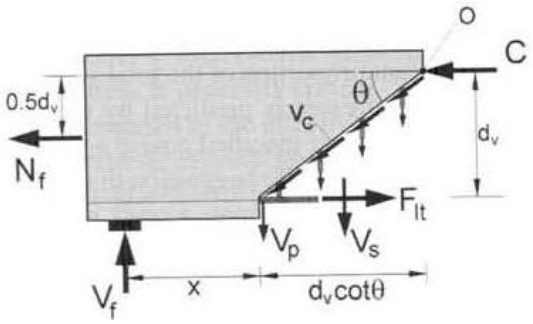

Figure 3-12: Basic shear resisting mechanism assumed by Bentz (2006).

The proposed approach for shear assessment assumes that:

- stirrups (transverse reinforcing) are undeteriorated with no loss in strength due to corrosion, and
- the interaction between longitudinal and transverse reinforcement is uncompromised.

The following sections first introduce the CAN/CSA A23.3-04 shear design provisions in 3.5.1 and then recommend two methods for determining the shear capacity of a spalled girder analogous with the CAN/CSA A23.3-04 “simplified” and “general” methods (Cl. 3.5.2 and 3.5.3).

3.5.1 CSA Shear Capacity

Canadian design codes allow designers to use either of two methods for computing the shear capacity of a reinforced concrete member. In both cases, the shear resistance is a combination of contributions from both the concrete and steel, as defined below:

S6-06, Cl. 8.9.3.4 $$V_c = 2.5\beta f_{cr} b_v d_v \quad (3.9)$$

S6-06, Cl. 8.9.3.5 $$V_s = \frac{\phi_s A_v f_y d_v \cot\theta}{s} \quad (3.10)$$

S6-06, Cl. 8.9.3.3 $$V_r = V_c + V_s \quad (3.11)$$

The General Method, is based on the modified compression field theory. Canadian standards provide simple formulae for computing the size and strain effects that contribute to the computation of V_c and V_s . The parameter characterizing aggregate interlocking on cracked concrete, β , is defined as:

A23.3, Cl. 11.3.6.4 $$\beta = \frac{0.40}{(1+1500\varepsilon_x)} \frac{1300}{(1000+S_{ZE})} \quad (3.12)$$

The strain effect is characterized by the average longitudinal strain in a member at mid-depth, which can be estimated according to the following relationship:

A23.3, Cl. 11.3.6.4 $$\varepsilon_x = \frac{\frac{M_f}{d_v} + V_f}{2E_s A_s} \quad (3.13)$$

The angle of inclination of the diagonal compressive stress is based on the strain effect as follows:

A23.3, Cl. 11.3.6.4 $$\theta = 29 + 7000\varepsilon_x \quad (3.14)$$

Design codes are structured for easy design and as a result the method becomes iterative for evaluation. As an alternative, the code also provides a Simplified Method. This method treats the mid-depth strain as constrained. If the yield strain for steel is 0.002, any mid-depth strains greater than half of 0.002 would result in flexural failure. Therefore, the mid-depth strain should be less than 0.001. The Simplified Method considers the upper bound to be:

S6-06, Cl. 8.9.3.6 $\varepsilon_x = 0.8\times10^{-3}$

A23.3, Cl. 8.9.3.6 $\varepsilon_x = 0.85\times10^{-3}$

If these are applied to Equation 3.14 and Equation 3.12 then:

S6-06, Cl. 8.9.3.6 $\theta = 42°$

S6-06, Cl. 8.9.3.6 $\beta = 0.18$

The method is both simple and conservative. For the evaluation of a spalled concrete girder, two methods have been derived analogous to the CSA A23.3 Simplified and General methods.

3.5.2 Modified Shear Capacity based on CSA Simplified Method

Theoretically, for both the deteriorated and undeteriorated cases, a first assumption can be made that the applied load effects and material properties do not change as the result of spalling. To consider spalling, the modified area concept can also be applied for the shear verification. If we consider the change in mid–depth strain due to bond loss, ε_x can be modified to ε_x' for the spalled case as follows:

$$\frac{\varepsilon_x'}{\varepsilon_x} = \frac{\left[\dfrac{\dfrac{M_f}{d_v} + V_f}{2E_s A_s'}\right]}{\left[\dfrac{\dfrac{M_f}{d_v} + V_f}{2E_s A_s}\right]} = \frac{A_s}{A_s'}$$

$$\varepsilon_x' = \frac{A_s}{A_s'}\varepsilon_x \tag{3.15}$$

Given the Simplified Method assumption that $\varepsilon_x = 0.8\times10^{-3}$, ε_x' can be computed based on the modified bar area.

Substituted ε_x' into Equation 3.12 and Equation 3.14, a spalled β' and θ' can be determined as follows:

$$\beta' = \left(\frac{0.4}{1+1500\varepsilon_x'}\right)\left(\frac{1300}{1000+S_{ze}}\right) \tag{3.16}$$

$$\theta' = 29 + 7000\varepsilon_x' \tag{3.17}$$

Similarly, a spalled V_c', V_s', and V_r' can be computed for the section. Numerically *cot* θ becomes negative as ε_x become large. To solve this problem, the upper bound of $\varepsilon_x = 3.0\times10^{-3}$ defined by CSA A23.3 Cl. 11.3.6.4 (f) is imposed as the maximum permissible value of ε_x'. This limit should be obeyed in the computation of a spalled shear capacity.

This method maintains the conservative nature of the Simplified Method and therefore a more refined method may be needed if the structure is insufficient according to the

Simplified Method. Section 3.5.3 discusses the development of a General Method for evaluation.

3.5.3 Modified Shear Capacity based on CSA General Method

The direct application of the General Method for the case study structure is not a straight forward task. Since the structure is statically indeterminate and subject to a moving (vehicular) load, at a given section along the span of the structure, factored moment and shear (M_f and V_f) combinations need to be checked for each position of the code truck along the span. In general, the code truck positions that cause the maximum values of M_f and V_f will not be the same. The computation of ε_x for the application of the General Method at each section along the structure subject to a large number of load effect combinations (i.e. for each truck position) can thus be a very time-consuming task. As a simple approximation, the largest absolute factored moment and shear may be combined to determine ε_x for the purpose of calculating the shear resistance. That is, although the worst case moment and shear may not coincide with the same truck position, using a combination of the two extreme values will result in a conservative assessment. The maximum shear and moment for each position along the structure can be taken from the moving load envelopes shown previously in Figure 3.6 and 3.7.

Once the factored moment and shear values are selected, they can be used to calculate the mid-depth strain as follows:

$$\varepsilon_x' = \frac{\left|\frac{M_f}{d_v}\right| + \left|V_f\right|}{2E_s A_s'} \tag{3.18}$$

To determine the resistance, Equations 3.16 and 3.17 can be used along with the modified area concept. Chapter 4 discusses the application of this concept in a computer program and presents the assessment results when applied to the case study structure.

3.6 Reliability Analysis

Even though significant reductions in strength may occur when a structural component is subject to deterioration, the structural performance of the component may still be adequate. This section provides an approximate means for estimating the remaining reliability of deteriorating structural components and full bridge structures deterministically. First, the reliability index concept is introduced and its application to bridge evaluation according to CAN/CSA S6-06 is described. Based on this concept of structural evaluation, an approximate reliability method is proposed to determine the reliability index for each individual girder. Following this, the concept is expanded to allow the estimation of a reliability index for the entire structure.

3.6.1 CSA Target Reliability Index

The philosophy behind structural evaluation according to CAN/CSA S6-06 is to maintain a consistent level of risk of loss of human life for each structural element of a bridge. However, structures that experience regular inspection, show warning before failure, and can redistribute loads to other elements, have a reduced probability of loss of life in the event of failure compared to those that do not exhibit these traits. A consistent level of risk is maintained by a combination of the probability and consequence of failure as shown in Figure 3-13 (Figure C14.1 in CAN/CSA S6-06).

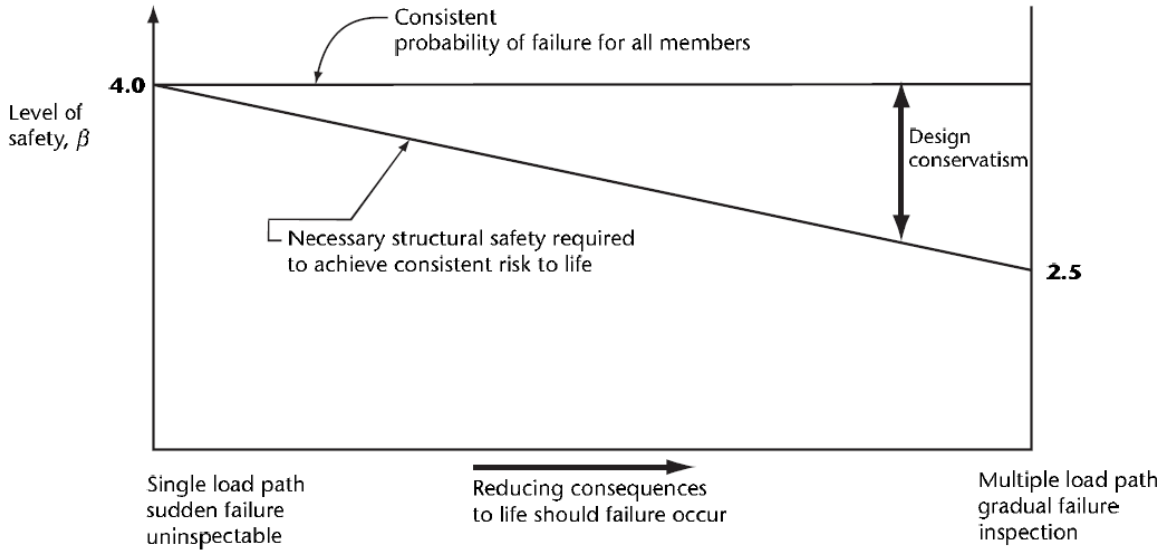

Figure 3-13: Relationship between risk and reliability (CAN/CSA S6-06).

CAN/CSA S6-06 bridge evaluation categorizes the target reliability index based on the system and element behaviour and the level of inspection. Each are described below.

Table 3.1: System behaviour (CAN/CSA S6-06).

Category	Description
S1	Element failure leads to total collapse.
S2	Element failure probably will not lead to total collapse.
S3	Element failure leads to local failure only.

Table 3.2: Element behaviour (CAN/CSA S6-06).

Category	Description
E1	Element being considered is subject to sudden loss of capacity with little or no warning.
E2	Element being considered is subject to sudden failure with little or no warning but will retain post-failure capacity.
E3	Element being considered is subject to gradual failure with warning of probable failure.

Table 3.3: Inspection level (CAN/CSA S6-06).

Category	Description
INSP1	Component is not inspectable.
INSP2	Inspection is to the satisfaction of the evaluator, with the results of each inspection recorded and available to the evaluator.
INSP3	The evaluator has directed the inspection of all critical and substandard components and final evaluation calculations account for all information obtained during this inspection.

Based on this categorization, the target reliability index can be calculated between 2.5 and 4 for normal traffic loading using Table 3.4.

Table 3.4: Target reliability index, β, for normal traffic and for PA, PB, and PS traffic (CAN/CSA S6-06).

System behaviour	Element behaviour category	Inspection level		
		INSP1	INSP2	INSP3
S1	E1	4.00	3.75	3.75
	E2	3.75	3.50	3.25
	E3	3.50	3.25	3.00
S2	E1	3.75	3.50	3.50
	E2	3.50	3.25	3.00
	E3	3.25	3.00	2.75
S3	E1	3.50	3.25	3.25
	E2	3.25	3.00	2.75
	E3	3.00	2.75	2.50

For the case study structure, the factors were selected based on engineering judgment as shown and discussed in Table 3.5.

Table 3.5: Reliability index factors for the case study structure.

Component	Category	Discussion
Traffic	Normal	Traffic designated as *Normal*.
System Behaviour	S2	The strength of the slab indicates that element failure *probably will not lead to total collapse*.
Element Behaviour	E1	Anchorage failure is sudden without warning or post-failure capacity.
Inspection Level	INSP2	Inspection conditions are satisfactory but not ideal.

On this basis, a target reliability index of 3.5 was selected from Table 3.4 for this structure.

3.6.2 CSA Reliability Evaluation

CAN/CSA S6-06 specifies modified load factors for the evaluation of existing structures at any given target reliability index. The load factors are separated for the live load and dead load components, which are defined in Table 3.6.

Table 3.6: Dead load components for evaluation (CAN/CSA S6-06).

Category	Description
D1	Dead load of factory-produced components and cast-in-place concrete, excluding decks.
D2	Cast-in-place concrete decks, wood, field-measured bituminous surfacing, and non-structural components.
D3	Bituminous surfacing where the nominal thickness is assumed to be 90mm for the evaluation.

Table 3.7 and Table 3.8 provide load factors to be used for evaluation based on the desired reliability index.

Table 3.7: Maximum dead load factors, α_D (CAN/CSA S6-06).

	Target reliability index, β								
Dead load category	**2.00**	**2.25**	**2.50**	**2.75**	**3.00**	**3.25**	**3.50**	**3.75**	**4.00**
D1	1.03	1.04	1.05	1.06	1.07	1.08	1.09	1.10	1.11
D2	2.06	1.08	1.10	1.12	1.14	1.16	1.18	1.20	1.22
D3	1.15	1.20	1.25	1.30	1.35	1.40	1.45	1.50	1.55

Table 3.8: Live load factors, α_L, for normal traffic (evaluation levels 1, 2, and 3) for all types of analysis (CAN/CSA S6-06).

	Target reliability index, β						
Spans	**2.50**	**2.75**	**3.00**	**3.25**	**3.50**	**3.75**	**4.00**
All Spans	1.35	1.42	1.49	1.56	1.63	1.70	1.77

Graphically, the relationships between the target reliability index and the various load factors are shown in Figure 3-14.

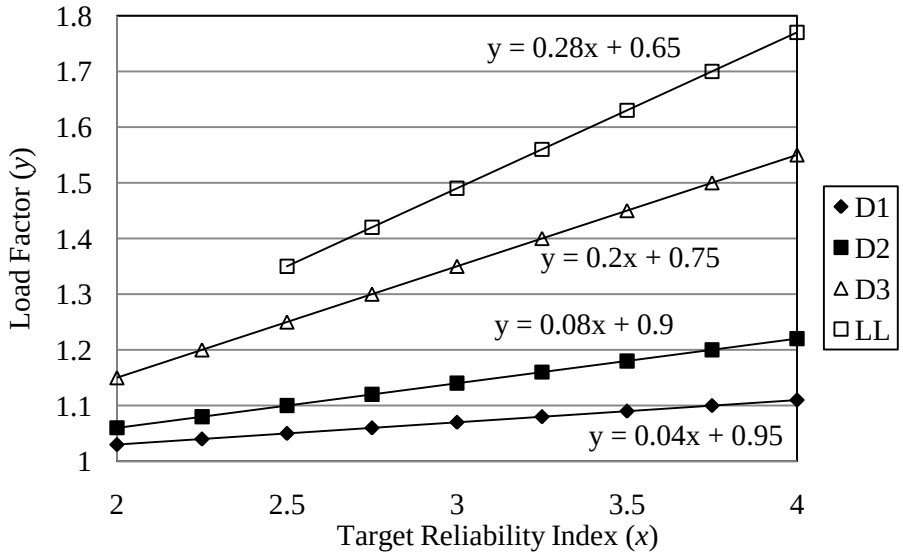

Figure 3-14: Load factors for various target reliability indices.

The case study structure has only D1, D2 and LL components. The lines can be represented by the following formulas:

For the girders: $$\alpha_{D1} = 0.04\beta + 0.95 \quad (3.19)$$

For the slab: $$\alpha_{D2} = 0.08\beta + 0.9 \quad (3.20)$$

For the live load: $$\alpha_{LL} = 0.28\beta + 0.65 \quad (3.21)$$

3.6.3 Reliability of Deteriorated Bridge

For a deteriorated structure, the reliability index is a function of the difference between the remaining capacity and the solicitation. For the reliability analysis of the deteriorated bridge, the reliability index was set as the unknown and the procedure was reversed. Once the reliability index is determined, it can be evaluated against the target indices provided in above to evaluate structural adequacy.

For the case study structure, the total load effect consists of dead and live components:

$$S = S_{D1} + S_{D2} + S_{LL}$$

The factored relationship is:

$$S_f = S(\alpha_T) = S_{D1}(\alpha_D) + S_{D2}(\alpha_D) + S_{LL}(\alpha_L)$$

where α_T is the difference between the spalled resistence, R', and the applied load, *S*, i.e.:

$$\alpha_T = \frac{R'}{S}$$

$$\frac{R'}{S} S = S_{D1}(\alpha_{D1}) + S_{D2}(\alpha_{D2}) + S_{LL}(\alpha_L)$$

Substituting equations 3-19, 3-20 and 3-21:

$$R' = S_{D1}(0.04\beta + 0.95) + S_{D2}(0.08\beta + 0.9) + S_{LL}(0.28\beta + 0.65)$$

Re-arranging for β:

$$\beta = \frac{R' - (0.95)S_{D1} + (0.9)S_{D2} + (0.65)S_{LL}}{(0.04)S_{D1} + (0.08)S_{D2} + (0.28)S_{LL}} \tag{3.22}$$

For moment and shear the relationships becomes:

$$\beta_M = \frac{M_r' - (0.95)M_{D1} + (0.9)M_{D2} + (0.65)M_{LL}}{(0.04)M_{D1} + (0.08)M_{D2} + (0.28)M_{LL}} \tag{3.23}$$

$$\beta_V = \frac{V_r' - (0.95)V_{D1} + (0.9)V_{D2} + (0.65)V_{LL}}{(0.04)V_{D1} + (0.08)V_{D2} + (0.28)V_{LL}} \quad (3.24)$$

At any location along the span, the reliability index is a function of the deteriorated resistance and the solicitation. The reliability index can be evaluated against those proposed by the analysis discussed in Section 3.6.1. This analysis assumes that the uncertainties in the development lengths and material strengths are the same for both design and assessment. In reality, the concrete strength associated with the girder soffit is highly uncertain and even more-so than new concrete. Therefore, a more refined reliability analysis taking these uncertainties into account explicitly is required. Such an analysis has been conducted within the scope of the project and is presented in Chapter 6.

3.6.4 Full Bridge Reliability

The reliability index determined in Section 3.6.3 only applies to the structural element being assessed (i.e. the girder) – not the structure as a whole. Although, assuming the failure of one girder will cause the failure of the whole structure is conservative, it may be an oversimplification. Therefore, it may be desirable to consider the beneficial effects of redundancy in multi-girder bridges. Various methods can be adopted for this purpose. Finite element analysis (FEA) studies of damaged structures may be carried out, for example, to determine the effect of losing a single girder on the overall capacity of the structure. Herein, it is proposed that the effect of system behaviour of the multi-girder structure can be considered using a relatively simple approach, wherein the two adjacent girders are assumed to carry the tributary load acting on all three girders, when a single girder fails.

In using this approach, it is implicitly assumed that the slab's strength is sufficient to distribute a single truck axle load transversely between the two intact girders (see Figure 3-16). For the case study structure, the slab strength is confirmed in Appendix A-8 using simple design checks.

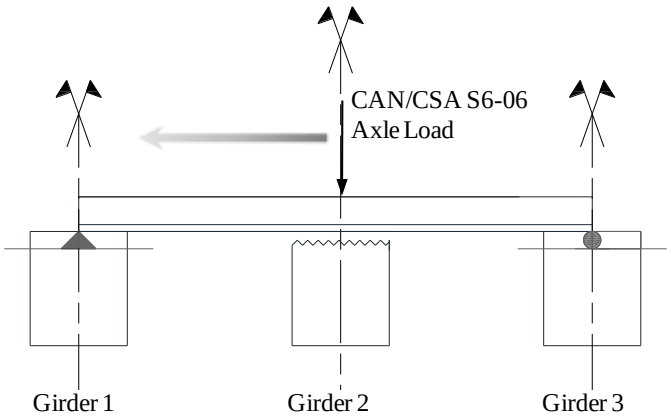

Figure 3-15: Slab strength evaluation.

A simplified reliability estimate for the whole bridge may consist of a comparison between the sum of the resistances of all the girders and the total applied load. This approach does not, however, consider the transverse distribution of the damage and load transfer. A more refined approximation would involve evaluating the reliability index for groups of adjacent girders. Such an analysis is performed herein for sets of three girders analyzed using the same method proposed in Section 3.6.3, i.e.:

$$\beta = \frac{\sum_{i=1}^{3}\left[M_{ri}^{'} - (0.95)M_{D1i} + (0.9)M_{D2i} + (0.65)M_{LLi}\right]}{\sum_{i=1}^{3}\left[(0.04)M_{D1i} + (0.08)M_{D2i} + (0.28)M_{LLi}\right]} \tag{3.25}$$

If the analysis is conducted for girders grouped in three, it can be repeated, moving across the width of the structure as shown in Figure 3-16. The analysis should be continued until the other side is reached. The reliability index for the whole structure is then taken as the minimum index of all the sets. This is analogous to modelling the structure as a series system with a high level of correlation between the performances of each of the components in the system. This correlation assumption is thought to be reasonable, given that all of the girders are subjected to similar traffic loads and environmental conditions and were all fabricated at the same time by the same contractor.

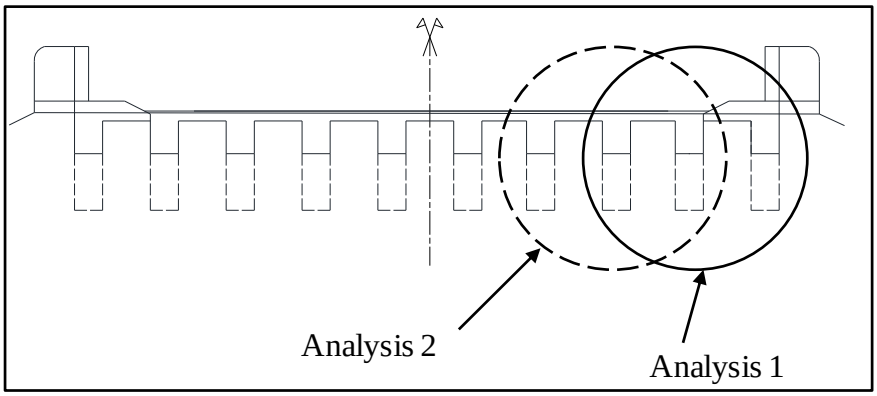

Figure 3-16: Girder grouping for full structure analysis.

Chapter 4

Deterministic Analysis and Results

4.1 Introduction

The concept presented in Chapter 3 is best applied at multiple locations along the length of a girder to evaluate the member's residual capacity. Both load effects, and resistance, clearly vary along the length of a member. Geometric variations such as girder arching may also vary significantly contributing to the flexural and shear capacities along the length of a girder. In addition, a full scale structure generally requires reinforcement splices along its length. An accurate model, such as that proposed in Chapter 3, considers strength variations that occur as bars terminate with butt or staggered lap splices. A program is developed in Matlab (2010) to conduct a multi-point analysis that considers strength and deterioration variations to assess the capacity incrementally along each girder and ultimately the entire bridge structure. In Section 4.2 the program was applied to a single girder to evaluate its moment and shear capacities and reliability index. Next, Section 4.3 expands the program for a multi-girder or full-bridge analysis. The program is then used to perform two short sensitivity studies (Section 4.4). Finally, the code is expanded to consider section loss and bond deterioration. The complete full bridge analysis program developed in this chapter has been named BEST (Bridge Evaluation Strength Tool).

4.2 Single Girder Matlab Program

The modified area concept can easily be adapted to computer programming. The program developed herein allows the user to evaluate the resistance of a single girder at a specified number of points along its length. The program was developed in three steps corresponding with: modified area, moment resistance and shear resistance computation.

4.2.1 Modified Area

To calculate the modified area, as discussed in Section 3.3.2, the algorithm described in Figure 4-1 was followed.

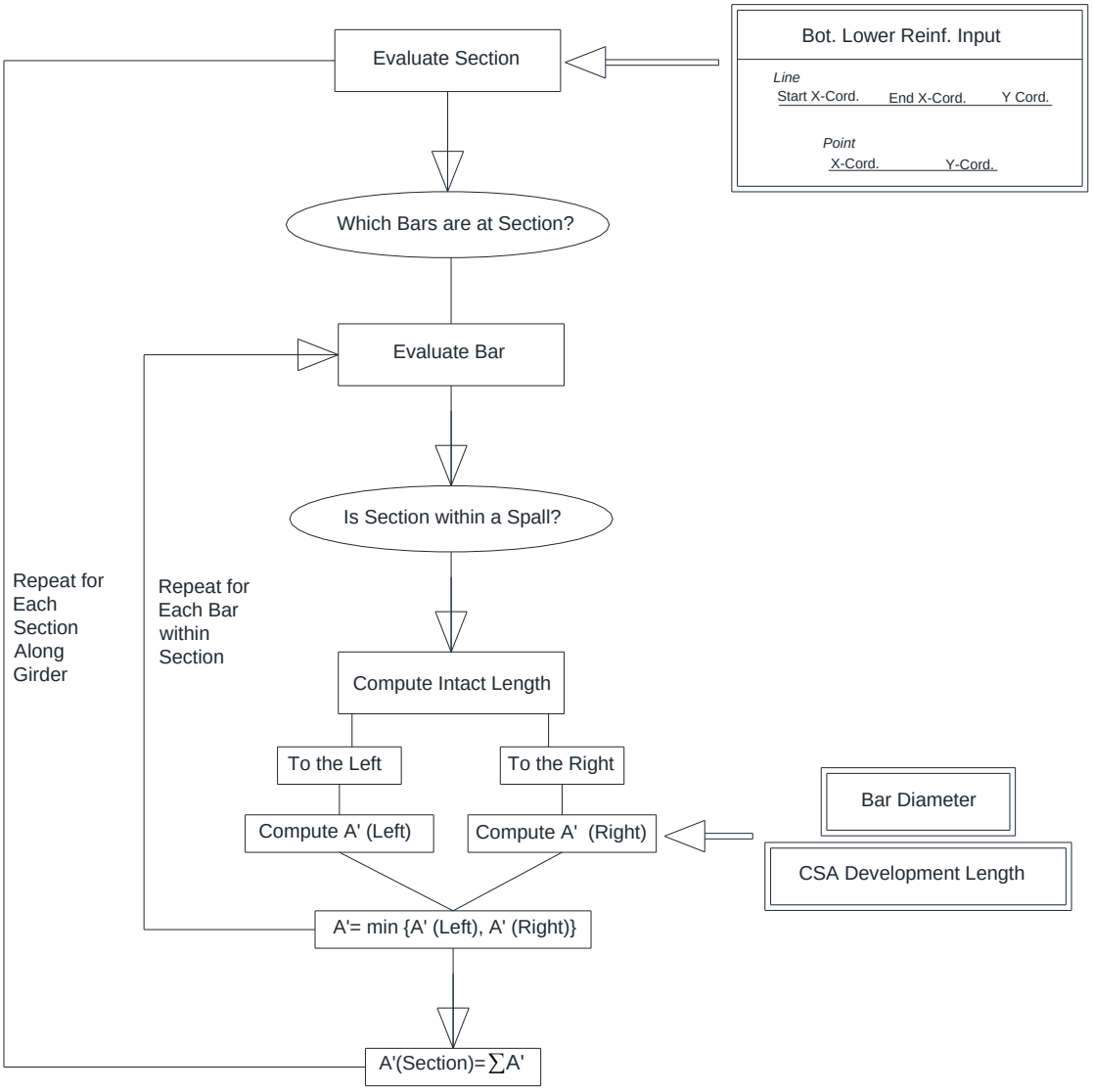

Figure 4-1: Algorithm for the computation of the modified area.

First, a single section is considered. Each bar within that section is evaluated to its left and right to determine if its remaining intact length is sufficient for development. A modified area is computed for each case and the minimum is selected as the modified area for that bar. The total spalled area across the cross section is the sum of all of the bars in the section.

4.2.1.1 Input

The program uses line data to describe the reinforcement and point data to describe the spalling. Autocad (2010) was used to generate the data. The spalling/reinforcement superposition drawings from Appendix A-4 were uploaded and used for this purpose. Points were added at all locations where reinforcement intersects a spalled region as shown in Figure 4-2.

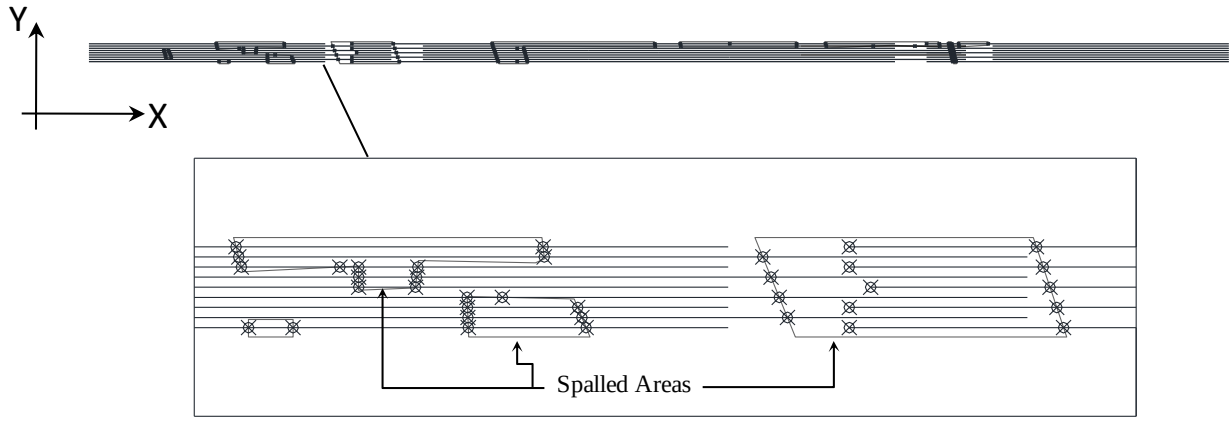

Figure 4-2: Reinforcement plan-spalling survey superposition for program input.

The Data Extraction function in Autocad (2010) was used to create text files with global point and line coordinates to characterize the spalling relative to the reinforcement. The reinforcement text file (Input File #1), shown in Appendix B-1, describes each rebar as a line with global *X* direction start and end coordinates and a single global *Y* coordinate. A second text file (Input File #2) is created by Autocad for point (spalling-reinforcement intersection) identification with *X* and *Y* coordinates. A sample is shown in Appendix B-2. The program works from the left since the global axes position themselves as such. It incrementally reads to the right, with the first point indicating the beginning of a spalled region. The spalled region ends at the next point. Points are also added at the left end of any rebar that starts within a spalled region. The required development length and the typical bar areas are also added as input in a separate input text file (Input File #3). A sample is featured in Appendix B-3.

4.2.1.2 Target formation

The program reads the input data within the Matlab directory and begins to rearrange it. Based on equivalent *Y* coordinates the program relates the spalling points with their associated reinforcing bar. Appendix B-5 shows the target formation for one section within the first segment of the program. This represents the useable form to which the data has been re-arranged. The target formation for a number of sections was checked with hand calculations at an early stage in the program development. From this arrangement, the minimum areas are next selected for each bar and the total modified and unmodified reinforcement areas computed for the section.

4.2.2 Moment Resistance

The program uses the modified areas to compute a modified moment resistance using the procedure described in Figure 4-3.

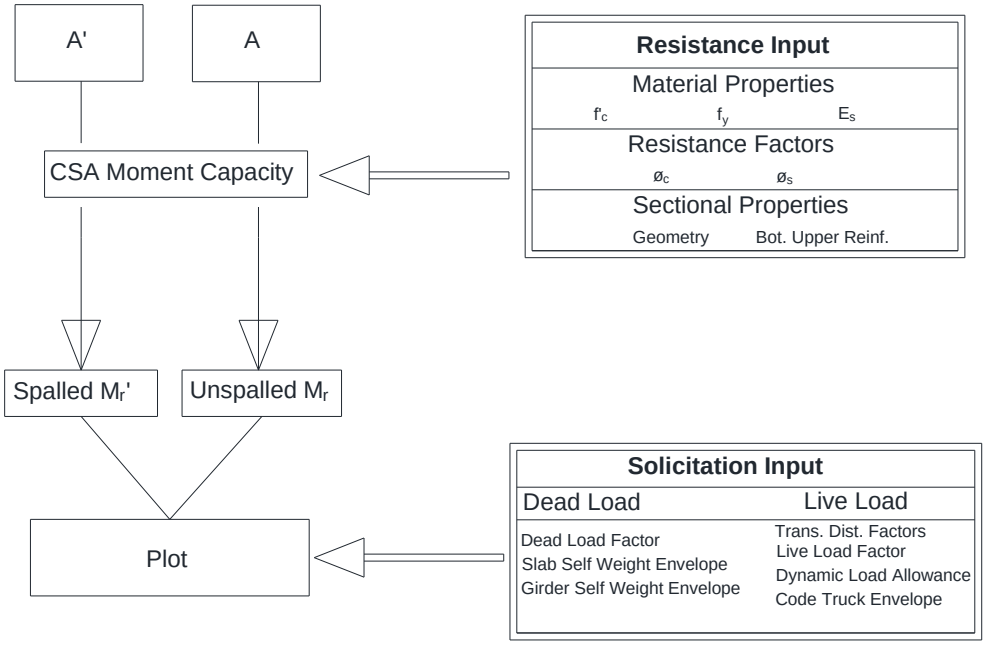

Figure 4-3: Algorithm for the computation of flexural capacity using the modified area concept.

Both spalled and unspalled moment resistance are found using the modified and unmodified bar areas. Moment capacities were determined using CAN/CSA A23.3-04 rectangular stress block theory. Bottom upper reinforcement was added (with no spalling effects considered) while top upper reinforcement was conservatively ignored. In its current state, the program is capable of analyzing T-beam as well as rectangular girder sections for flexure.

4.2.2.1 Program Input for Modified Moment Capacity

Input fields were separated into resistance (Input File #3) and solicitation (Input File #4) data files. Sample input files can be found in Appendix B-3 and Appendix B-4 respectively. Solicitation input consists of text files generated using the SAP program discussed in Section 3.2.4.1, copied to Input File #4. The dead loads, self weight of the slab and girder, and the live load truck envelopes are kept separate in the input and are simply combined arithmetically within the body of the program with the user specified transverse distribution factor, dynamic load allowance (DLA), and load factors.

4.2.2.2 Program Output for Modified Moment Capacity

The program generates plots to graphically describe the deteriorated moment resistance. Figure 4-4 shows the moment evaluation of Girder 2 in the case study structure (all girders are of the same design). In the figure, the origin corresponds with the north girder support. The south girder support corresponds to an X-coordinate of 1357 inches. In this analysis, the girder was divided into 300 sections along its length, represented by points on the X-axis of the plot.

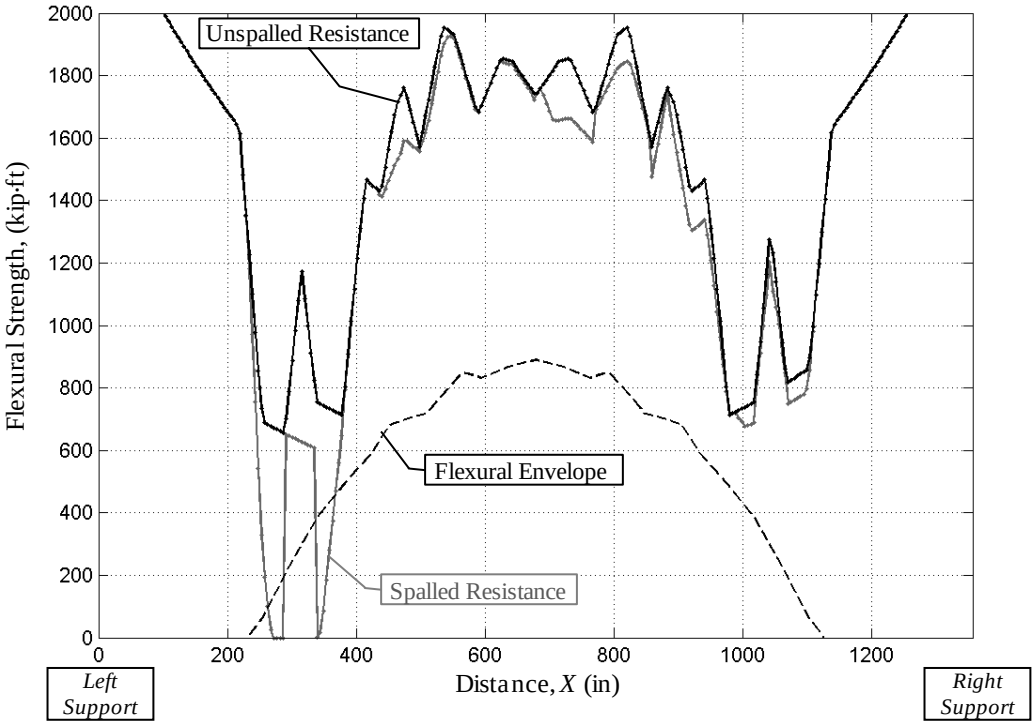

Figure 4-4: Flexural evaluation of Girder 2.

The dashed line indicates the envelope of the maximum moment due to the CL-625-ONT truck (CAN/CSA S6-06) located at any position along the bridge span. The remaining curves in this figure represent the factored unspalled and spalled moment resistances, as indicated. The curved shape of the both resistance curves is a result of the change in cross-section along the span (i.e. the girder arch). The impact that exposing longitudinal reinforcement has on the member's strength is clearly visible. It is immediately evident that spalling has the greatest effect on the strength of this girder near the general splice locations. Locations where the resistance drops below the moment envelope are obvious areas of concern.

4.2.3 Simplified Method Shear Resistance

Next, the shear assessment method based on the CSA Simplified Method, developed in Section 3.5.2, was added to the Matlab code to evaluate the girders residual shear capacity. The algorithm in Figure 4-5 was followed for the shear resistance computation based on this method.

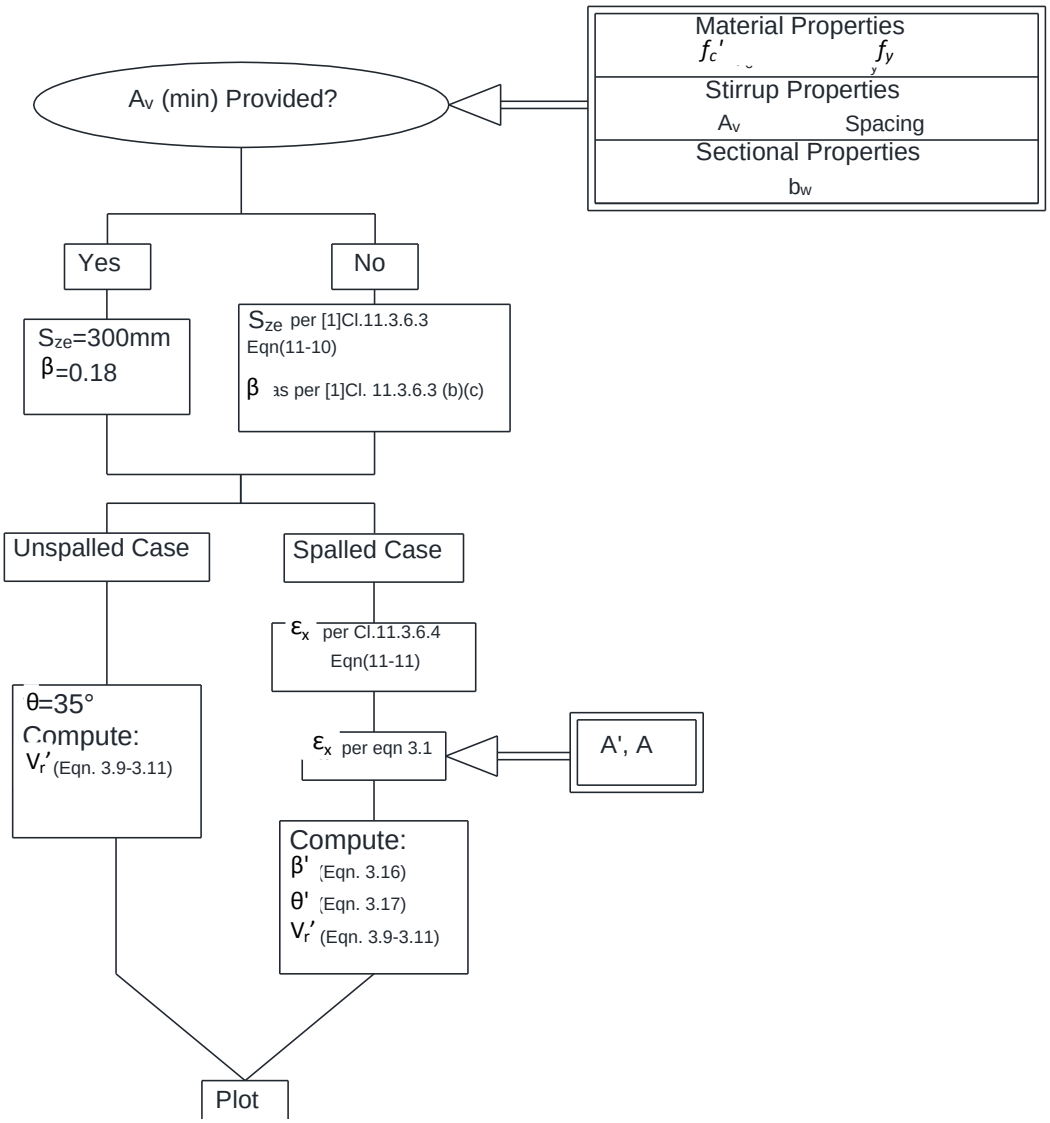

Figure 4-5: Algorithm for the computation of the shear capacity using the Simplified Shear Method.

4.2.3.1 Program Input for Simplified Shear Method

An input field was added to Input File #3 to allow the user to specify the stirrup spacing and any changes in this spacing along the length of the girder (Appendix B-3). For the case study structure, minimum stirrups (as per CAN/CSA A23.3-04) were only provided within the 12 inch stirrup spacing sections to a distance of 252" (6400 mm) from the face of each support. At the time of construction it is likely that provisions for minimum stirrups were not as

stringent. Therefore, the developed program is adapted to both cases - where minimum stirrups are provided and where they are not. To do this, the equivalent crack spacing parameter, S_{ze}, must be computed. This parameter depends on S_z, which is the lesser of d_v or the maximum distance between layers of bars. This requires the user to input both top and lower reinforcement details. The program, at this point, assumes that both the top upper and bottom lower bars continue along the full girder length. It then uses the user defined input of the bottom upper and top lower bars to compute S_z. The result is a slight approximation, however one that can be easily resolved with the improvement of the user interface.

4.2.3.2 Program Output for Simplified Shear Method

Like the moment resistance, the shear resistance is plotted along the length of the girder. The output for Girder 2 is shown in Figure 4-6.

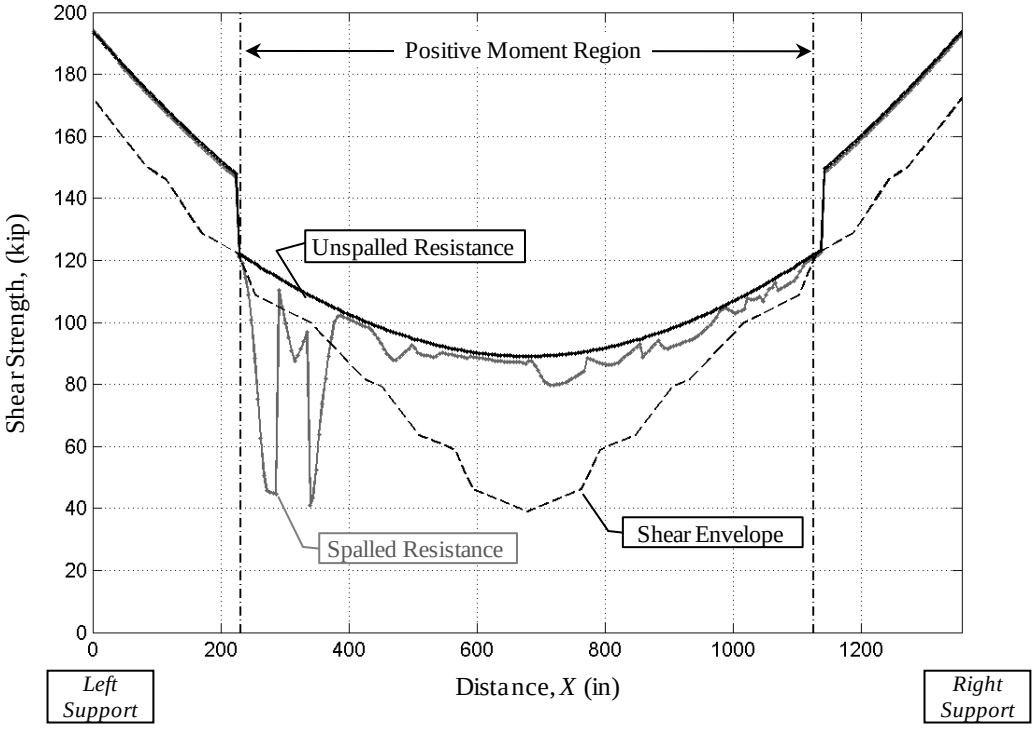

Figure 4-6: Shear evaluation of Girder 2: Simplified Method.

The dashed line represents the absolute factored shear envelope. In Figure 4-6, the plotted shear resistance has a curved shape, due to the arching of the concrete cross section. The

sudden jumps at 252” (6.4 m) and 1116” (28.35 m) from the left support represent changes in the stirrup spacing. Since the observed spalling is contained to the girder soffit, the shear resistance is only modified in the positive flexural zone (indicated on the plot), where the bottom reinforcement is in tension.

4.2.4 Shear Resistance General Method

The shear resistance General Method discussed in Section 3.5.3 was also added to the Matlab code. The algorithm in Figure 4-7 was followed for this method.

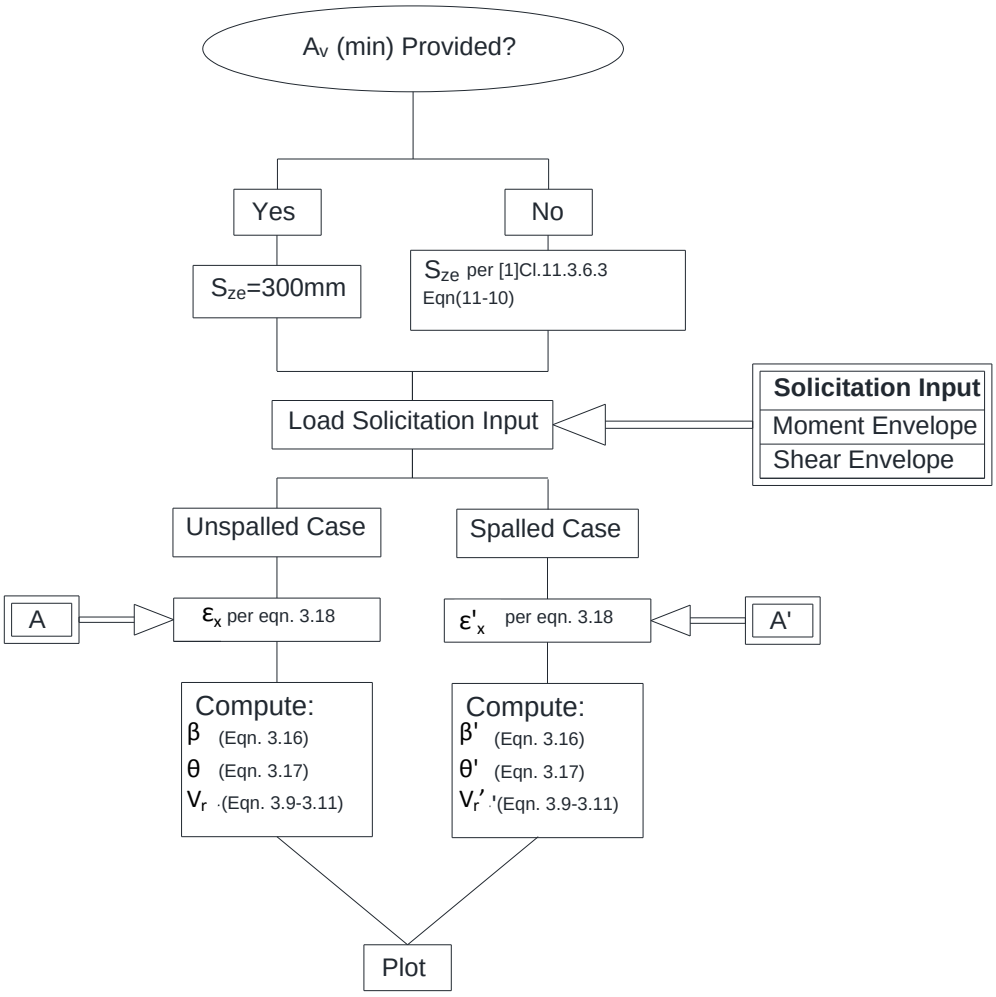

Figure 4-7: Algorithm for the computation of the shear capacity using the General Shear Method.

4.2.4.1 Program Input for General Shear Method

The proposed General Method employs envelopes of the solicitation data. The moment and shear envelopes are pre-determined within the code. The only adaption required is to adjust the data series to be coincident with the points being analyzed along the girder. Linear interpolation was used to approximate the moment and shear envelopes at each analysis point.

4.2.4.2 Program Output for General Shear Method

The shear analysis output is shown graphically in Figure 4-8, again, for Girder 2.

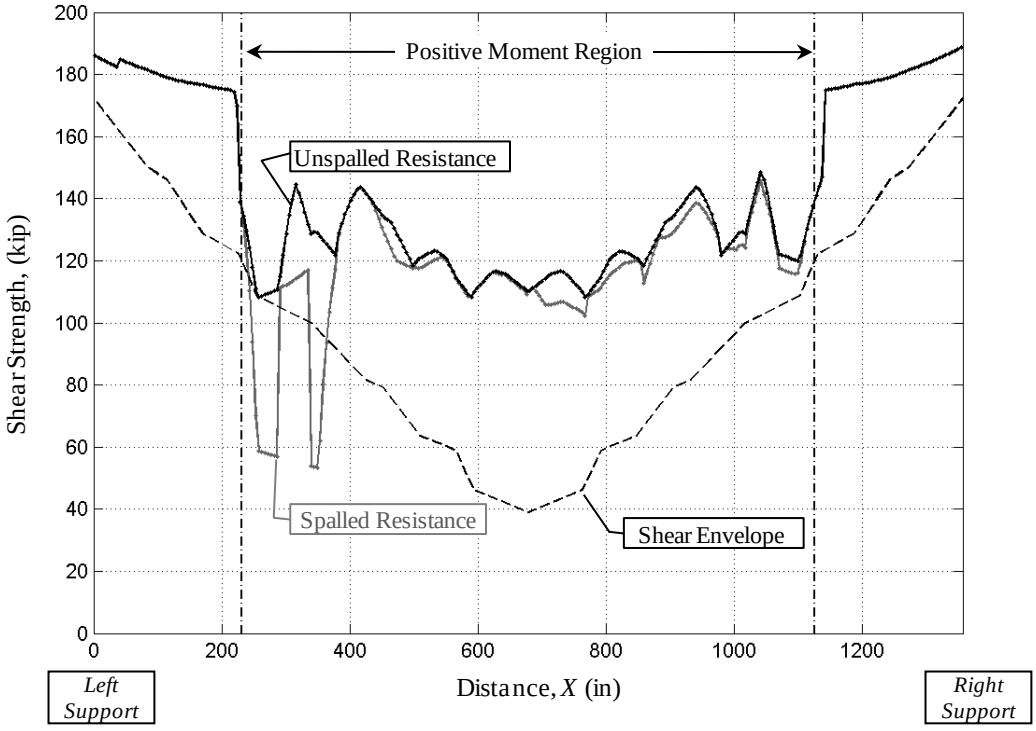

Figure 4-8: Shear evaluation of Girder 2: General Method.

In the computation of the strain at mid-height, ε_x, the modified longitudinal bar area is used and is subsequently responsible for the changes in the shape of the resistance plot. Sections where the shear resistance drops below the shear envelope are areas of particular concern from a structural safety standpoint.

To show more clearly the loss of strength with the exposure of longitudinal reinforcement along the girder, the ratio between the unspalled and spalled capacities for each method is generated and shown in Figure 4-9.

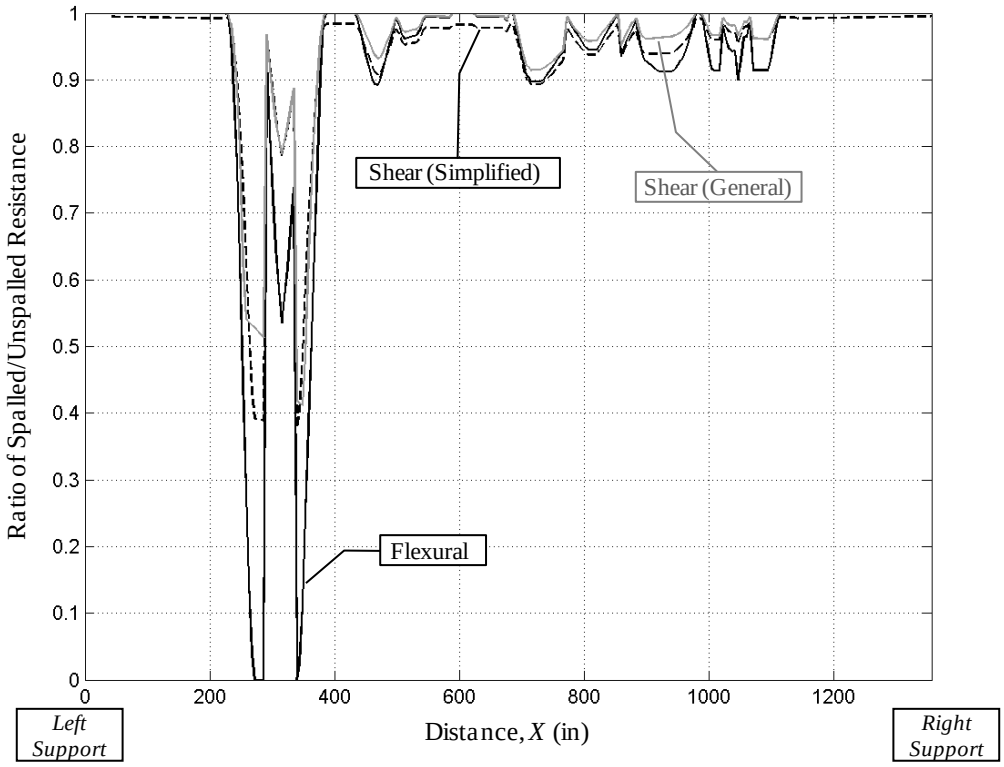

Figure 4-9: Effect of the loss of anchorage on Girder 2 of the case study structure.

If the bridge engineer is comfortable with the initial design, then Figure 4-9 simply and clearly indicates areas of concern and possible strengthening locations.

4.2.5 Reliability Index

The bridge reliability was determined using the method proposed in Section 3.6.3. No additional input was required for this analysis. For Girder 2, the reliability index for the spalled moment, and both shear methods was plotted as output shown in Figure 4-10.

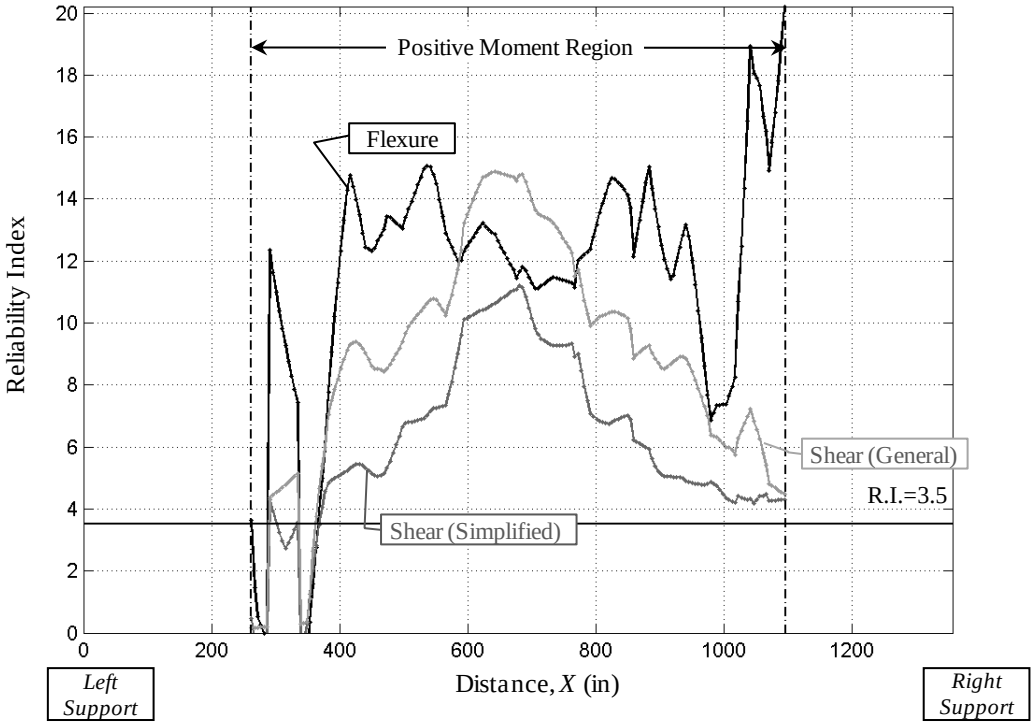

Figure 4-10: Approximate reliability index of Girder 2.

Since the examined deterioration only affects the positive moment region, this region is identified in Figure 4-10. The target reliability index, assumed to be 3.5, is also indicated in this figure. Any point along the girder where the calculated reliability index drops below 3.5 can be deemed as unsafe from a structural safety standpoint. The overall girder is unsafe if the target index at any point along the span does not exceed this limit.

4.3 Full Bridge Analysis Program

The analysis up to this point does not take advantage of structural redundancy. To account for this, the concept proposed in Section 3.6.4 was integrated into the Matlab code. The schematic in Figure 4-11 describes the additional computational framework required.

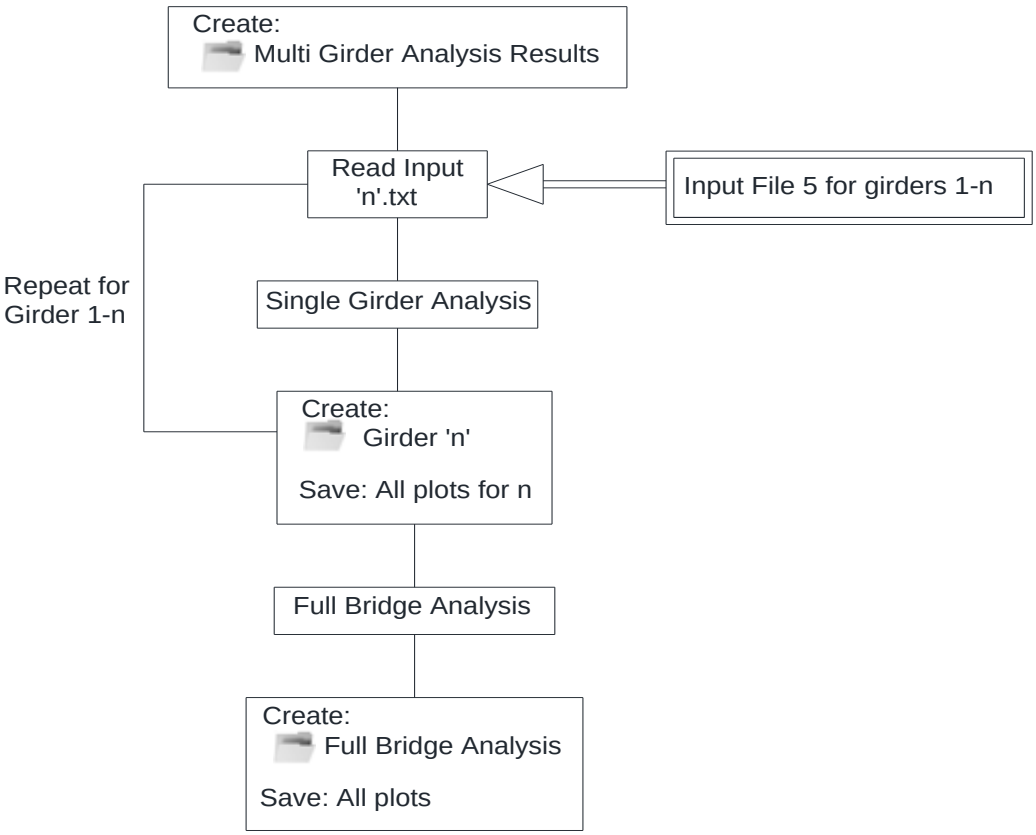

Figure 4-11: Algorithm and file organization for multi-girder analysis.

4.3.1.1 Full Bridge Analysis Input

For a multi-girder or full structure analysis, managing the input data is a complex task. The resistance and load input data remains the same as that for the single girder analysis but the deterioration data (point and line coordinate text files) must be compiled for every girder. To simplify the input, the point and line data for each girder was compiled into single text files named based on the girder number and placed within a Matlab directory. A sample input file can be found in Appendix B-6. As Matlab evaluates each girder, in order from Girder 1 to Girder n, it scans the directory for the associated text file, reads it, and completes the analysis.

4.3.1.2 Full Bridge Analysis Output

The organization of the output for a multi-girder analysis is also a complex task. To catalogue each of the girder results, a sub-directory for the multi-girder analysis results is created. Within this directory, folders are automatically created for all the girder plots during the program run sequence. Figure 4-11 explains the program output organization.

The multi girder program also generates plots for the entire bridge structure and catalogues them in the directory. The first plot is a combination of all moment resistance plots as shown in Figure 4-12.

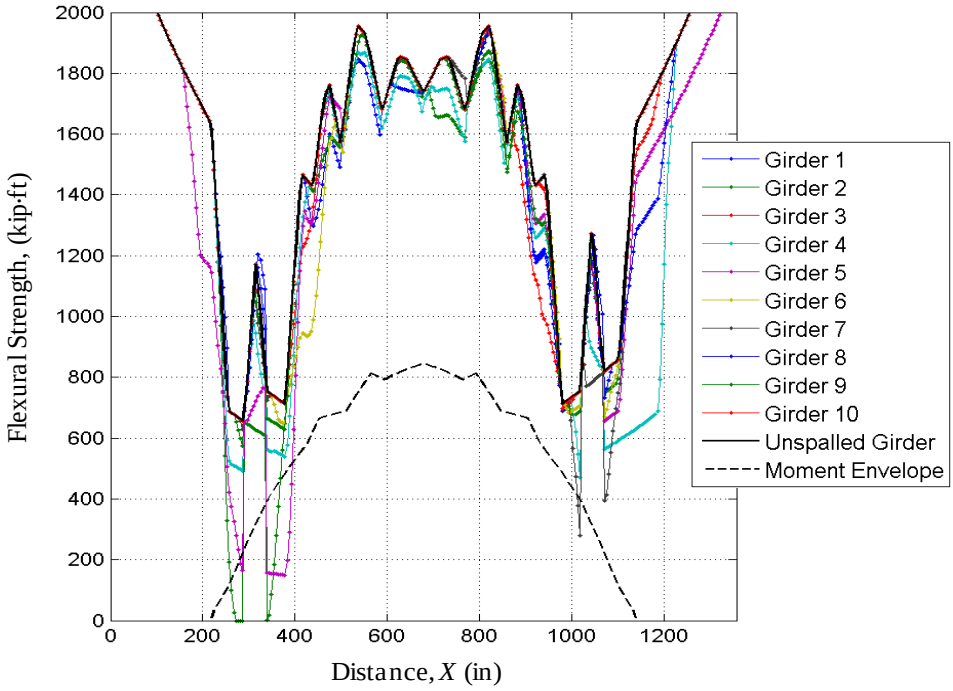

Figure 4-12: Spalled moment resistance for each girder in the bridge.

In this figure, the spalled moment resistance for each girder is plotted against the unspalled resistance and applied moment envelope. The minimum girder resistance can also be determined at each point, as shown for flexure and both shear methods in Figure 4-13. These plots describe the minimum girder resistance or an envelope of the weakest girder points and can be used as a quick check to determine if any girders in the entire bridge are insufficient and if further analysis is required.

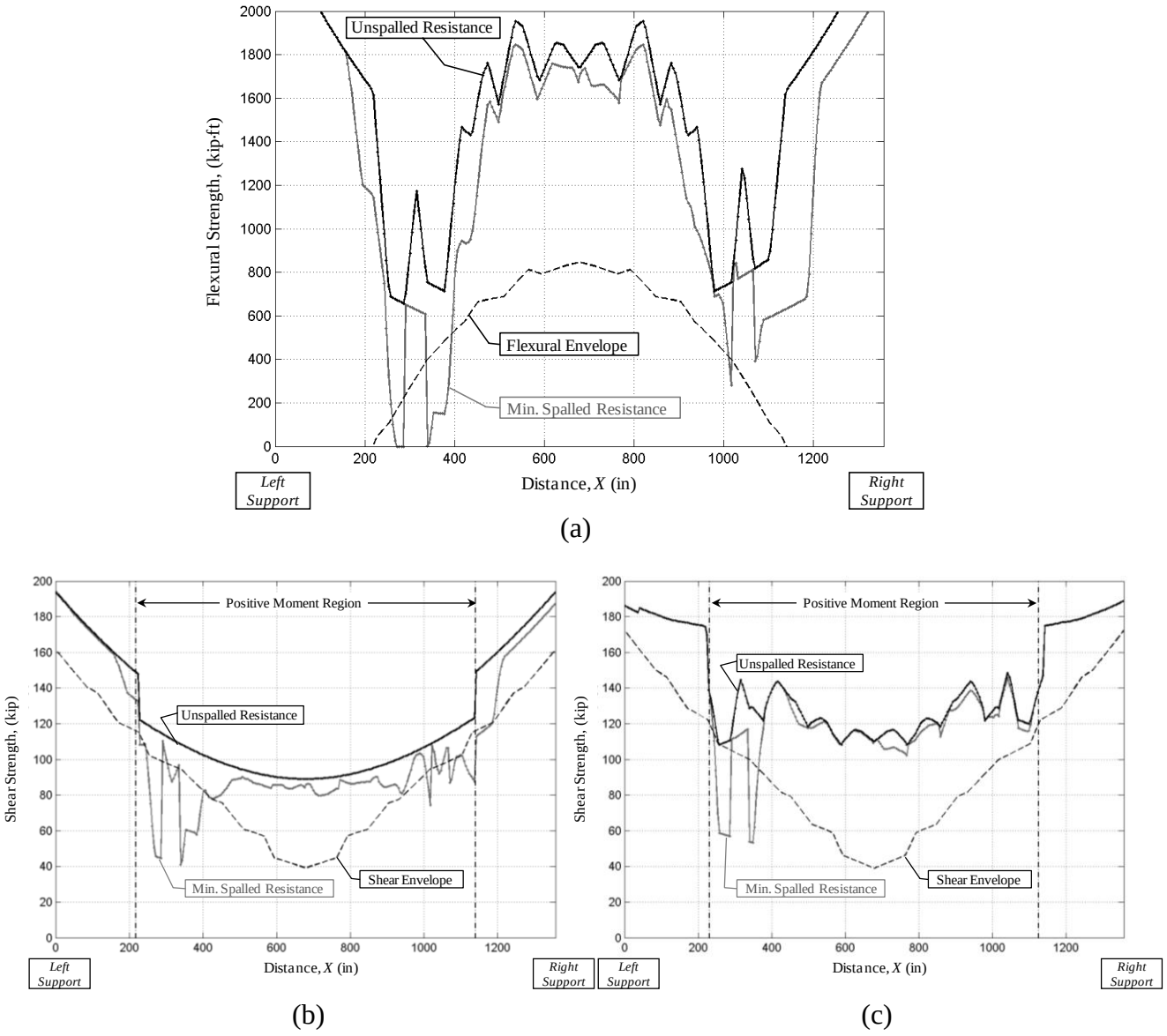

Figure 4-13: Minimum spalled girder resistance for (a) Flexure, (b) Simplified Shear and (c) General Shear Methods.

To consider structural redundancy, the method of girder groups proposed in Section 3.6.4 is applied. In Figure 4-14 the results of the full bridge analysis are plotted for the flexural, Simplified shear Method, and General shear Method verifications. Each curve represents the minimum factored resistance ratio (resistance ÷ load effect) at each point along the span of all groups of three (adjacent) girders analyzed. Although these curves still drop below 1.0 at

some locations along the span (indicating that the structure fails the verification at these locations), the benefits of considering system behaviour are apparent.

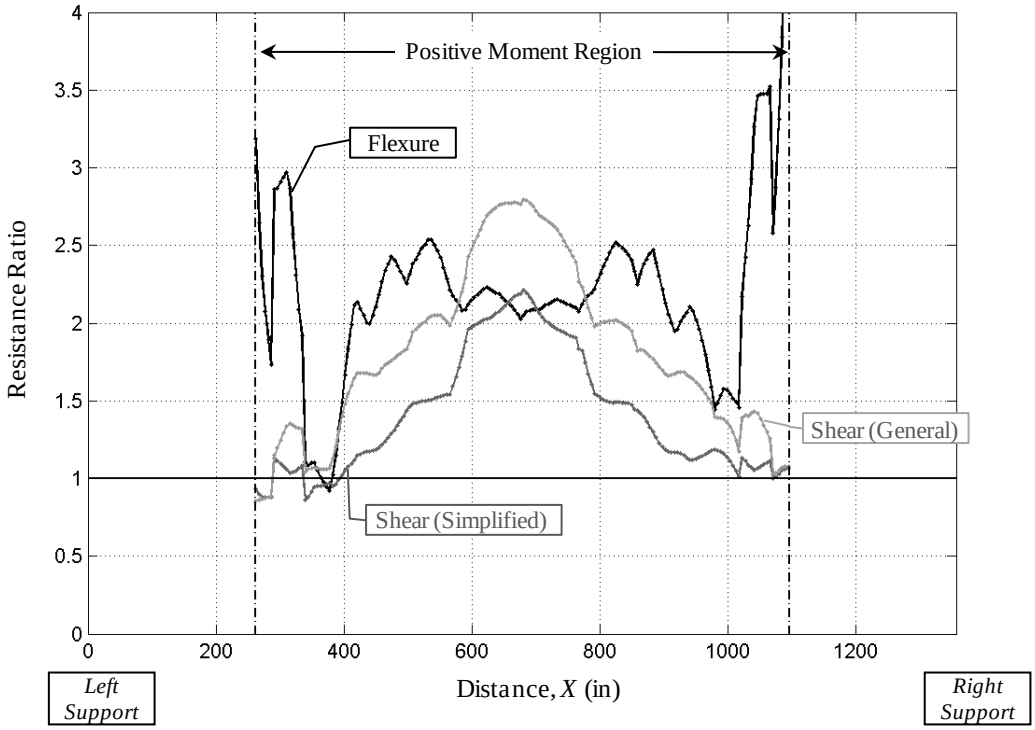

Figure 4-14: Full bridge case study structure analysis using girder grouping presented as resistance ratio.

Next the approximate reliability analysis concept presented in Section 3.6.4 was employed, and the reliability index for each set of three girders transversely across the structure was determined. Finally, the minimum reliability index for any group of three girders is found at each point and plotted as the full bridge reliability output as shown in Figure 4-15. The absolute minimum is taken as the reliability index for the whole structure.

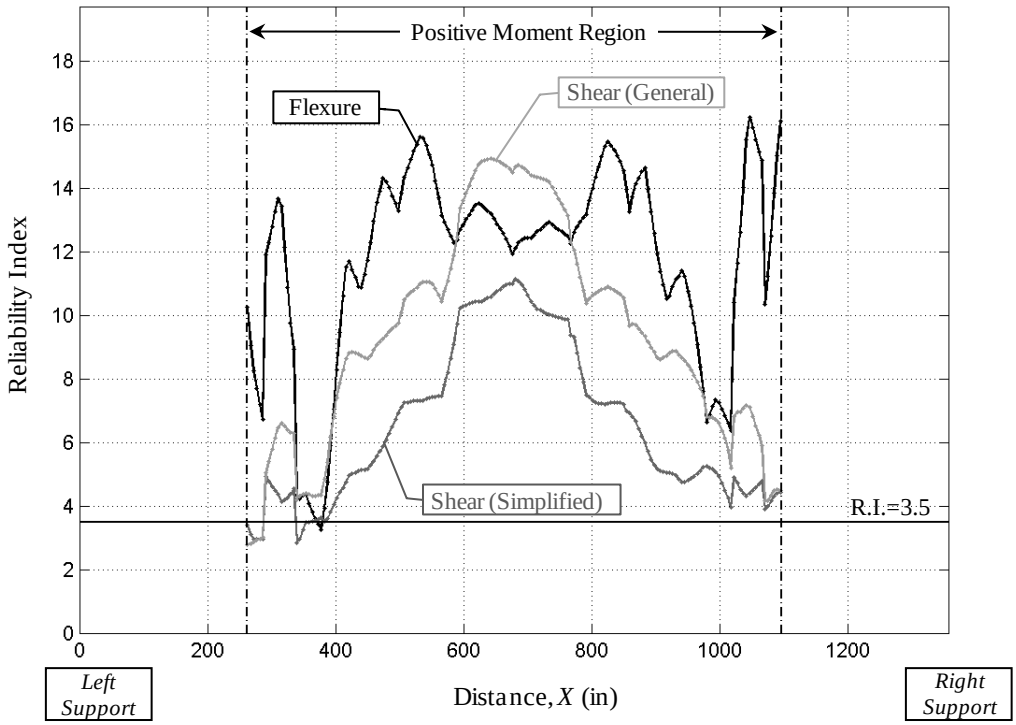

Figure 4-15: Full bridge approximate reliability.

This result shows that the structure does not meet the minimum target reliability index of 3.5. Analysing Figure 4-15, it can be seen that, for the examined case study structure, the resistance ratio and approximate reliability index produce relatively consistent results. The impact of load sharing is significant for the overall performance of the structure.

4.4 Sensitivity Analysis

The accuracy of the results presented in the previous section depends on the validity of the assumptions listed in Section 3.3. To understand the impact of development length and concrete strength adjacent to the reinforcement, two simple sensitivity studies were conducted.

4.4.1 Variation of f'c

The analysis results in Section 4.3 assume that there is no reduction in the concrete strength or development length (due to bond deterioration) in the unspalled regions of the girder

soffit. To better understand the effect of concrete strength loss due to corrosion and weakening of the concrete-steel bond in the intact sections, a sensitivity study was conducted. To do this, the concrete compressive strength for the calculation of the required development length was systematically varied. A loop was added to the multi-girder program that decreased the concrete compressive strength in increments of 2 MPa from the specified 20 to 0 MPa. The concrete strength for the compression block and flexural calculations remained unchanged.

4.4.1.1 Results of f'c Sensitivity Study

Since, at full concrete strength, the bridge is insufficient (See Figure 4-15), a hypothetical failure criterion of a reliability index of 2.5 was instituted for this study. The graphical output at each strength level was assessed to determine if failure had occurred. The following table summarizes the results, where the indicated concrete strength is the minimum acceptable to negate failure.

Table 4.1: Variation of f_c' results.

Component	***Minimum value for β >2.5***		
	f_c' (MPa)	**l_d (Req'd) (mm)**	**l_d Multiplier**
Moment	4–6	1704–2087	1.9–2.3
Simplified Shear Method	<2	>2954	>3.2
General Shear Method	8–10	1320–1476	1.4–1.6

From the results in Table 4.1, shear appears to be the critical failure mode. Using the Simplified Method, failure did not occur.

4.4.1.2 Applications of Strength Variation Analysis

The results of a sensitivity study on the compressive strength of the intact concrete could provide useful information for site inspections. If testers were aware, before going to the field, that the concrete compressive strength of the concrete needs to be at least (in this case) 10 MPa, they can test a number of locations along the bridge soffit to ensure this limit is met. A limit such as this can also be used to simplify the application of new, Nondestructive Testing (NDT) methods.

4.4.2 Future Deterioration Estimate

To showcase how the BEST computer program could be used to forecast bridge performance, the spalled regions were systematically scaled up to model future deterioration. It is understood that as time progresses, new spalled regions develops and existing ones increase in size as the nearby concrete (and steel) deteriorates. The following figure shows the scaling of spalled regions by area as assumed in the analysis.

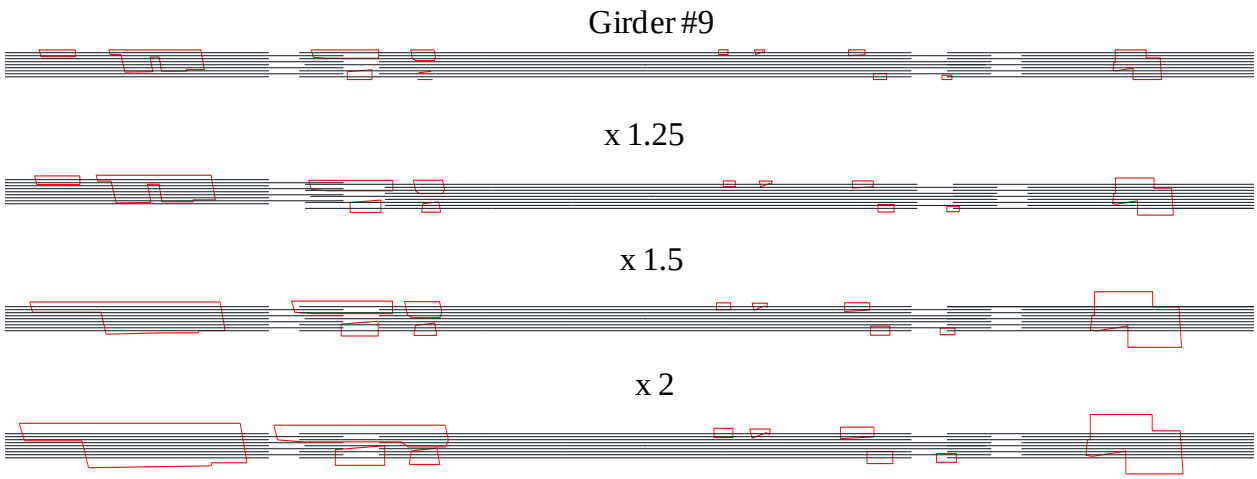

Figure 4-16: Spalling scale-up analysis.

The results of this study are shown in Appendix B-7. Although the results are as predicted, i.e. a decrease in capacity as the spalled area increases, the following should be noted from the study: It is not sufficient to simply model the effect of spalling over time by increasing the required development length. As the spalled regions increase in size, they may begin to affect adjacent bars that previously were fully developed. Therefore the effect of spalling over time is difficult to quantify and would greatly benefit from addition research to study the development of spalling with time.

4.5 Corrosion Section Loss Model

In the presented formulation, up to this point, it has been assumed that the steel rebar itself is not significantly deteriorated. Using the methodology described in Chapter 2, a reduction in the rebar yield strength, i.e. based on Equation 4.1, can be introduced. To demonstrate this,

the empirical model by Cairns et al. (2005) and Lee and Cho (2009) with α_y = 0.012 was selected for the current study. The selected model is identified in Figure 4-17. Other empirical models could be used in place of the adopted model. However, this model was chosen as it gives average predictions compared with the other models in Figure 4-17 and was validated using a relatively large database of test results.

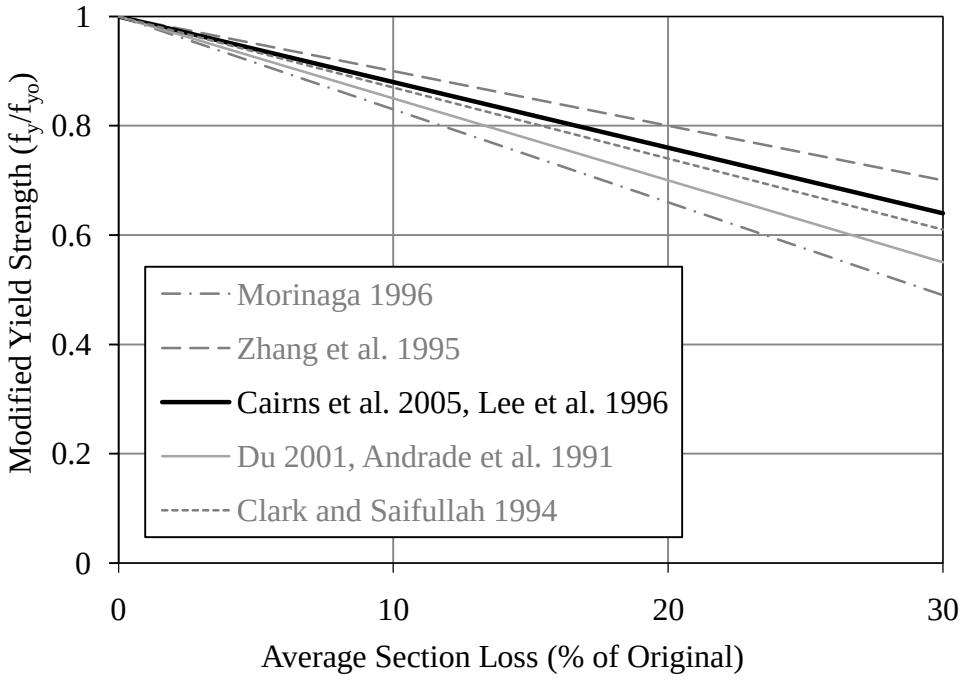

Figure 4-17: Selected empirical model for residual yield strength of corroded bars.

The following relationship was thus added to the multi-girder program:

$$f_y = (1.0 - 0.012 Q_{corr}) f_{yo} \qquad (4.1)$$

The program does not further modify the bar's cross-sectional areas, but rather modifies the bar's yield strength according to Equation 4.1.

4.5.1 Corrosion Model Input

A new field was added to the input file to allow the user to enter an average percent corrosion for both intact concrete sections, Q_i, and sections of steel within spalled regions, Q_s. The exposure of steel within spalled regions is greater when the protective concrete cover is no

longer in place. The corrosion levels, at this time, are unknown for the case study structure and therefore the degree of corrosion was left as a user input. For application to actual structures, this parameter could be measured or estimated.

4.5.2 Corrosion Model Output

For demonstration purposes, 15% corrosion within spalled regions and 6% corrosion in intact concrete was used. The full output for this case is provided in Appendix B-8 for Girder 2. For the full bridge analysis, the resistance ratio and reliability index shifted to that shown in Figure 4-18 and Figure 4-19.

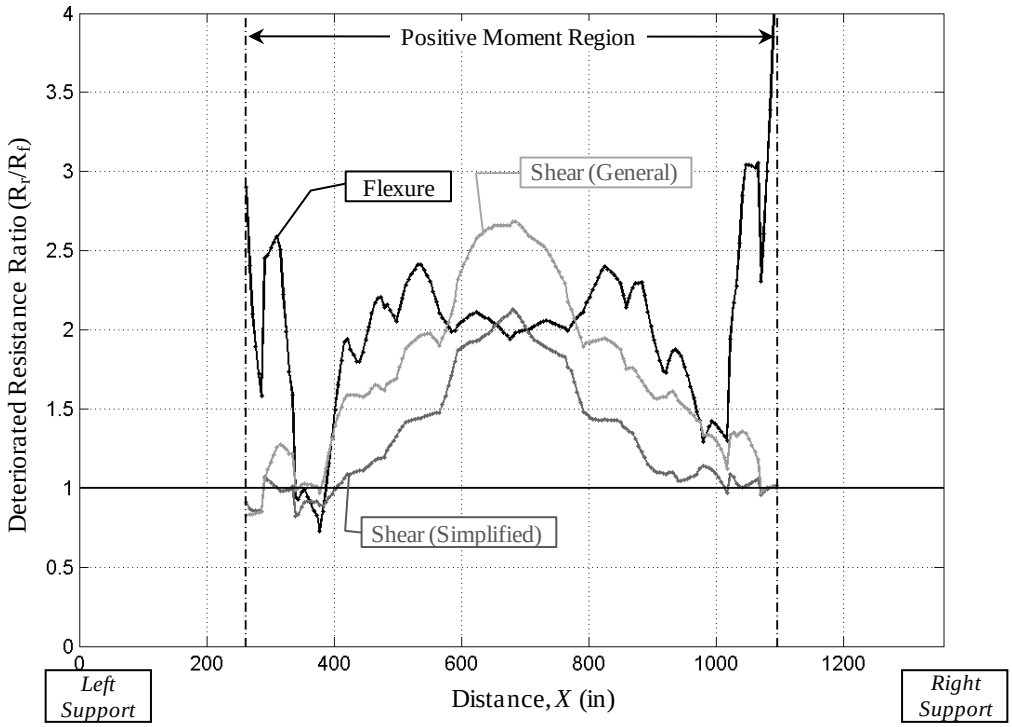

Figure 4-18: Full bridge resistance ratio with section loss model.

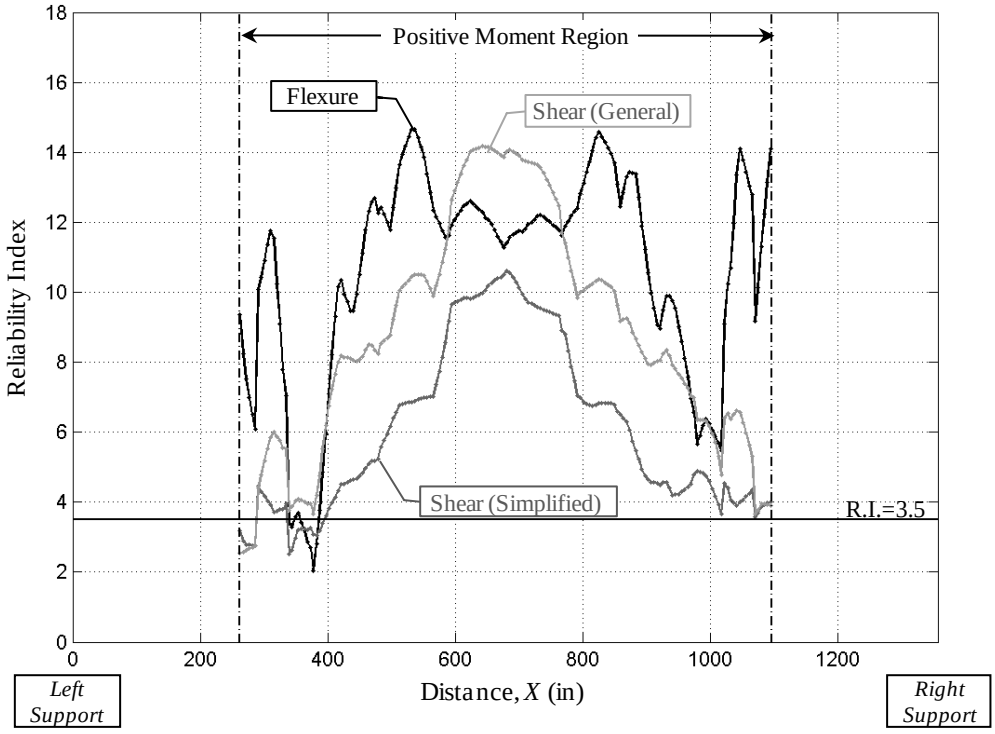

Figure 4-19: Full bridge reliability with section loss model.

The results show, as expected, a shift downward in the calculated resistance ratio and reliability index due to spalling and structural deterioration.

4.6 Bond Deterioration Model

In the analysis procedures described in Chapter 2, it has been assumed that the intact concrete adjacent to the spalled regions can continue to provide the same bond as it did in the new structure. However, if spalling has occurred, there is sufficient evidence that reinforcing corrosion has also taken place and the bond strength between reinforcing steel and concrete has deteriorated. For the purpose of this study, the empirical model proposed by Bhargava et al. (2007) (see Figure 4-20) was selected based on the range of test data and consideration given in this reference of previous studies.

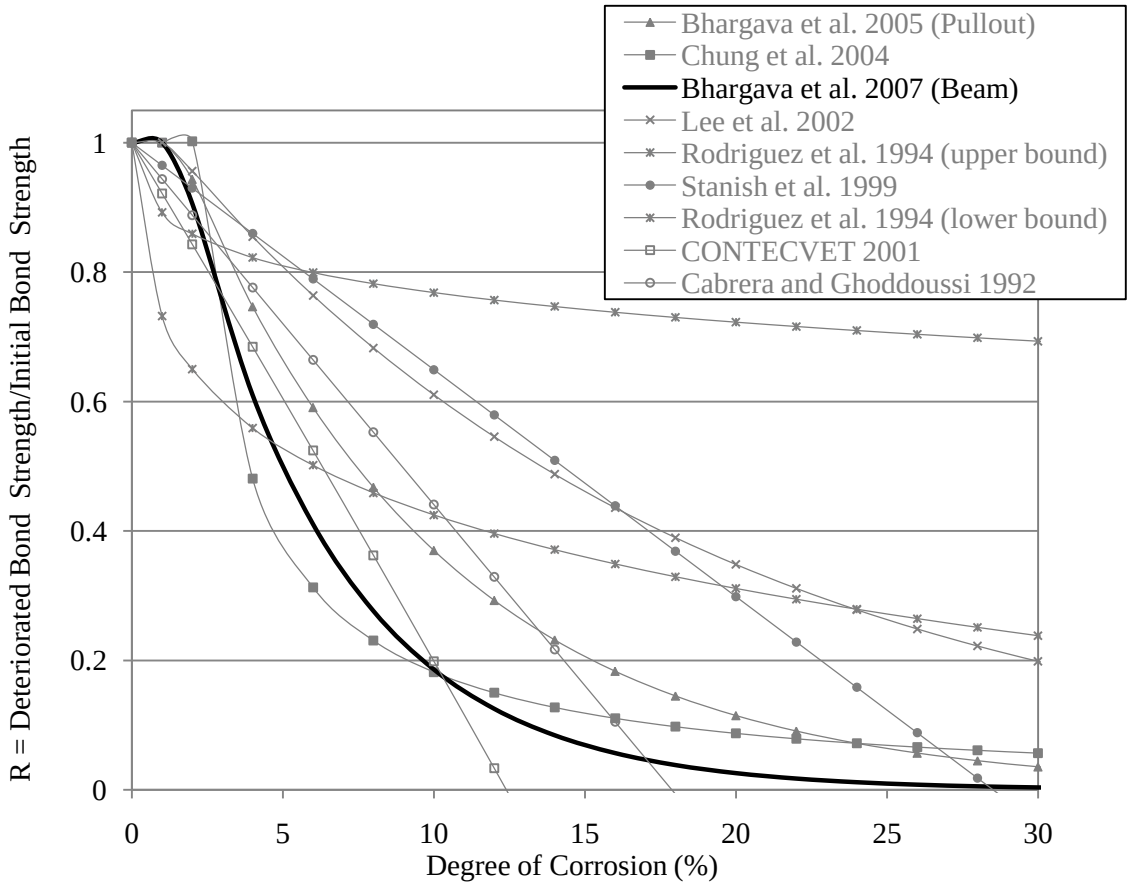

Figure 4-20: Selected empirical relationship for steel deterioration.

The model assumes that longitudinal cracking occurs at 1.5% corrosion (X_p = 1.5%) and:

$$R = 1.0 \text{ for } X_p \le 1.5\% \tag{4.2}$$

$$R = 1.34e^{-0.198X_p} \text{ for } X_p > 1.5\%$$

where,

X_p = average section loss as a percentage of the original cross section area

R = ratio of the current to the original bond strength

For this model, the average corrosion, X_p, is equivalent to Q_i, or the average corrosion level within the intact sections.

This model was easily integrated into the multi-girder program. With the addition of this model and the case of Q_s=15% and Q_i=6%, the results of the full bridge analysis are presented in Figure 4-21 and Figure 4-20.

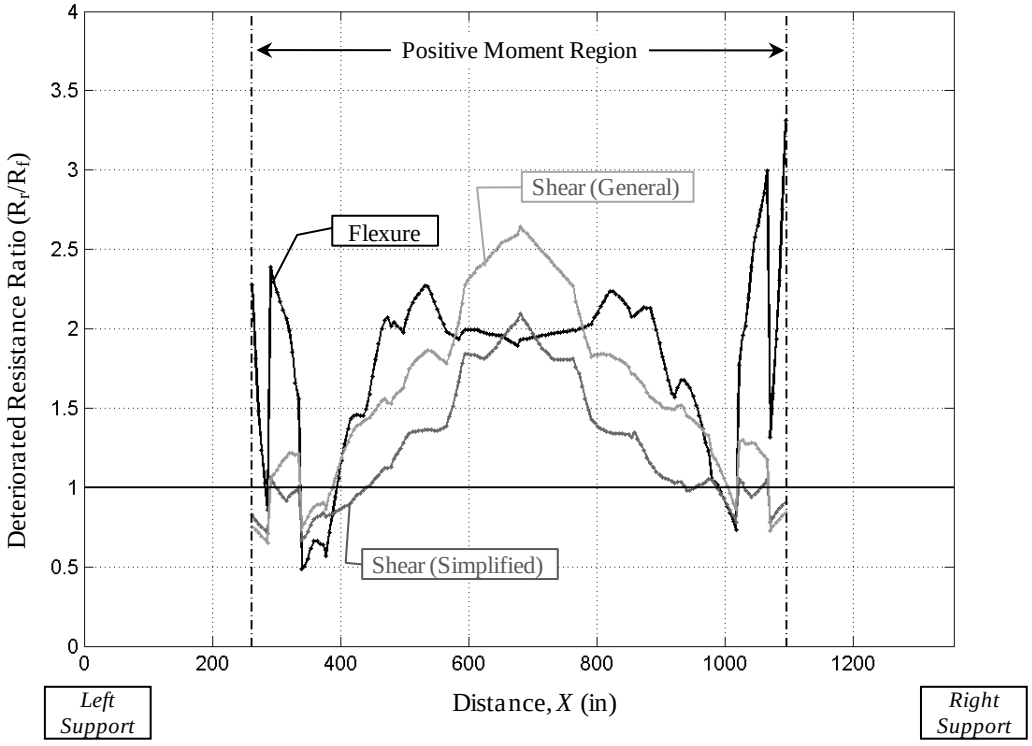

Figure 4-21: Full bridge resistance ratio with section loss and bond deterioration.

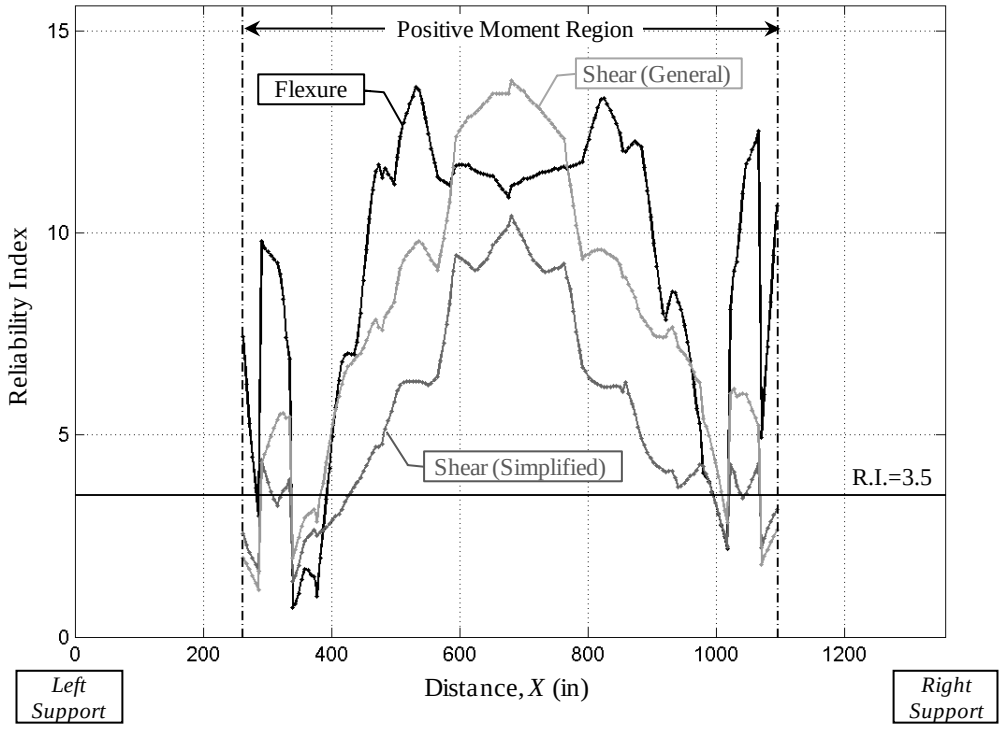

Figure 4-22: Full bridge reliability with section loss and bond deterioration.

Appendix B-9 presents the results for Girder 2. Each plot shows an additional shift and reduced capacity. Figure 4-20 shows the impact that as a little as 6% corrosion has on the overall reliability of the structure.

4.6.1 Program Applications

The BEST computer program, in its current form, is capable of analyzing any RC structure. Since load effects are an input field, the program is not limited to rigid frame structures. For example, a three span continuous structure, as shown in Figure 4-23, can also be modelled using the program developed herein. The envelopes shown in the same figure are for the CSA S6-06 CL-625 Truck and would be the program solicitation input for the 3-span structure.

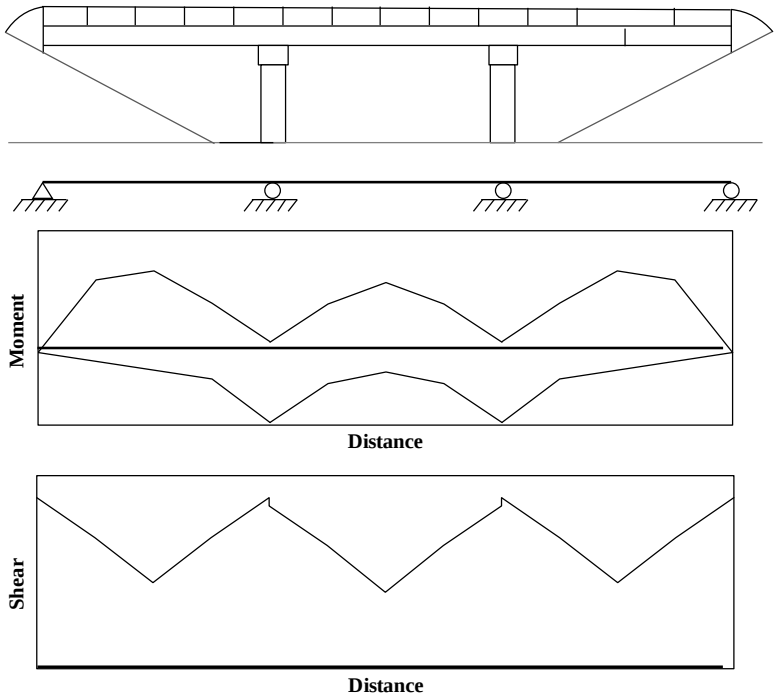

Figure 4-23: Moment and shear envelopes for a 3-span continuous girder.

In addition, because the load effects are input by the user, the user can control the accuracy of the model and subsequently the program. As a quick check, or analysis, the user may decide to use simple hand calculations to generate the load effects. For example, the analysis of the case study structure used the finite element model discussed in Section 3.2.4.1. As a simple, quick analysis, the bridge evaluator may decide to use an average cross section and analyse the structure as fixed-fixed or simply supported. In this case, the user controls the accuracy of the program and is cautioned to use 'safe' judgment.

Although, the CSA transverse distribution model was used for this analysis, any transverse distribution model that utilizes similar distribution factors may be used. Similarly, the required development length was calculated using CSA provisions, but other code or empirical relations may be used.

Since load and resistance factors are user specified, the user can easily perform both nominal and factored analyses for the given structure. Nominal analysis, for example (with load and resistance factors all set to equal 1.0), may be used to predict laboratory test results.

The section depth and stirrup spacing may also be varied along the length or the girder, as is the case with the arched case study structure

4.6.2 Program Limitations

The program currently has a number of restrictions in place so that it could be simply created and interpreted. The program, in its current form, only allows for two layers of bottom reinforcement to be considered for flexural resistance. These bars, however, must have a constant bar diameter. Future versions of the program can expand the input if these features are found to limit users. The geometry is also limited to rectangular and T-shaped sections. Since this covers the majority of conventionally reinforced bridges, adaption to other geometries at this time may not be a priority.

Also, the program is currently limited to the CSA approach for calculating flexural and shear resistance. Little work would be required, however, to create versions of the program for other national standards.

Chapter 5

Experimental Program and Results

5.1 Introduction

A pilot laboratory study was conducted to do the following:

a) determine if the proposed modified area concept and BEST computer program can predict the behaviour of a mechanically spalled concrete beam with exposed reinforcement,
b) determine if planes of weakness are created between the spalled patches,
c) determine the effect, if any, of asymmetric spalling on a concrete beam's strength, e.g. spalling occurring only on one half of a girder with the other half intact,
d) determine the effectiveness of a mortar patch (as currently utilized in industry) to restoring bond and strength, and
e) explore FRP repairs for bond, flexural and shear strength restoration.

The current chapter describes this pilot study and presents the main results.

5.2 Test Program

Twelve test beams were fabricated in total. They are divided into reference, spalled and deterioration specimens as indicated by the matrix shown in Table 5.1.

Table 5.1: Test matrix.

Series	ID	Specimen Layout	Development	% Span Spalled	Anticipated Failure	Target Study
Ref.	1	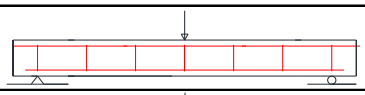	Full	None	Flexure	• calibration
Spalled Series	2	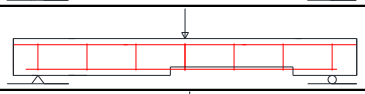	45%	42%	Bond	• correlation to BEST program
	3	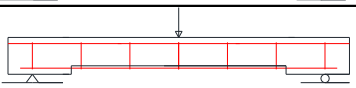	45%	73%	Bond	• the effect of Asymmetrical spalling
	4	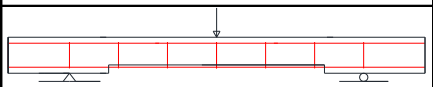	Full	73%	Flexure	• study arch action. • strength maintained or increased
	5	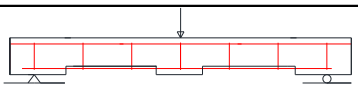	60%	63%	Bond	• effect of intact section positioning • layout reduces potential support confining
	6	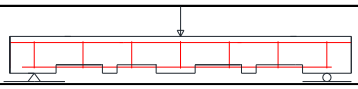	60%	63%	Bond	• effect of small intact section fracture • layout reduces potential support confining

Series	ID	Repair	Specimen Layout	Anticipated Failure	Target Study
Rehabilitation Series	7	SikaTop 123 Plus	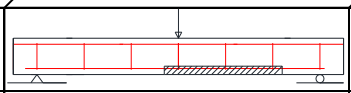	Patch, shear or bond	• study SikaTop for bond restoration • test SikaTop in shear
	8	SikaTop 123 Plus + Long. FRP	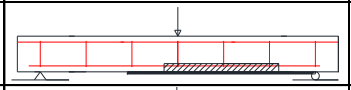	Shear, or FRP	• test effects of Long. FRP over SikaTop
	9	SikaTop 123 Plus, Long. & U-Wrap FRP	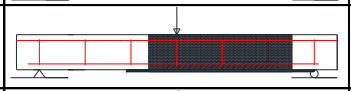	Shear, or FRP	• test effects of FRP over SikaTop • u-wrap and long. FRP application
	10	SikaTop 123 Plus + U-Wrap FRP	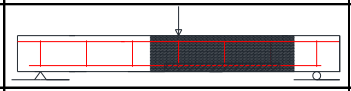	Shear, or FRP	• test effects of u-wrap FRP over SikaTop
	11	Sikacrete-08 SCC	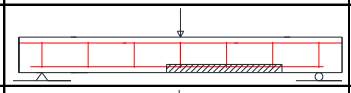	Patch, shear or bond	• study SCC for bond restoration • test SCC in shear
	12	Sikacrete-08 SCC	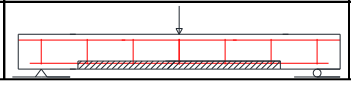	Patch, shear or bond	• study SCC for bond restoration • test SCC in shear

Detailed specimen drawings are provided in Appendix C-1.

5.2.1 Test Specimens

A scaled-down rectangular cross section, as shown in Figure 4-13**,** was selected to reduce material costs and utilize existing formwork.

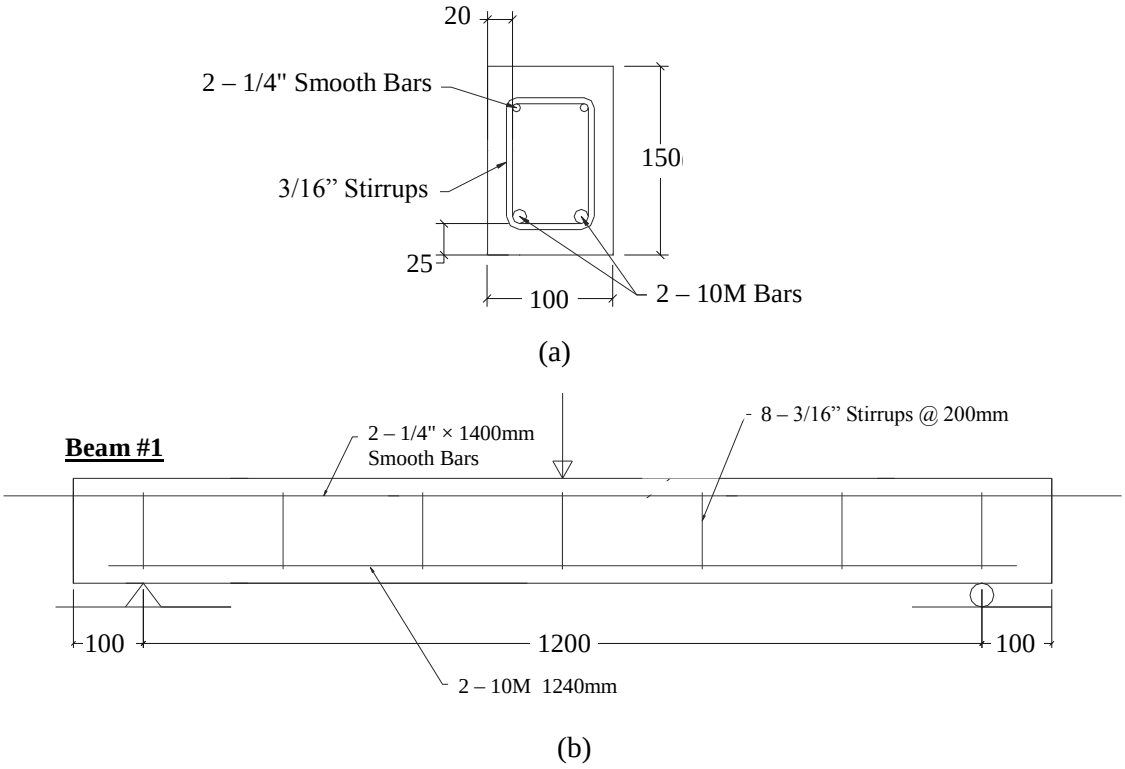

Figure 5-1: Typical test specimen (a) Cross section and (b) Elevation.

The beams were designed for an underreinforced flexural failure. The design calculations are provided in Appendix C-2.

5.2.2 Material Properties

Reinforcing Steel

10M 400 grade longitudinal reinforcing steel was used. Canadian steel was specified for quality and consistency. The reinforcing bars were wired brush cleaned before the repairs were applied.

Concrete

A concrete compressive strength of 20-25 MPa was specified to replicate the concrete originally specified on the case study structure. 9 mm aggregate was specified in view of the reduced scale of the tested beams. The concrete was cured under wet burlap and plastic to keep it moist. Concrete cylinders were tested at 7, 14, 21, and 28 days. The 28 day compressive strength was 16.1 MPa.

5.2.3 Deterioration

Artificial spalling was achieved using cast-in foam blocks. The blocks were chipped out at 7 days to create pockets to simulate spalling as shown in Figure 5-2.

Figure 5-2: Cast-in foam blocks for spalling simulation.

For the test specimens set to be repaired, the surface was roughened using a needle peener to achieve the results shown in Figure 5-3.

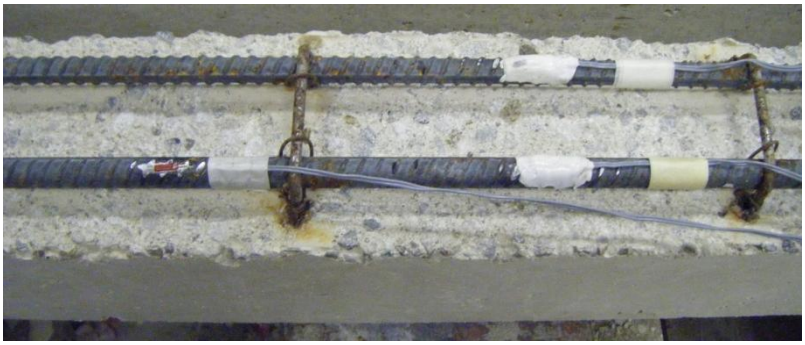

Figure 5-3: Surface roughened by needle peener and strain gauge installation.

5.2.4 Instrumentation

Strain gauges were added at the locations shown in Appendix C-1. FLA-5-11 gauges were used with an M-Cote adhesive. Those subsequently covered by repair materials were coated with wax and SB tape as shown in Figure 5-3.

5.2.5 Rehabilitation

To compare rehabilitation techniques, a number for products were used. Two patching materials were utilized, as well as a fibre-reinforced polymer (FRP) wrap.

SikaTop 123 Plus

SikaTop 123 Plus mortar was used to represent a typical trowel applied mortar patch currently used by MTO. The product is a two component, polymer modified, cementitious, fast setting mortar. It has a migrating corrosion inhibitor with a freeze thaw resistance defined as *good* (Sika 2011). The specified compressive strength at 7, 24, and 28 days is 20, 37, and 50 MPa respectively. The specified bond strength at 1 and 28 days is 7 and 17 MPa. The mortar is limited to repair thickness between 3 and 38 mm (Sika 2011).

For repairing Specimens 7-10, the SikaTop 123 Plus mortar was scrubbed into saturated surface dry (SSD) substrate and trowel applied as shown in Figure 5-4.

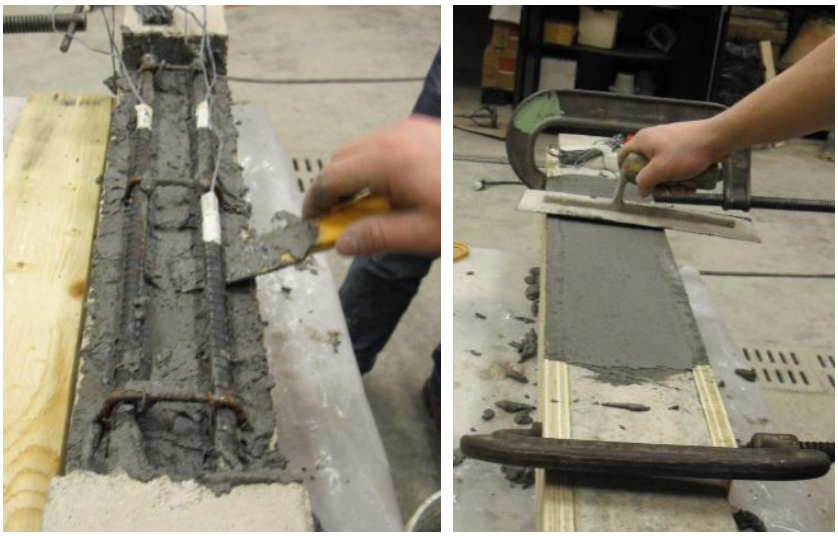

Figure 5-4: SikaTop 123 application.

Sikacrete 08 SCC

Sikacrete 08 SCC is a product currently being considered for use by the MTO. It is a highly flowable, cement-based concrete pump or pour applied grout. It is de-icing salt resistant with good (>300 cycle) freeze-thaw resistance (Sika 2011). Its application is limited to repair thicknesses between 25 and 200 mm. The specified compressive strength is 11 and 31 MPa at 24 hrs and 31 days respectively. For the repair of Specimens 11 and 12, the beams were placed back in the forms and the product was poured on SSD substrate as shown in Figure 5-5.

Figure 5-5: Sikacrete-08 SCC application.

FRP Wraps

SikaWrap Hex 103C was used for the FRP repairs. It is a high strength, high modulus, unidirectional carbon fibre fabric. The ply thickness is 1.016 mm. It was used with the suggested Sikadur 300 high strength, high modulus, two-part epoxy. Together, the specified average 7 day tensile strength and elastic modulus were 849 and 70,552 MPa respectively. For the repair of Specimens 8-10, the fabric was first pre-impregnated and then rolled into the roughened epoxy covered substrate.

5.3 Test Results and Discussion

In this section, the results for each reference, spalling and rehabilitation series are as follows. Both ultimate and serviceability related performance metrics are discussed.

5.3.1 Reference Beam

Beam 1 was unspalled and serves as a reference for all other test specimens. As shown in Appendix C-2, the beam was designed for shear failure. Even though minimum stirrups (as per CAN/CSA A23.3-04) were provided, it is expected that the stirrups did not contribute to the shear strength due to the mortar strength, stirrup spacing, use of round 9 mm aggregate and the use of smooth wire stirrups. In fact, many older bridge structures are shear sensitive and do not meet modern shear standards. For example, minimum stirrups were not provided along the majority of the case study structure girder span.

Using the actual 28 day concrete compressive strength (16.1 MPa) and the specified steel strength (400 MPa), the strength of the member is shown as case (a) in Table 5.2. To understand the failure, case (b) was created with the average concrete strength at the day of testing (18 MPa) and an anticipated actual steel strength of 450 MPa. These are more realistic actual material strengths. Actual results indicate that, overall, the beam is shear sensitive.

Table 5.2: Strength approximations of Beam 1.

	Simplified Method			General Method			Flexural Strength	Actual
Case	**Vc**	**Vs**	**Vr**	**Vc**	**Vs**	**Vr**	**Mr**	**Failure Load**
(a)	17.22		41.27	30.3		30.3	23.90	26.40
(b)	18.26		18.26	31.8		31.8	26.74	

*Strengths shown in applied load (kN).

In fact, the beam is on the verge of flexure and shear failure and interestingly, the conservatism of the each code strength approximation is well displayed. That is, potentially the conservatism in the flexure strength is higher than that of the General shear Method.

Herein, the material strengths proposed in case (b) are used and it has been assumed that the stirrups do not contribute to the shear strength of the member.

5.3.2 Spalling Series

The results of the spalling series tests are discussed in terms of member strength and ductility.

Member Strength

The predicted strengths for each test specimen using the BEST program are shown in Table 5.3 (converted to applied load values). The resistances predicted by the proposed flexural and shear methods are shown in this table. The selected lowest (critical) strengths are highlighted and compared to actual test results. BEST selects the lowest of flexure and shear strengths for the member. Test:predicted values range between 1.55-1.21. In each case, the estimate is conservative. Based on this estimate, the failure mode should be characterized as a shear-bond failure. In reality, however, the actual observed failure of each member (other than Beam 4) was flexure-bond or 'pure' anchorage failure. Therefore, it is anticipated that the strengths governed by flexure are likely a more accurate representation. As shown in Table 5.3, test:predicted values range between 1.28-0.87 for this case.

Table 5.3: Strength approximation for spalling series beams.

Series	Beam ID	Specimen Layout	Spall Pattern	Development	% Span Spalled	Actual* Failure Load (kN)	Predicted Strength* Flexure	Simplified Method	General Method	Selected	Test/Predicted Flexure Only	Flexure or Shear
Spalled Series	2	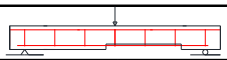	45%	42%	17.16	13.40	11.10	20.30	11.10	1.28	1.55
	3	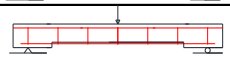	45%	73%	16.64	13.40	11.10	20.30	11.10	1.24	1.50
	4	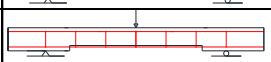	Full	73%	24.20	26.70	18.26	27.15	18.26	0.91	1.33
	5	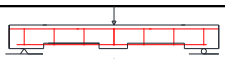	60%	63%	17.36	18.20	13.20	23.14	13.20	0.95	1.32
	6	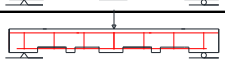	60%	63%	15.91	18.20	13.20	23.14	13.20	0.87	1.21

*Strengths in applied load (kN).

As anticipated, Beam 2, which had asymmetrical simulated spalling, failed in bond. The crack pattern for the beam is shown in Table 5.4. The BEST program predicted strength appears to be highly conservative. It is likely that this conservatism is due to additional confining stress over the right support, which is not considered by BEST. The bond strength in this section is increased due to the intersection of the inclined shear path with the anchorage zone and bearing surface. Beam 3 has the same development length (180 mm), but is spalled symmetrically over 73% of the span. Marginal differences in strength between Beam 2 and Beam 3 indicate that the symmetric nature of spalling has little or no effect because failure in both cases was due to bond.

In Beam 4, the longitudinal bars were fully anchored by extending them past the supports. The results for this beam serve as a good example of a shift from shear failure to arch action. Steel gauge strains indicate a shift upward of the neutral axis and a change in failure mode to concrete crushing failure. The crack pattern, shown in Table 5.4, matches those observed by Cairns and Zhao (1993). High deflections, exceeding one degree of rotation, are apparent. In actual bridge structures, deflections of this magnitude are visible and likely detectable. For the case of full development, BEST anticipates the strength to be equal to that of the unspalled beam.

In Beam 5, 240 mm of development length is provided, to accommodate a spalling pattern in which 90 mm is intact on each side of the centrally placed load. The results indicate that BEST is less conservative (unconservative in flexure) for this case due to the apparent inability of the central intact section to engage and contribute to anchorage. It is likely that a section of this nature acts similarly to a pivot for the longitudinal reinforcing steel. The vertical cracks near the central intact section (shown in Table 5.4) support this theory. A simple approach may be to neglect intact section near the load point(s). In this case, if the intact section is removed, the test:predicted ratio for flexure increases from 0.95 to 1.525.

Table 5.4: Test specimen crack patterns.

Series	Beam ID	Cracked Specimen
Ref.	1	
Spalled Series	2	
	3	
	4	
	5	
	6	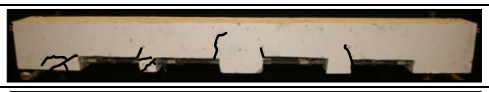
Rehabilitation Series	7	
	8	
	9	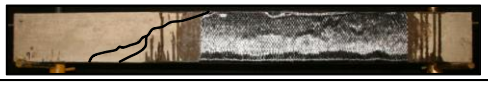
	10	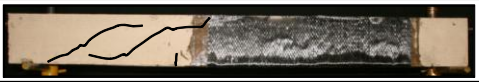
	11	
	12	

Beam 6 had similar short intact sections within the span. In this beam, the central section was shortened to 60 mm on each side of the centrally placed load and additional small intact sections (60 mm) were created further away on either side. The total development length provided was the same as that for Beam 5 (230 mm). A further strength reduction is seen for Beam 6, due in part to the fracture of one of the short intact sections before the final pullout failure. The cracked section is shown in Figure 5-6. The fracture of intact sections depends on the shear strength of the section, which is a function of the concrete strength, intact length and depth of spalling. It also depends on the tensile force in the reinforcing bar at that

section. In fact, it may be conservative to ignore short intact sections. By removing the contribution of the 60 mm sections (which fractured) the test:predicted ratio increases from 0.87 to 1.19. Both Beams 5 and 6 also have reduced anchorage sections over the supports (150 and 120 mm respectively) and likely the bond strengths are therefore not as enhanced by support confining stresses.

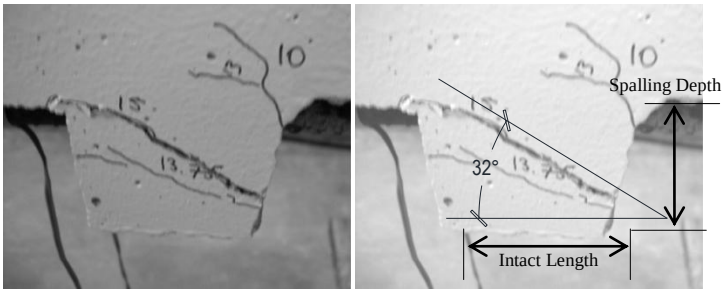

Figure 5-6: Beam 6 intact section cracking.

Ductility

Load versus deflection curves were created for each specimen to evaluate the effect of each spalling case on ductility. Deflection was measured at the mid-span below the applied load. Figure 5-7a compares Beam 1 to each spalling case except Beam 4 (arch action). Figure 5-7b shows the ductility of Beam 4. All spalling cases appeared to be less stiff, but, ultimate failure was pullout in each case. For Beam 5, there are obvious jumps where the bars slipped within the short intact sections or the intact sections fractured. The sudden deflection jump for Beam 6 is likely due to a slip or a bump of the dial gauge and experimental error.

Deflections are very high and cracking is severe for the case of full development and arch action (Beam 4). Likely under service load levels, the additional deflection would be undetectable, but near the ultimate load level the plot plateaus and deflections are significant. The maximum tensile stress in the bar is constant and results in elongation of the bar along its entire exposed length.

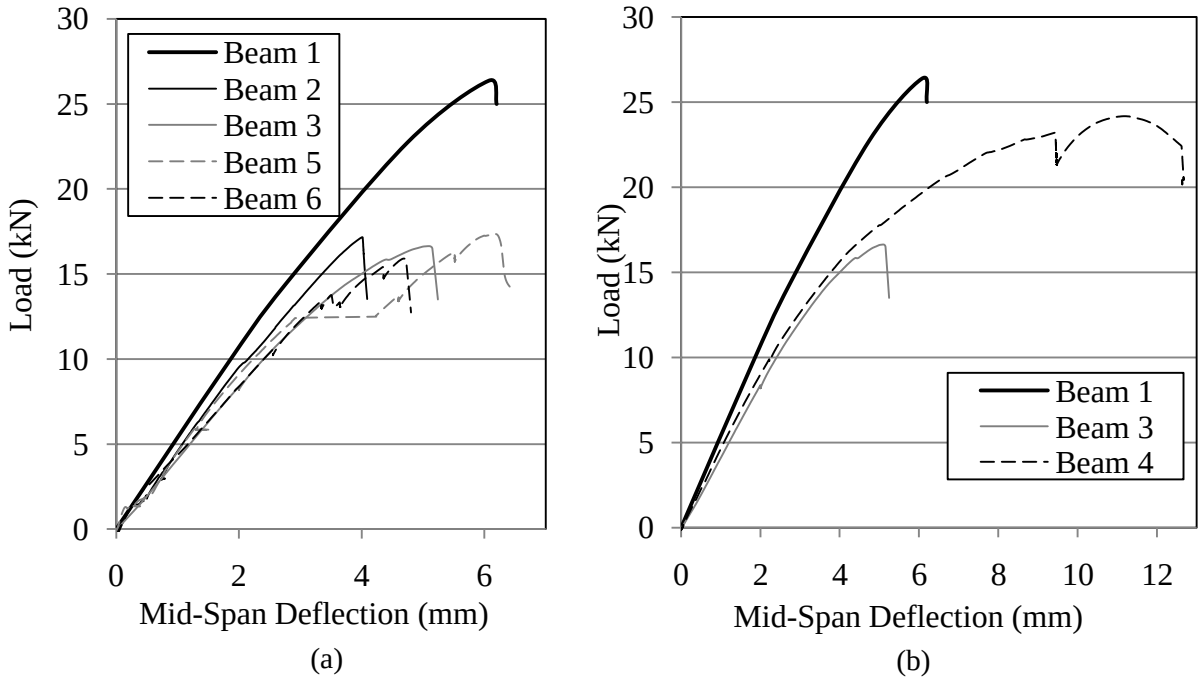

Figure 5-7: Spalling Series load-deflection curves for (a) Spalling configurations and (b) Arch action.

5.3.3 Rehabilitation Series

Member Strength

All repairs (except the ones applied to Beam 12) were applied to the same spalling case as Beam 2. If the repair was sufficient, then the strength of the spalled (right) side of the beam was sufficiently restored to force shear failure to the left (substrate) side of the beam. As shown in Table 5.5, each repair was sufficient to restore the bond and subsequently the beam strength. In Table 5.5 the strengths are compared to the unspalled beam as the repaired:unspalled ratio. The variations in this ratio are likely governed by the experimental variation of the shear strength of the substrate concrete. Both the mortar patch and SCC repair were easy to trowel apply and appeared to bond well to the relatively weak substrate. FRP repairs remained bonded through the duration of testing, although cracking (as shown in Table 5.4) appeared under the longitudinal repair (Beam 8). The mortar patch repair on its own (Beam 7) appears to result in a significant strength gain, however this result is unexplainable and likely due to inherent variability in the specimen strengths.

For Beam 12, the SCC repair was applied to the spalling case from Beam 3 (73% of the span spalled). The strength of the repair and increase in the tension stiffening effect appear to result in an increase in the beam shear strength or shift of the failure mode closer to flexure.

Table 5.5: Rehabilitation series test results.

Series	Beam ID	Specimen Layout	Repair	Failure Load (kN)	Repaired Beam/ Beam 1	Max Deflection (mm)	Preliminary Discussion
Rehabilitation Series	7	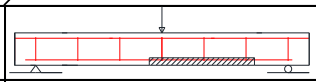	SikaTop 123 Plus	32.50	1.23	8.54	• Shear failure in substrate • Patch bond to substrate is good • 18% stiffer than beam 1.
	8	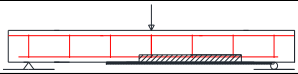	SikaTop 123 Plus + Long. FRP	30.13	1.14	5.01	• Shear failure in substrate • 34% stiffer than beam 1.
	9	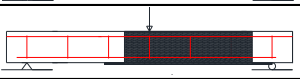	SikaTop 123 Plus, Long. & U-Wrap FRP	27.78	1.05	4.03	• Shear failure in substrate • 37% stiffer than beam 1.
	10	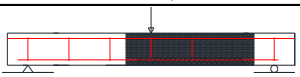	SikaTop 123 Plus + U-Wrap FRP	27.05	1.02	5.39	• Shear failure in substrate • 27.6% stiffer than beam 1.
	11	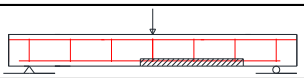	Sikacrete-08 SCC	24.51	0.93	4.18	• Shear failure in substrate
	12	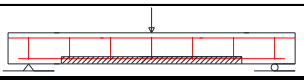	Sikacrete-08 SCC	33.36	1.26	14.38	• Shear failure in substate • Strengthened in shear by arch action • Vey large deflections at loads over ref. beam

*All Specimens have 45% Development

Ductility

Each repair resulted in an increase in member stiffness (as shown on Figure 5-8). This outcome is somewhat unexpected. The stiffness increase shown in this figure can be attested to an increase in tension stiffening resulting from the higher strength of the repair materials compared to the substrate concrete. Even in those beams repaired by patch materials, the SCC and mortar have a sufficient bond and compression strength to increase tension stiffening, thus increasing the overall stiffness of the beam. The application of FRP materials further enhances this effect.

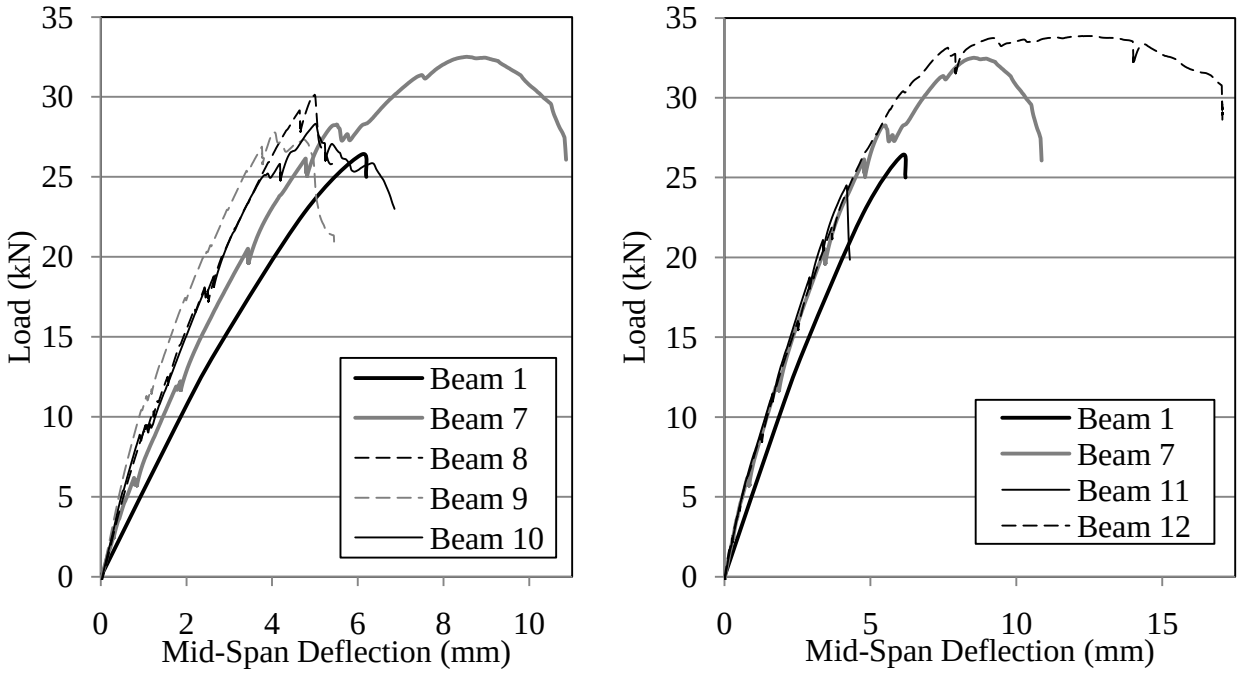

Figure 5-8: Rehabilitation Series load-deflection curves for (a) Sikacrete, FRP and (b) SCC repairs.

5.4 Summary

Based on the test specimens analyzed, the BEST computer program provides conservative estimates for the strength of beams within a test:predicted ratio of 1.21-1.55. However, the failure is better represented by flexural pullout, in which the calculations produce test:predicted ratios between 0.87-1.28. It appears that the simplified shear method produces overly conservative strength estimates.

The distribution of spalling was varied for Beams 2-6. Negligible strength differences were found between symmetric and asymmetrical spalling. Centrally located intact sections are unable to fully contribute to the strength of the beam. Similarly, short sections can fracture and fail to contribute to bond at higher load levels. Arch action was demonstrated by fully anchoring longitudinal bars past the supports. Small strength loss occurred as the failure mode shifted from shear to concrete crushing and mid-span deflections increased substantially.

Both patch materials (SikaTop 123 and Sikacrete-08 SCC) used for spalling rehabilitation appear to effectively restore bond and member strength over spalled sections. Additionally, the use of FRP, even over half of the beam length, has a stiffening effect.

Chapter 6

Reliability Analysis

6.1 Introduction

In this chapter, a full reliability analysis is conducted with the following goals:

- to use the modified area concept and BEST program as a basis for the reliability analysis of a deteriorated RC bridge structure with exposed reinforcement,
- to develop realistic statistical distributions for parameters involved in the probabilistic analysis of an RC member based on the CAN/CSA code equations,
- to assess the viability of the approximate reliability method presented in Section 3.6 as a simple approximation of a bridge structure's reliability,
- to find a relationship between the deterministic resistance ratio and reliability index for sections along the length of a spalled RC bridge girder, and
- to conduct sensitivity studies to examine the effect on the structural reliability of further deterioration of concrete compressive strength, further spalling and the subsequent reduction in the provided bar development.

6.2 Probabilistic Analysis Methods

Monte Carlo Simulation (MCS) techniques were used for this analysis and were run using the existing BEST computational framework. The procedure used herein is referred to by Melchers (2002) as direct sampling, or the 'crude' Monte Carlo approach. The probability of failure, p_f, is determined by sampling each variable over N trials, so that:

$$p_f \approx \frac{1}{N}\sum_{j=1}^{N} I\left[G(x_j) \le 0\right] \tag{6.1}$$

The process counts limit state violations, $G(x) \leq 0$ using an indicator function $I[G(x_i) \leq 0]$, which is equal to 1 if $G(x) \leq 0$ is true and 0 if $G(x) \leq 0$ is false. The limit state function represents the difference between resistance and solicitation (load effect), i.e.:

$$G = R - S \tag{6.2}$$

If a normal distribution is assumed for *G*, the reliability or safety index, β, can be related to the mean, μ, and standard deviation, σ, of *G* as follows:

$$\beta = \frac{\mu}{\sigma} \tag{6.3}$$

The reliability index can also be related to P_f as follows:

$$\beta = -[\Phi(P_f)] \tag{6.4}$$

The reliability index is related to the distance between the mean of *G* and *G* = 0, and the standard deviation, σ, of *G*, as shown in Figure 6-1.

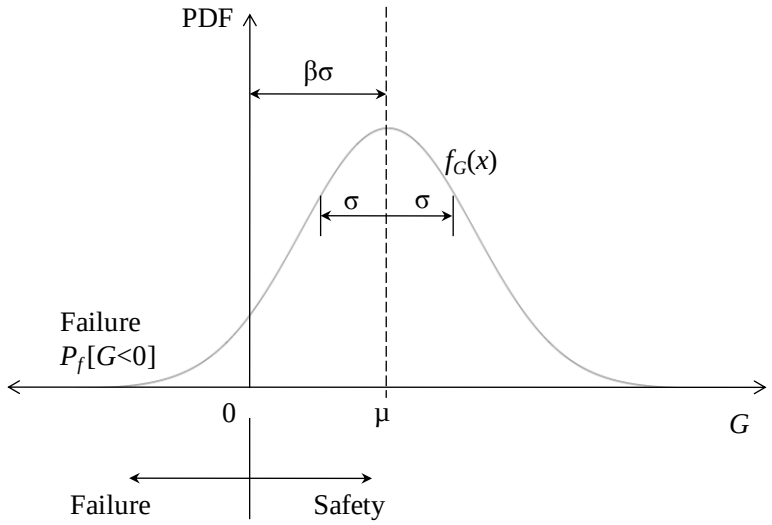

Figure 6-1: Probability density for *G*.

In other words, β provides a measure of the distance, in terms of standard deviations, between the mean of the safety function and the most likely point of failure. For practical

use, CAN/CSA S6-06 tabulates the relationship between the reliability index and probability of failure (see Table 6.1).

Table 6.1: Relationship between probability of failure and reliability index (CAN/CSA S6).

Reliability index, β	Notional probability of failure, p_f	
2.0	2.3×10^{-2}	or 1:44
2.5	6.2×10^{-3}	or 1:160
3.0	1.4×10^{-3}	or 1:740
3.5	2.3×10^{-4}	or 1:4 300
4.0	3.2×10^{-5}	or 1:31 500
4.5	3.4×10^{-6}	or 1:294 000

The reliability index, of course, can be compared to the target index computed in accordance with CSA/CAN S6-06 as discussed in Section 3.6.1. The target index is generally based on acceptable degrees of risk to the general public as shown in Table 6.2.

Table 6.2: Acceptable degree of risk in society (MacGregor 1976).

	Yearly death rate per person per year	
Activity	**For those concerned**	**For the total population**
Motorcycle Racing	5×10^{-3}	
Mountain Climbing	5×10^{-3}	
Mining	7×10^{-4}	
Swimming	1×10^{-4}	2×10^{-5}
Automobile travel		3.6×10^{-4}
Airplane travel	1×10^{-4}	
Fire in buildings		2×10^{-5}
Poisoning		1.1×10^{-5}
Lightning		5×10^{-7}
Structural Collapse		
During Construction	3×10^{-5}	
All others		2×10^{-7}

It is important to note that for the MCS analysis to be accurate a sufficient number of failures must be achieved. A number of general rules are available as described in Melchers (2002).

6.3 Statistical Modelling of Input Parameters

The basis of crude MCS consists of sampling from each of the statistical distributions assigned to each of the variables in the limit state function. For the current study, each of the variables shown in Figure 6-2 and Figure 6-3 were considered and the uncertainty of each was estimated in order to facilitate the reliability analysis.

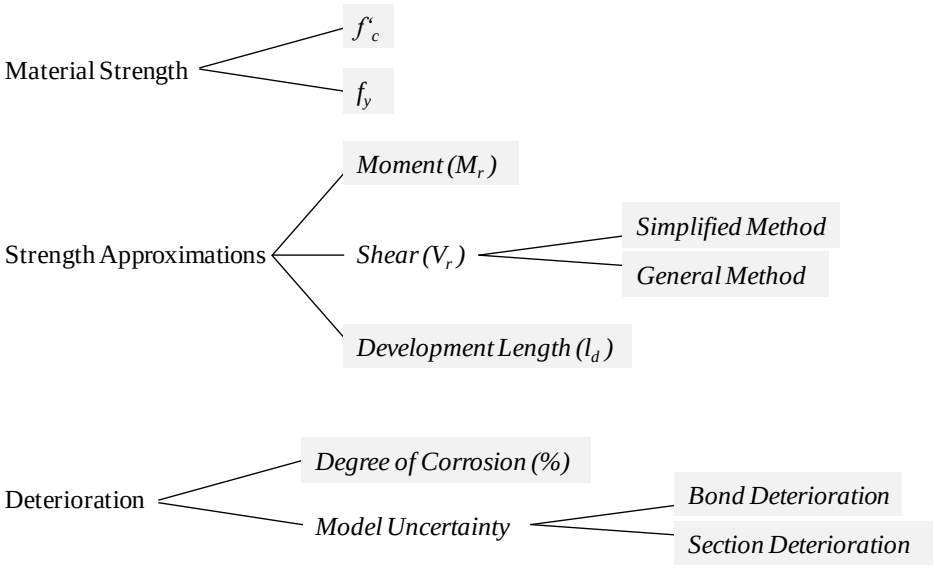

Figure 6-2: Probabilistic variables for bridge resistance.

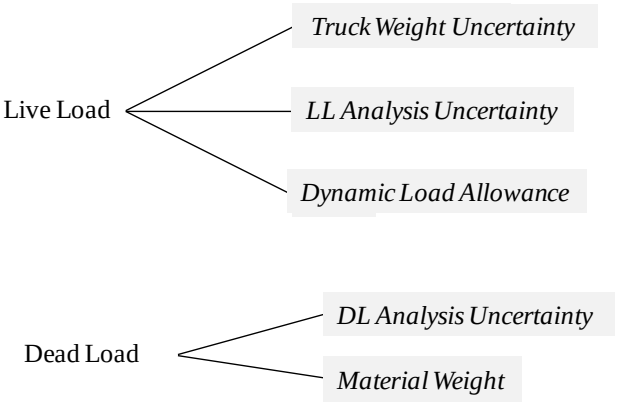

Figure 6-3: Probabilistic variables for bridge solicitation.

Reliability analysis requires uncertainties to be estimated for each variable. The assumed statistical properties for the bias factors associated with each variable are shown in Table 6.3.

Table 6.3: Bias Factors for probabilistic analysis.

Uncertainty Description			Bias Factor			
			Dist. Type	Mean	CoV	Source
Loading	**Live**	LL Annual Extreme Event (Moment)	Gumbel	1.247	0.058	[CSA-S6 Calib.]
		LL Annual Extreme Event (Shear)	Gumbel	1.285	0.059	[CSA-S6 Calib.]
		LL Analysis	Normal	0.93	0.12	[CSA-S6 Calib.]
		DLA	Normal	1.1	0.072	[CSA-S6 Calib.]
	Dead	Self Weight	Normal	1.05	0.1	[CSA-S6 Calib.]
		DL Analysis	Normal	0.93	0.12	[CSA-S6 Calib.]
Resistance (*R*)	**Material Strength (*M*)**	f'_c	Normal	1.25	0.131	[Bartlett and MacGregor 1994]
		f_y	Lognormal	1.115	0.1	[Cheung and Li 2002]
	Professional Factor (*P*)	Moment (M_r)	Normal	1.14	0.13	[Nowak and Szerszen 1998]
		Shear (Simplified)	Normal	1.34	0.176	[Bentz 2010]
		Shear (General)	Normal	1.19	0.129	[Collins et al. 2008]
		Development Length (L_d)	Normal	0.785	0.161	[modified Rezansoff and Sparling 1996]
	Deterioration (*D*)	Degree of Corrosion				
		Model for Bond Deterioration				
		Model for Section Loss				

The parameters for deterioration (*D*) are still under investigation. At this time, the analysis does not consider cross section loss and bond deterioration due to corrosion. A sample input file for the reliability analysis is shown in Appendix D-1.

6.3.1 Statistical Resistance Modelling

The resistance of a structure, *R*, is defined by Nowak and Grouni (1994) as being made up of nominal resistance, R_n, multiplied by the uncertainty involved in the material properties, *M*, fabrication (geometry), *F*, and a professional/analysis factor, *P*.

$$R = R_n \cdot M \cdot F \cdot P \tag{6.5}$$

At this point, fabrication errors (and geometric variations) are ignored. Since geometric variations factor into both resistance and load effects they may have a cancelling effect. The variability in bar sizes is generally small (Melchers 2002) and therefore omitted from the current study. Likewise, to simplify the analysis, the spatial variations of each parameter have not been modelled in this analysis thus far. In this section the selection of each parameter distribution is discussed.

Concrete Strength

The uncertainty associated with the concrete compressive strength according to Cheung and Li (2002) has a bias (mean) of 0.805 and coefficient of variation (COV) of 15% with a lognormal distribution. Based on Melchers (2002), these values appear to be reasonable and generally at the lower end of relevant work. However, it is expected that these commonly used factors do not capture the difference between specified and delivered concrete strengths, but rather compare batches of cylinders of constant mix design. In an extensive report, Bartlett and MacGregor (1994) studied *in situ* cores taken from structures built in Alberta between 1988 and 1993 and found the average *in situ* strength to be 1.2 times the specified strength (for shallow structure depths) with a COV of 18.6%. They noted that the data was normally distributed. This value captures and encompasses variations in batch and location strengths. Bailey (1996) suggests a bias of 1.28 and 11% COV for *in situ* concrete. It is important to note that quality control varies significantly around the world and throughout history. For this Canadian study, the values by Barlett and MacGregor (1994) were selected.

Steel Strength

Cheung and Li (2002) suggest reinforcing steel has a strength ratio bias of 1.115 with a CoV of 10%. Mirza and MacGregor (1982) show very good agreement to this (mean of 1.115 and COV 6.4%). They suggest a lognormal distribution. In his analysis Bailey (1996) uses a mean of 1.25 with a COV of 8%. The statistics presented by Cheung and Li (2002) are representative for old steel that likely has lower strengths with higher levels of variability resulting from poor quality control.

6.3.1.1 Professional Factors

Professional factors account for the difference between tested strengths and strengths predicted using the deterministic CAN/CSA design code equations. When applied to the reliability analysis they, in essence, remove the implicit conservatism in standard design approximations.

It is important to note, at this point, that when test-to-predicted values are used to derive a professional factor, it is implicitly assumed that the tests are perfectly accurate. That is geometric variations and concrete strengths are consistent between test specimens and the computation of predicted values. Herein, this assumption has been made and test-to-predicted ratios are simply used as professional factors in which variations in material strengths and geometric conditions are additionally applied as per Equation 6.5.

Flexure

For flexure, most current standards use a rectangular stress block as an approximation. Nowak and Grouni (1994) recommend professional factors based on their simulation of moment-curvature relationships with comparisons to test results. They found that the strengths had a mean of 1.02 and COV of 6%. These values are consistent with work by Ellingwood et al. (1980), Mirza and Mcgregor (1982) and Isreal (1986). Panesar and Bartlett (2006) suggest strain hardening increases test results by 16%. Based on these values, a mean of 1.18 (1.02+0.16) may be justified, but relies on the assumption that the member is underreinforced to be accurate. Factors by Nowak and Szerszen (1998) with a mean of 1.14 and CoV of 135 are used herein.

Shear General Method

For establishing the CAN/CSA A23.3 General Method for shear design, Collins et al. (1996) compared test-to-predicted strengths of 580 beam specimens. They found the ratio had a mean of 1.39 and COV of 0.197. However, the General Method has evolved significantly since then. These statistics were confirmed by Somo and Hong (2006) using the computer

program Response 2000 (based on the modified compression field theory) to derive statistical data with comparisons to a database of experimental shear strengths. For shear span to depth ratios greater than two they found the program had a resistance ratio mean of 1.26 and COV of 0.33. However, these values should stand as a lower bound since the General Method code equations are more conservative than the program. A review of current standards by Collins et al. (2008) examined a database of 1849 tests. They recommended the statistical distribution to their data had a mean of 1.21 and a CoV of 15.3%. They also fitted a normal distribution to the unconservative half of the data with a mean of 1.19 and CoV of 12.9%. It is important to, in this case, base the analysis on the unconservative half of the data, because there are a number of failure modes that artificially enhance shear strength and few that artificially reduce it. The result is a skewed (conservative) distribution. Herein, the recommendations by Collins et al (2008) were adopted for the General Method professional factor. These factors should not be extended to span-to-depth ratios less than 2 (or 2.5) since the code formulae do not accurately predict the strengths of deep beams (due to arch action). It is important to note that herein the General Method is used with the modified area concept and is an approximation. Maximum shear and flexure load effects are used. Therefore this analysis is implicitly conservative.

Simplified Method

For the CAN/CSA Simplified Method, Polak and Dubas (1996) suggest a mean of 1.12 and a COV of 0.19, but this work was based on CAN/CSA A23.3-M94 standards. Sun (1999) suggests a mean of 1.26 and COV of 0.246 using another database of test results. Sun suggests a normal or Gumbel distributions. Somo and Hong (2006) suggest a mean of 1.43 and COV of 0.43 after analyzing their database of results. Most recently, Bentz (2010) analyzed a database of tests using three accuracy levels. The least of these corresponded to the CAN/CSA Simplified Method. He found the data on the unconservative half was normally distributed with a mean of 1.34 and a coefficient of variation of 17.6%.

Development Length

The CAN/CSA A23.3 computation of development length is based on ACI Committee 408. An evaluation by Rezansoff and Sparling (1995) of tension lap splices found small differences between the two in overall prediction accuracies. A Report by ACI Committee 408 (ACI 408R-03) suggests its formulae have a test-to-predicted ratio mean of 1.284 and COV of 0.135. Rezansoff and Sparling (1996) however found that the strength ratio has a mean of 1.46 (0.161 COV) and 1.54 (0.203 COV) for CSA 23.3 and ACI 408, respectively. This analysis uses CAN/CSA A23.3-04 for development. Therefore, a normal distribution was assumed with a bond-strength ratio mean of 1.46 and COV of 0.161. The required development length is inversely related to the strength. Therefore, for development, a mean of 1/1.46 = 0.685 was selected. A CRSI report (2001) suggests adding 10% to development lengths for vintage steel bars as a good rule of thumb. Therefore, the required development length was varied normally about a mean of 0.785 with a COV of 0.161.

6.3.2 Statistical Solicitation (i.e. Load) Modelling

The uncertainty in the dead load is the result of variations in the self weight and the structural analysis method used. For the current analysis, a simple 2-D SAP 2000 frame was used, but the transverse analysis was completed using CAN/CSA S6-06. For this case, the CAN/CSA-S6 Calibration report suggests the factors listed in Table 3.7 for *simplified code methods*, and the self-weight uncertainty associated with *cast-in-place* components.

Extreme event statistics were calculated using the approach described in the CAN/CSA-S6 Calibration Report using annual truck data. The report relied on data with a sample size of 13391 trucks, driven over bridges of varying length. They develop Gumbel distributions for each traffic class, as defined by the average daily truck traffic or ADTT. For this analysis, it has been assumed that the bridge supports an ADTT of 500 trucks (less than the design Class A Highway).

6.4 Reliability Index Results

In this section, Girder 2 of the case study bridge is analyzed using MCS with the statistical variables described in the previous section. The results are presented for flexure and shear.

6.4.1 Single Girder: Flexure

Analyzing a large number of section along the girder using the 'crude' MCS approach is not efficient computationally. Therefore, for the flexural analysis, first the resistance was scaled down to induce a sufficient number of failures in 10 000 trials to facilitate the determination of the critical section. In this case, the flexural capacity was scaled down by a factor of 0.5 and the critical section was determined to be around 420 inches from the left support. The results of this analysis are shown on Figure 6-4.

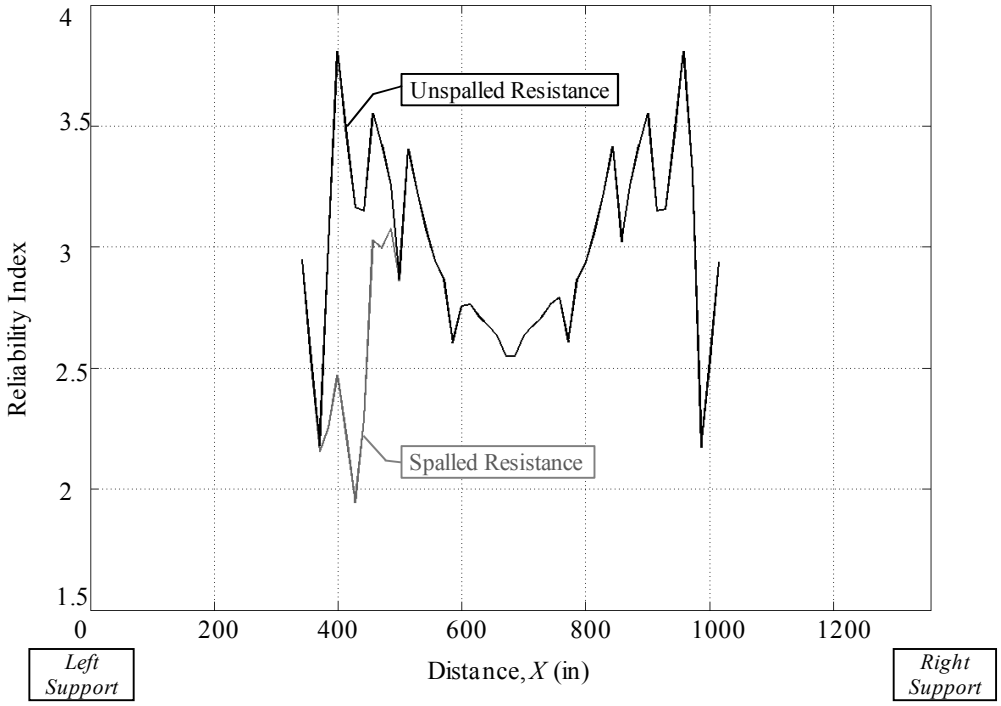

Figure 6-4: Flexural reliability index.

Once the critical section was determined, a second analysis was performed, focusing on 10 sections around the critical section, the full capacity was assumed and the number of trials was increased to 2 million. The results of this analysis are shown in Figure 6-5.

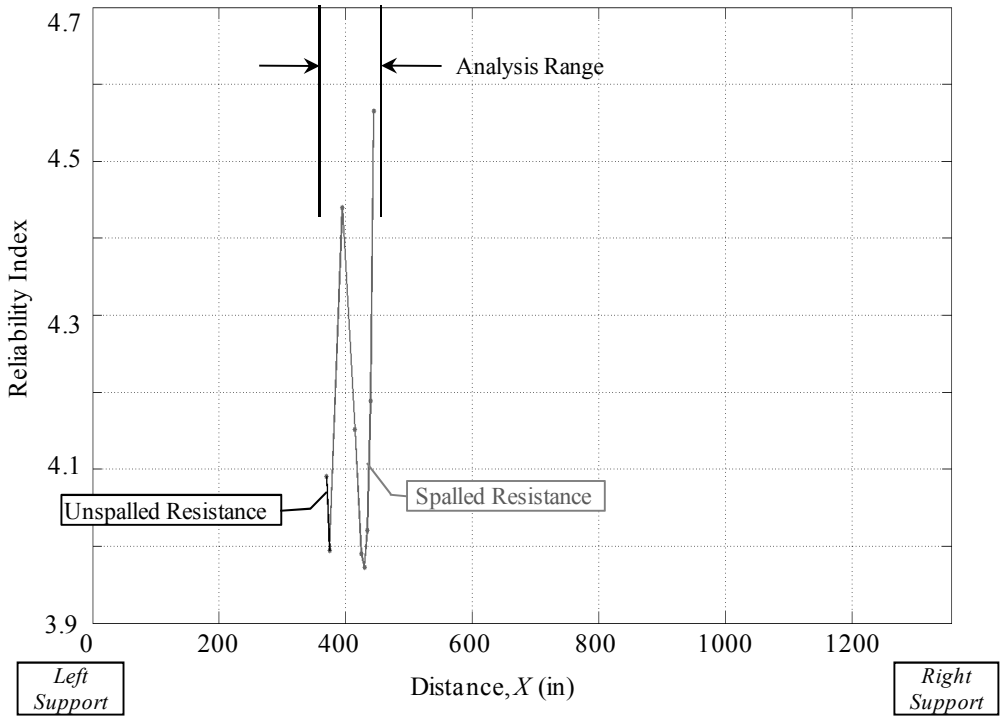

Figure 6-5: Reliability Index determined by MCS analysis at critical section.

In this analysis, at the critical section a minimum reliability index of 3.973 was calculated. Therefore, this value is the lower bound reliability of the girder analysed.

Section 3.6 of this thesis proposes an approximate reliability analysis, based on CAN/CSA S6. The results of the MCS analysis and approximate analysis are both summarized on Table 6.4 and compared graphically in Figure 6-6.

Table 6.4: Critical section in flexure reliability: Analysis summary.

Analysis	Exposure	Min. R.I.	Location	Failures (in $2 \cdot 10^6$ trials)
Approx. Analysis	Unspalled	6.86	979.2	N/A
	Spalled	5.961	377.8	N/A
MCS Analysis	Unspalled	3.994	374.5	65
	Spalled	3.973	429.5	71

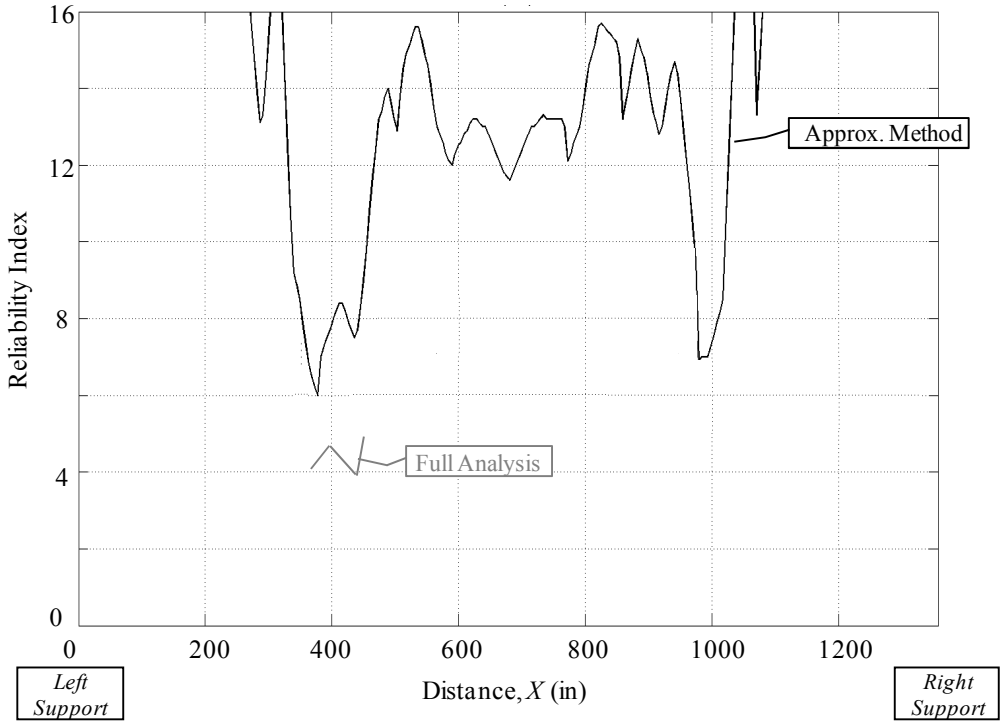

Figure 6-6: MCS vs. approximate reliability analysis for flexure.

The results indicate an approximate-to-actual ratio of 1.50. Although the general trends are similar for both models, the approximate method is unconservative. It is expected that, in reality, the MCS is detecting and including additional sources of uncertainty that the approximate method doesn't. These might include conservatism in the development length calculation and discrepancy between load or resistance factors and the actual statistical data for each. In addition, the simplified method assumes normal distributions for each load effect component. These are varied for the Monte-Carlo simulation.

6.4.2 Single Girder: Shear Simplified Method

The MCS analysis was repeated for the simplified shear method presented in Section 3.5.2. Sufficient failures were reached within 100,000 trials analysed at 100 sections along the girder length and, as a result, scaling of either the load effect or capacity was not required. The probabilities of failure and reliability indices determined by this analysis are presented in Figure 6-7 and Figure 6-8, respectively.

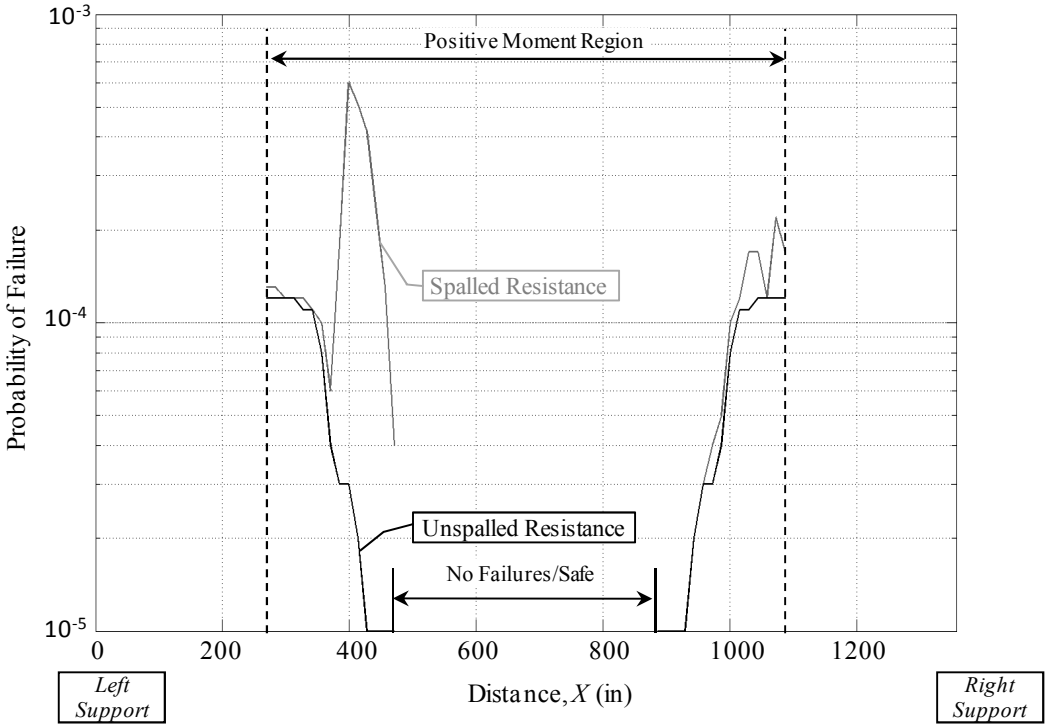

Figure 6-7: Probability of failure for shear (Simplified Method) using MCS.

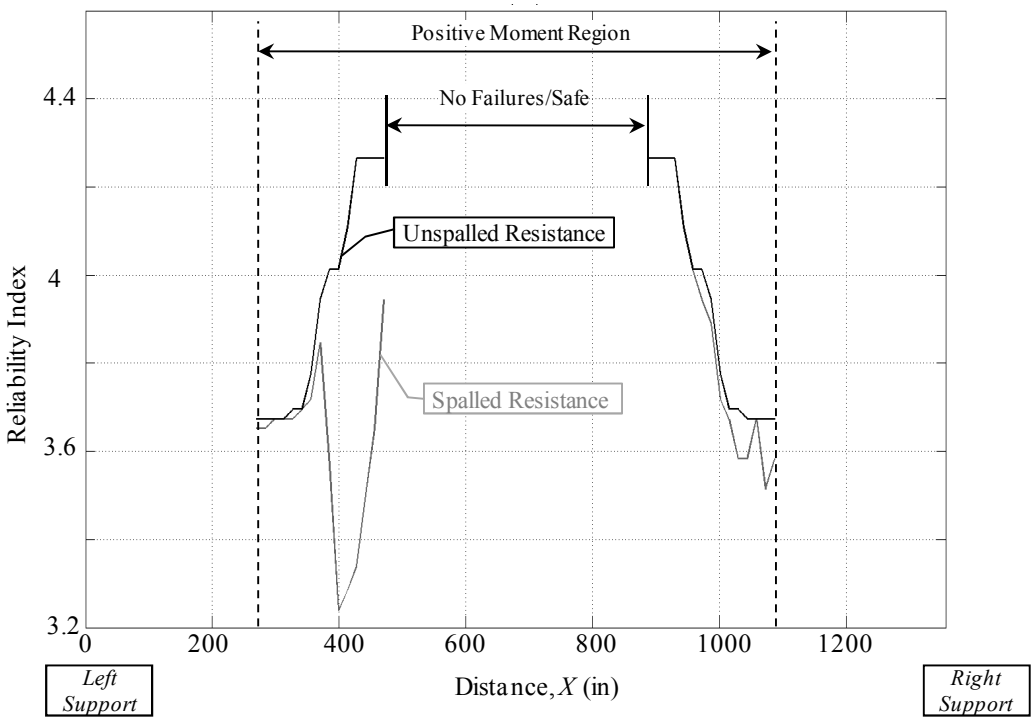

Figure 6-8: Reliability Index for shear (Simplified Method) using MCS.

A minimum reliability index of 3.239 was simulated by MCS at the critical section. A clear distinction between the spalled and unspalled analyses is apparent. Again, the results for the critical section analysis are summarized in Table 6.5.

Table 6.5: Critical section in shear (Simplified Method) reliability: Analysis summary.

Analysis	Exposure	Min. R.I.	Location	Failures (in 10^5 trials)
Approx. Analysis	Unspalled	4.54	1017	N/A
	Spalled	3.40	416.3	N/A
MCS Analysis	Unspalled	3.673	270-313 & 1044-1087	12
	Spalled	3.239	398.9	60

Comparing the results, the approximate-to-actual analysis ratio is approximately 1.05 and the location of the critical section appears to be very well estimated. Figure 6-9 directly compares the MCS and approximate analysis with very good correlation observed.

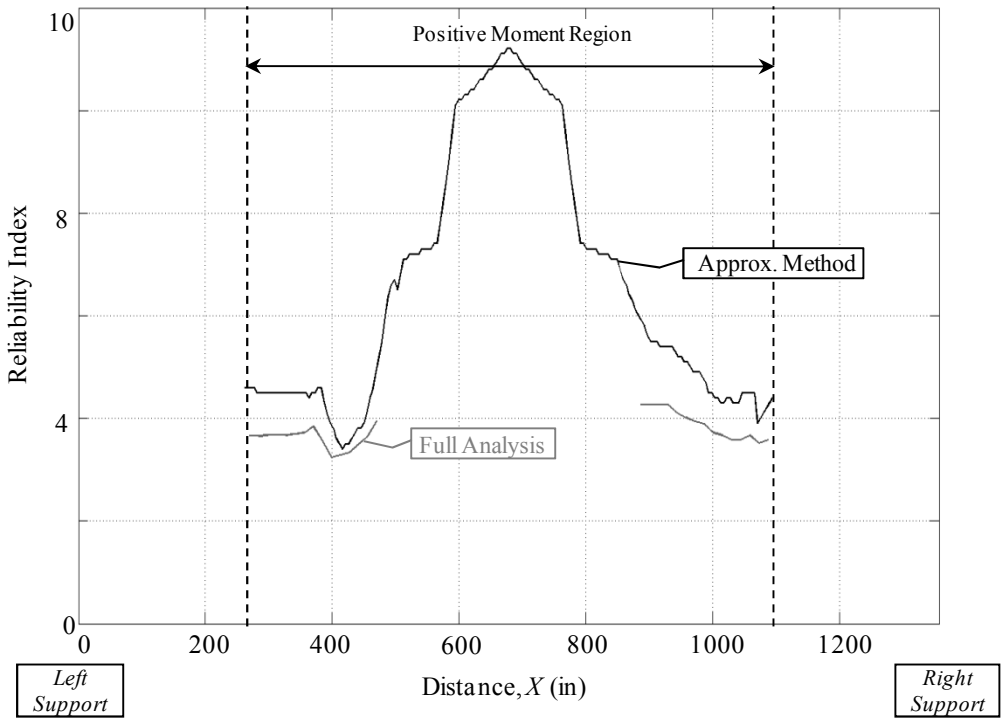

Figure 6-9: Full vs. approximate reliability analysis for Simplified Shear Method.

6.4.3 Single Girder: Shear General Method

Finally, the analysis was repeated for the General Method for shear design proposed in Section 3.5.3. Once again, the resistance had to be scaled down to induce failures and identify the critical section. For this analysis, as shown in Figure 6-10, the capacity was scaled down by a factor of 0.3.

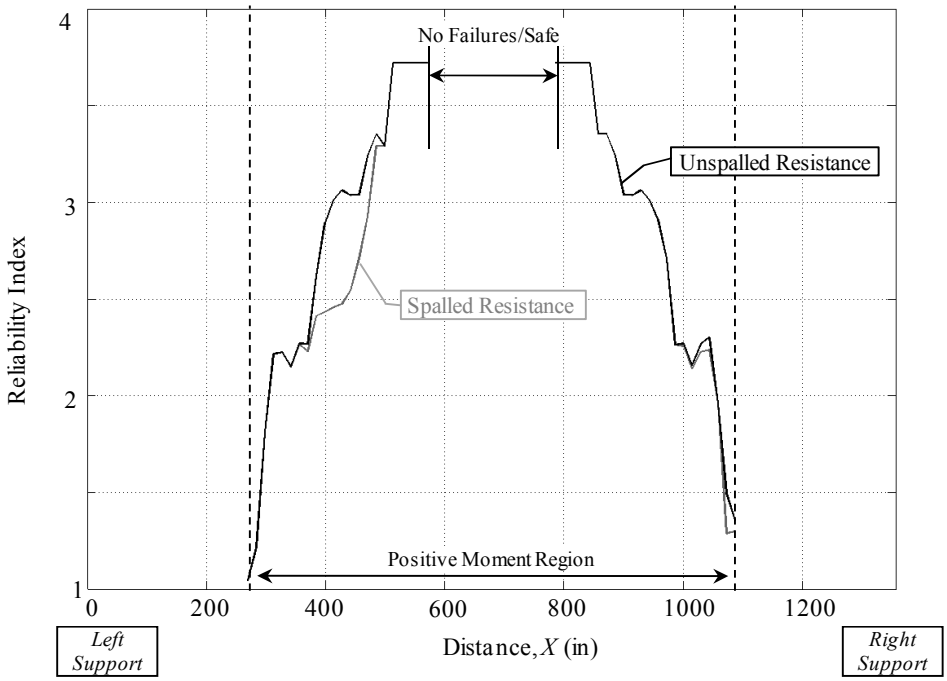

Figure 6-10: Shear (General Method) reliability index.

Focusing the analysis on the identified critical locations did not improve the simulation and the result was zero failures in 2 million trials. The analysis was abandoned on the basis that the reliability index was greater than 4.89 (the index corresponding to one failure in two million trails) since no failures occurred on the simulations of this size.

Table 6.6: Critical section in shear (General Method) reliability analysis summary.

Analysis	Exposure	Min. R.I.	Location	Failures (in $2 \cdot 10^6$ trials)
Approx. Analysis	Unspalled	3.96	262.4	N/A
	Spalled	3.96	262.4	N/A
Full Analysis A	Unspalled	>4.89	1096	0
	Spalled	>4.89	261.3	0

In fact, the approximate analysis does a good job of suggesting a high index for this case but fails to accurately predict the reliability index.

6.4.4 Single Girder: Total Reliability

The reliability of this girder is governed by shear. Overall, the approximate method estimated the index within an *Approximate:Actual* analysis ratio of 1.05. From this MCS analysis, the reliability index determined (3.239) is less than the target reliability index of 3.5 calculated in Section 3.6.1 using CSA/CAN-S6.06. Likewise, the approximate analysis prediction of 3.4 is consistent with the MCS index and does not meet this target. Interestingly, for the unspalled girder, the index (3.67) exceeds the target and therefore when longitudinal reinforcement is exposed this girder can be deemed insufficient due to the deterioration.

It should be noted, however, that theoretically, both shear methods should generate equal reliability indices. It is concluded that the reliability analysis based on the General Method needs to be further examined to find an exploration for this discrepancy.

In a practical sense, a deterministic approximation of the reliability index may be more useful than one based on the approximate reliability analysis. Such an approximation would allow an evaluator to use a reliability index for comparisons between structures and the target index defined by CSA/CAN S6-06. Repairs and replacements could be prioritized based on this index and a limiting criterion. In Figure 6-11, the results of the full reliability analysis are compared to the deterministic resistance ratio (resistance ÷ load effect). There appears to be a linear relationships between the resistance ratio and reliability index for both flexure and shear (based on the Simplified Method for the shear design).

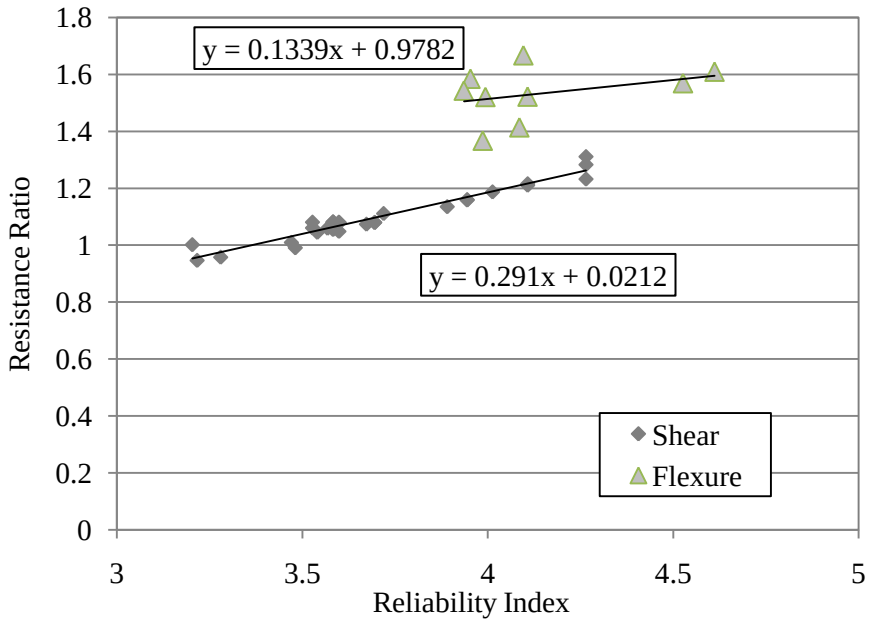

Figure 6-11: Resistance ratio and reliability index for flexure and shear.

The relationship may also be consistent enough for a single relationship to represent both flexural and shear results as shown in Figure 6-12.

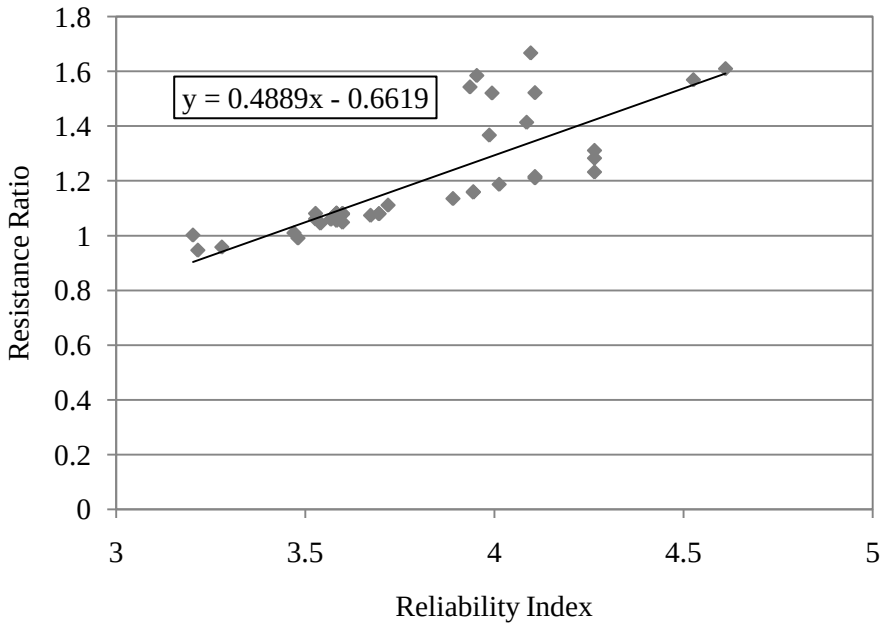

Figure 6-12: Resistance ratio and reliability index for both analyses.

The presented analysis is only for Girder 2. To establish an empirical relationship that can be used for a wider range of structure configurations, loading conditions and spalling scenarios, a larger number of comparisons are required.

Chapter 7

Conclusions and Recommendations

7.1 Conclusions

The conclusions presented in this chapter were drawn from: (1) the deterministic analysis presented in Chapters 3 and 4, (2) the laboratory study presented in Chapter 5, and, (3) the probabilistic (reliability) analysis presented in Chapter 6 of this thesis.

7.1.1 Deterministic Analysis

Based on the deterministic analysis presented herein, the following conclusions are drawn:

- When sections of reinforced concrete (RC) bridge girder reinforcement are exposed, development becomes critical and in many cases the required development length may no longer be provided.

- For the investigated case study bridge, the remaining structural capacity is directly related to the spatial distribution of the spalling relative to bar cutoffs and splices.

- The modified area concept offers a viable method for estimating an RC girder's flexural or shear strength when full development is no longer provided.

- A multi-point analysis program, employing the modified area method, offers a viable tool for the rapid assessment of spalled RC bridge girders.

- In general, the consideration of system effects improves the bridge condition estimate, since the spalled regions will generally vary from one girder to the next.

- The proposed full bridge analysis utilized by the program BEST efficiently considers system effects and strength deficiencies that arise from adjacent deteriorated RC girders, considering the pattern of deterioration across the structure.

- Rebar section loss and bond deterioration can also be considered in the analysis by incorporating existing empirical models of these effects. In general, lower calculated resistance ratios will result when these effects are included in the analysis.

7.1.2 Laboratory Work

The following conclusions were drawn from the pilot laboratory study:

- The BEST computer program provides accurate (and conservative) estimates for the strength of the test specimens with exposed reinforcement.

- The symmetry of spalling (or lack thereof) along a beam or about a point of loading likely does not affect the strength if development length is compromised.

- If development is provided, arch action can create a shift from shear failure to concrete crushing. High ductility can provide adequate warning of failure.

- Intact sections centred under the load point may act like a pivot and do not fully contribute to bond. On real bridges, symmetric spalling is improbable and under a moving truck load these sections may engage when the truck is in other positions.

- Intact sections with a length and depth of spalling resulting in premature local shear failure (such as Beam 6) can only be partially counted on for bond. As a conservative estimate, these sections may be ignored. Further work is required to establish length limits for unspalled sections to be considered in the development length calculation that could be implemented in the BEST computer program.

- Both SikaTop 123 and Sikacrete-08 SCC appear to effectively restore bond and member strength over spalled sections.

- When spalled region repairs are applied to a relatively weak substrate concrete, the increase in tension stiffening can result in increased member stiffness.

7.1.3 Reliability Analysis

The following conclusions were drawn from the reliability analysis:

- Statistical parameters were derived for the probabilistic evaluation of any RC bridge. This analysis uses statistical distributions as professional factors associated with CAN/CSA code equations for flexure, shear, and development length in a probabilistic study.

- Based on comparisons with the Monte-Carlo analysis, the approximate reliability analysis presented herein, appears to provide a viable estimate of the reliability of a spalled bridge structure deterministically.

- With a broader range of studies, an empirical relationship between the deterministic resistance ratio and the reliability index may be established. A formula based on the deterministic resistance ratio such as the one presented herein could allow bridge evaluators to quickly assess and compare structures, prioritizing repairs and replacements based on the deterministic reliability index.

7.2 Recommendations for Future Work

To further advance this field of the study, a number of possibilities have been identified.

7.2.1 Further Development of BEST Computer Program

The BEST computer program presented herein requires further development, before it can be considered an industry-ready tool. The following advancements are recommended:

- To evaluate the potential of the program, a multi-span conventionally RC bridge with spalling could be analyzed using the existing program. A number of critical sections could arise for such a structure if concrete surrounding the soffit steel is removed or deteriorated.

- At this time, the program does not consider the combined influence of axial load and flexure that occurs in rigid frame structures (such as the case study structure). In this regard, it is conservative. Code provisions for considering combined load effects, including axial load, can easily be added to the current program, however

- The models for the effects of corrosion on bond strength and section loss can also be improved. For example, analytical models for the rebar bond strength in cracked concrete could be modified with corrosion parameters to better predict the bond strength between rebar and corroded concrete in intact sections.

- The program could be adapted to analyze 2-way slab or prestressed concrete bridges.

- Finally, a graphical user interface can easily be developed for the program. Easy to use displays for input fields would increase the appeal of the program to potential users.

7.2.2 Extension of Laboratory Studies

The BEST computer program should be further validated by expanded laboratory investigations. In the next round of laboratory testing, the following could be studied:

- Separate sets of flexure and shear sensitive beams should be designed. Simply comparing the strengths of spalled specimens with different levels of transverse reinforcement should indicate the role (if any) of transverse reinforcement on the strength of a beam with development deficiencies.

- The statistical significance of the results for each spalling configuration should be confirmed by expanding the number of test specimens. Ideally, specimens could be designed to reduce the impact of confining stress above supports. For example a splice within the span may be used to remove this source of inaccuracy.

- Further examination of intact section lengths could be used to develop an analytical model to relate bond strength to concrete strength and section length. Specimens similar to that shown in Figure 7-1 could be tested. The results of these tests could be used to generate intact length limits for BEST.

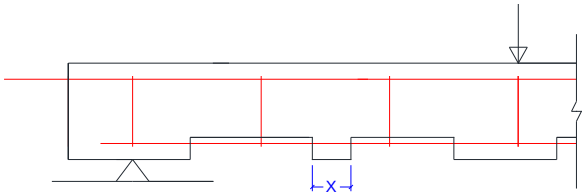

Figure 7-1: Specimen design for intact length (*X*) analysis.

- Further tests could examine partial spalling situations such as those in Figure 7-2. The results of such tests could be directly compared to BEST predicted strengths.

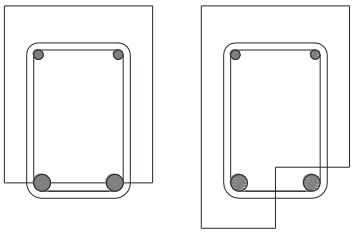

Figure 7-2: Test specimen for partial spalling evaluation.

7.2.3 Further Investigation of Rehabilitation Methods

Further research could be dedicated to investigating the effectiveness of rehabilitation methods. There is significant work required before SCC, mortar patches or FRP repairs are accepted as short term repair methods for restoring anchorage and strength. Even more work is required before they can be accepted as durable long term solutions.

Test specimens can be easily redesigned to analyze different spalling situations where the repair restores bond, completes splice, or restores shear strength. Although mortar and SCC

products restored bond and strength on the beams tested, they did not complete a splice. Specimens, such as that shown in Figure 7-3, represent a more realistic case.

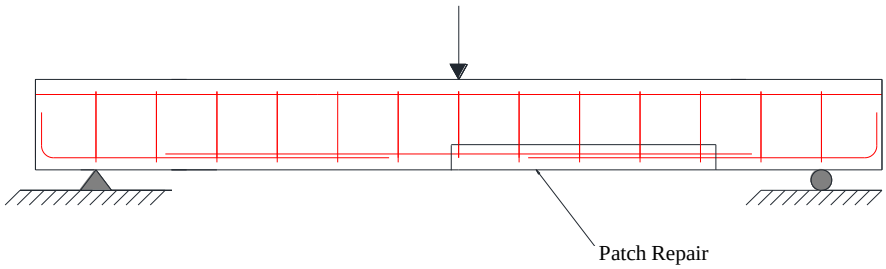

Figure 7-3: Proposed detail for splice repair evaluation.

A potential area of concern is the durability of patch materials. Repair materials are often subject to rapid deterioration due to corrosion, accelerated by corrosion products cast or trapped within the repair, and extensive cracking. Often high strength repairs show extensive flexural cracking as well as cracking relative to the substrate material due to material property differentials.

7.2.4 Improvements in Corrosion Measurement

There currently is a shortage of quick, useful methods for measuring corrosion effects on RC structures. For the BEST computer program to be a realistic representation of the corroded strength of a deteriorated bridge, there needs to be improved means of accurately approximating the degree of corrosion in-situ. The following potential avenues could be explored:

- Within spalled sections, if the corrosion appears to be uniform, then potentially a caliper can accurately measure the degree of corrosion. Field trials could be compared to extracted samples measured in the lab using the displaced water technique. If pitting corrosion is evident, then a dial gauge similar to the one proposed conceptually in Figure 7-4 may be useful.

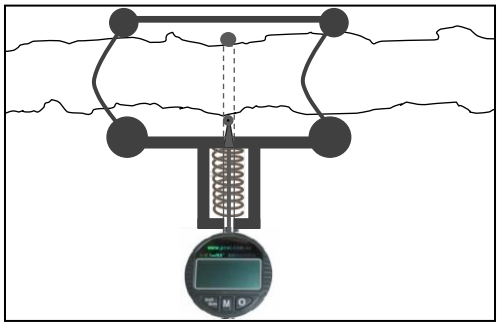

Figure 7-4: Concept for reinforcement corrosion pit gauge.

- For corrosion levels less than 10% section loss (due to accuracy concerns) perhaps, Nondestructive testing (NDT) methods such as ground penetrating radar (GPR) or eddy current techniques could be explored.

- For intact sections, a study could examine test specimens artificially corroded to relate the degree of corrosion with the first appearance of longitudinal cracking or crack width. Surface staining could be another clue to the degree of corrosion within intact sections.

- An alternative study could examine the degree of corrosion on sections taken from a decommissioned structure or a structure recently scaled in an attempt to relate the level of corrosion within intact sections to that of exposed reinforcement as a function of the amount of time the steel has been exposed.

Figure 7-5: Corrosion cracking, surface staining and section loss.

7.2.5 Effect of Corrosion on Other Components

There are legitimate concerns about the impact of corrosion on parts of the structure other than girder soffits. MTO officials have highlighted significant concerns about slab spalling.

In many cases, the severity has reached levels in which truck wheels are creating localized failure of the slab and falling through, as shown in Figure 7-6.

Future studies could examine the following:

- Examine localized spalling on bridge slabs and attempt to evaluate its impact on the global behaviour of the structure. Perhaps limits could be established with regards to a maximum spalled slab area before the global strength of the slab is compromised.
- MTO has also indicated a need for improved slab repair methods that are well anchored and not susceptible to "push-out" failure. Research is required for quick and durable repair methods.

Figure 7-6: Severe slab spalling (MTO).

In addition, there also exists a potential that girder compressive zones are deteriorated and concrete sections may be lost from these sections. For the case study structure, it was noted that the majority of corrosion was accelerated by salt spray from trucks. This spray hits the girders at an angle and in most cases does not reach the compressive concrete. However, this may not be the case for every structure, especially multi-span RC bridges where compressive concrete may be subject to high levels of corrosion. On a conventional RC bridge, corrosion can also be accelerated by poor drainage of chlorides applied to the bridge deck. Future work could investigate actual structures for concrete section loss at these other locations and, if necessary, simply add these effects to the existing BEST computational framework.

Bibliography

ACI Committee 222. 1988. Corrosion of metal in concrete. American Concrete Institute manual of concrete practice: Part 1. Detroit, USA, ACI 222R-85.

Al-Sulaimani, K., Basunbul M., and Rasheeduzzafar, I.A.1990. Influence of corrosion and cracking on bond behaviour and strength of reinforced concrete members. American Concrete Institute Structural Journal, **87**(2)**:** 220–231.

Amey, S. L., Johnson, D. A., Miltenberger, M. A., and Farzam, H. 1998. Temperature dependence of compressive strength of conversion-inhibited high alumina cement concrete. American Concrete Institute Structural Journal, **95**(1): 27-36.

Andrade, C. 1993. Calculation of chloride diffusion coefficients in concrete from ionic migration measurements. Cement and Concrete Research, **23(**3): 724–742.

Andrade, C., Alonso, C., Garcia, D., and Rodriguez, J. 1991. Remaining lifetime of reinforced concrete structures: effect of corrosion in the mechanical properties of the steel. *In* Proceedings of the International Conference on Life Prediction of Corrodible Structures, Cambridge, UK., 23-26 September 1991. National Association of Corrosion Engineers. pp. 12/1-12/11.

Auditor general report, 2009. 3.02 Bridge inspection and maintenance, Office of the Auditor General of Ontario. December 7 2009.

Azam, R. 2010. Behaviour of Shear Critical RC Beams with Corroded Longitudinal Steel Reinforcement. M.Sc. thesis, Department of Civil and Environmental Engineering, The University of Waterloo, Waterloo, Ont.

Bailey, S.F. 1996. Basic principles and load models for the structural safety evaluation of existing road bridges. Ph.D. Thesis No. 1467, École Polytechnique Fédérale de Lausanne, Switzerland.

Ballim, Y. and Reid, J.C. 2002. Reinforcement corrosion and the deflection of RC beams - an experimental critique of current test methods. Cement and Concrete Composites, **25**(6):635-632.

Bartlett, M. 2010. Behaviour of Partially-Repaired Reinforced Concrete T-Beams. Unpublished.

Bartlett, M.F. and MacGregor. J.G. 1994. Assessment of concrete strength in existing structures. Structural Engineering Report No. 198. University of Alberta, May 1994.

Bazant, Z. P. 1979. Physical model for steel corrosion in concrete sea structures-theory. ASCE Journal of Structural Division, **105**(6): 1137–1153.

Bentz, E.C. 2010. MC2010: Shear strength of beams and implications of the new approaches. *In* FIB/CEB Bulletin 57: Shear and punching shear in RC and FRP Elements, Proceedings of an International Conference, Salo, Italy, 15–16 October 2010, pp. 15–31.

Bentz, E. 2006. Summary of Development and Use of CSA 2004 Shear Design Provisions. *In* Advances in Engineering Structures, Mechanics. *Edited by* M. Pandey et al. Springer, Netherlands. pp. 67-80.

Berto, L., Simioni, P. and Saetta, A. 2008. Numerical modelling of bond behaviour in RC structures affected by reinforcement corrosion. Engineering Structures, **30**(5): 1375–1385.

Bhargava, K., Ghosh, A.K., Mori, Y., and Ramanujam, S. 2007. Corrosion-induced bond strength degradation in reinforced concrete - analytical and empirical models. Nuclear Engineering and Design, **237**(11): 1140-1157.

Cabrera, J.G. 1996. Deterioration of concrete due to reinforcement steel corrosion. Cement and Concrete Composites, **18**(1): 47–59.

Cabrera, J.G., and Ghoddoussi, P. 1992. The effect of reinforcement corrosion on the strength of the steel concrete bond. *In* Proceedings of the International Conference on Bond in Concrete, Riga, Latvia, 15-17 October 1992. pp. 10/11–10/24.

Cairns, J. and Abdullah, R.B. 1996. Bond strength of black and epoxy-coated reinforcement—a theoretical approach, ACI Materials Journal, **93**(4): 362–369.

Cairns, J. and Zhao, Z. 1993. Behaviour of concrete beams with exposed reinforcement. *In* Proceedings of the Institution of Civil Engineers – Structures and Buildings, **99**(2) May 1993. Institution of Civil Engineers, London, UK, pp. 141-154.

Cairns, J., Du, Y.G. and Law, D. 2005a. Criteria for and prediction of limit states of degradation of reinforced concrete structures. *In* Proceedings of 6th International Conference: Global Construction: Ultimate Concrete Opportunities, Dundee, UK, 5-7 July 2005.

Cairns, J., Plizzari G., Du, Y.G., Law, D.W., and Franzoni, C. 2005b. Mechanical properties of corrosion damaged reinforcement. American Concrete Institute Structural Journal, **102**(2): 256-264.

Cairns, J., Du, Y.G. and Law, D. 2008. Structural performance of corrosion-damaged concrete beam. Magazine of Concrete Research, **60**(5): 359-370.

Canadian Standards Association. 2004. CSA Standard A23.3-04: Design of Concrete Structures. Mississauga, O.N.

Canadian Standards Association. 2006. CAN/CSA S6-06: Canadian Highway Bridge Design Code. Mississauga, O.N.

Canadian Standards Association. 2007.Calibration report for CAN/CSA-S6-06: Canadian highway bridge design code.

Cheung, M.S. and Li, W.C. 2002. Reliability assessment in highway bridge design. Canadian Journal of Civil Engineering, **29**:799-805.

Chung, L., Cho, S.H., Kim, J.H.J., and Yi, S.T. 2004. Correction factor suggestion for ACI development length provisions based on flexural testing of RC slabs with various levels of corroded reinforcing bars. Engineering Structures, **26**(8): 1013–1026.

Clark, L.A., and Saifullah, M. 1994. Effect of corrosion rate on the bond strength of corroded reinforcement, *In* Corrosion and Corrosion Protection of Steel in Concrete, *Edited by* R. N. Swamy, Sheffield Academic Press, Sheffield, UK. pp. 591-602.

Collins, M.P., Bentz, E.C. and Sherwood, E.G. 2008. Where is shear reinforcement required? Review of research results and design procedures. ACI Structural Journal, **105**(5), 590-600.

Collins, M.P., Mitchell, D., Adebar, P.E. and Vecchio, F. J. 1996. A general shear design method. ACI Structural Journal, **93(**1): 36-45.

Comite Eurointernational du Beton (CEB), Federation Internation du Beton (FIB), 2000. Bond of Reinforcement in Concrete: State-of-Art, Bulletin No. 10.

Coronelli, D. 2002. Corrosion cracking and bond strength modeling for corroded bars in reinforced concrete. American Concrete Institute Structural Journal, **99**(3): 267–276.

Council of the Federation, 2005. Looking to the Future: A Plan for Investing in Canada's Transportation System [online]. Available from www.councilofthefederation.ca/ [cited April 27 2011].

CRSI. 2001. Evaluation of reinforcing bars in old reinforced concrete structures. Engineering Data Report Number 48. Concrete Reinforcing Steel Institute.

Du, Y. 2001. Effect of Reinforcement Corrosion on Structural Concrete Ductility. PhD thesis, Department of Civil Engineering, University of Birmingham, Birmingham, UK.

Ellingwood, B.R., Galambos, T.V., MacGregor, J.G. and Cornell, C.A. Development of a probability-based load criterion for American National Standard A58. National Bureau of Standards Special Publication 577, US Government Printing Office, Washington, DC, 1980.

El-Maadawy, T. and Soudki, K.A. 2007. A Model for Prediction of Time from Corrosion Initation to Corrosion Cracking. Cement and Concrete Composites, **29**(3): 168-175.

GEOCISA, Torroja Institute, 2001. CONTECVET: A validated user's manual for assessing the residual service life of concrete structures. British Cement Association et al., Madrid, Spain.

Hansson, C. M., Poursaee, A. and Laurent, A. 2006. Macrocell and microcell corrosion of steel in OPC and high performance concrete. Cement and Concrete Research, **36**(11): 2098–2102.

Hansson, C. M., Poursaee, A. and Jaffer, S. J. 2007. Corrosion of reinforcing bars in concrete. Available from the Portland Cement Association, Illinois USA, R&D Serial No. 3013.

Hope, B.B. and Ip, A.K.C. 1987. Chloride corrosion threshold in concrete. American Concrete Institute Materials Journal, **84**(4): 306–314.

Israel, M. S. 1986. Probabilistic basis of partial resistance factors for use in concrete design. Thesis. Johns Hopkins University.

Lee, H.S., and Cho, Y.S. 2009. Evaluation of the mechanical properties of steel reinforcement embedded in concrete specimen as a function of the degree of reinforcement corrosion. International Journal of Fracture, **157**(1): 81-88.

Lee, H.S., Tomosawa, F., and Noguchi, T. 1996. Effect of rebar corrosion on the structural performance of singly reinforced beams. *In* Durability of Building Materials and Components. *Edited by* C. Sjostrom. E&FN Spon, London. pp. 571-580.

Lee, H.S., Noguchi, T., and Tomosawa, F. 2002. Evaluation of the bond properties between concrete and reinforcement as a function of the degree of reinforcement corrosion. Cement and Concrete Research, **32**(8): 1313–1318.

Li, C., Zheng, J., Lawanwisut, W. and Melchers, R.E. 2007. Concrete delamination caused by steel reinforcement corrosion. Journal of Materials in Civil Engineering, **19**(7): 591–600.

Liang, M.T., Lin, L.H., and Liang, C.H. 2002. Service life prediction of existing reinforced concrete bridges exposed to chloride environment. ASCE Journal of Infrastructure Systems, **8**(3): 76–85.

Litvan, G.G., 1972. Phase Transitions of Adsorbates, IV: Mechanism of Frost Action in Hardened Cement Paste. Journal of the American Ceramic Society, **55**(1): 38-42.

MacGregor, J.G. 1976. Safety and limit states design for reinforced concrete. Canadian Journal of Civil Engineering. **3**(4):484-513.

Melchers, R. 2002. Structural reliability analysis and prediction, 2nd Edition. John Wiley & Sons.

Mindess, S. and Young, J.F. 1981. Concrete. Prentice-Hall, Inc., Englewood, N.J.

Mirza, S.A. and MacGregor, J.G. 1982. Probabilistic study of strength of reinforced concrete members. Canadian Journal of Civil Engineering. **9**(43):1-48.

Morinaga, S. 1996. Remaining life of reinforced concrete structures after corrosion cracking. *In* Durability of Building Materials and Components. *Edited by* C. Sjostrom. E&FN Spon, London. pp. 127-137.

Nowak, A.S. and Grouni, H.N. 1994. Calibration of the Ontario highway bridge design code 1991 edition. Canadian Journal of Civil Engineering, **21**: 25–35

Nowak, A.S. and Kulicki, J.M. 1996. New generation of U.S. bridge design codes. *In* Proceedings, IABSE Colloquium in Eurocodes, Vol. 74, Delft, The Netherlands. March 1996, pp. 535-540.

Nowak, A.S. and Szerszen, M.M. 1998. Bridge load and resistance models. Engineering Structures, **22**(11), 985-990.

Palsson, R. and Mirza, M.S. 2002. Mechanical response of corroded steel reinforcement of abandoned concrete bridge. American Concrete Institute Structural Journal, **99**(2): 157–162.

Panesar, D.K. and Bartlett, F.M. 2006. Load and resistance data for precast stringer highway bridges. Canadian Journal of Civil Engineering. Vol. 33, pp.1368-1378.

Pigeon, W. and Pleau, R. 1995. Durability of Concrete in Cold Climates. Modern Concrete Technology 4. E&FN Spon, U.K.

Poursaee, A. and Hansson, C.M. 2009. Potential pitfalls in assessing chloride-induced corrosion of steel in conrete. Cement and Concrete Composites, **39**(5):391-400.

Powers, T. C. 1945. A working hypothesis for further studies of frost resistance of concrete. Journal of the American Concrete Institute. **16**(4): 245-272.

Powers, T. C. and Helmuth, R. A. 1953. Theory of volume changes in hardened portland-cement paste during freezing. Highway Research Board Proceedings, 32: 285-297.

Renew Ontario Website, 2009 (http://www.mei.gov.on.ca/english/infrastructure/renew/).

Rezansoff, T. and Sparling, B.F. 1995. Correlation of the bond provisions of CSA A23.3-94 with tests on tension lap splices in beams. Canadian Journal of Civil Engineering, **22**(4): 755-769.

Rodriguez, J., Ortega, L., and Garcia, A. 1994. Corrosion of reinforcing bars and service life of R/C structures: corrosion and bond deterioration. *In* 'Concrete Across Borders', Proceedings of an International Conference, Odense, Denmark, 22–25 June 1993, pp. 315–326.

Rodriguez, J., Ortega, L.M. and Casal, V. 1997. Load carrying capacity of concrete structures with corroded reinforcement. Construction and Building Materials, **11**(4): 239–248.

SAP 2000 Version 12. 2009. Computers and Structures, Inc. Berkeley, California USA.

Sika Canada, 2011. Product data sheets. (available from http://can.sika.com)

Somo, S. and Hong, H. P. 2006. Modeling error analysis of shear predicting models for RC beams. Structural Safety, **28**(3), 217-230.

Stanish, K., Hooton, R., and Pantazopoulou, S. 1999. Corrosion effects on bond strength in reinforced concrete. American Concrete Institute Structural Journal, **96**(6): 915–921.

Thomas, M.D.A. and Bentz, E.C. 2000. Life-365 computer program for predicting the service life and life-cycle costs of reinforced concrete exposed to chlorides. Available from www.masterbuilders.com/support/pageEtools [cited May 25, 2011].

Tuutti, K. 1982. Corrosion of steel in concrete. Swedish Cement and Concrete Research Institute, Report 4-82, Stockholm, Sweden.

Zhang, P.S., Lu, M., and Li, X.Y. 1995. The mechanical behaviour of corroded bar, Journal of Industrial Buildings, 25(257): 41-44.

Appendix A

Appendix A-1 Structural Drawings

Appendix A-2 Spalling Surveys

Appendix A-3 Repair History

Appendix A-4 Reinforcement/Spalling Superposition

Appendix A-5 Bridge Loads

Appendix A-6 Structural Capacity

Appendix A-7 Transverse Distribution

Appendix A-8 Slab Strength

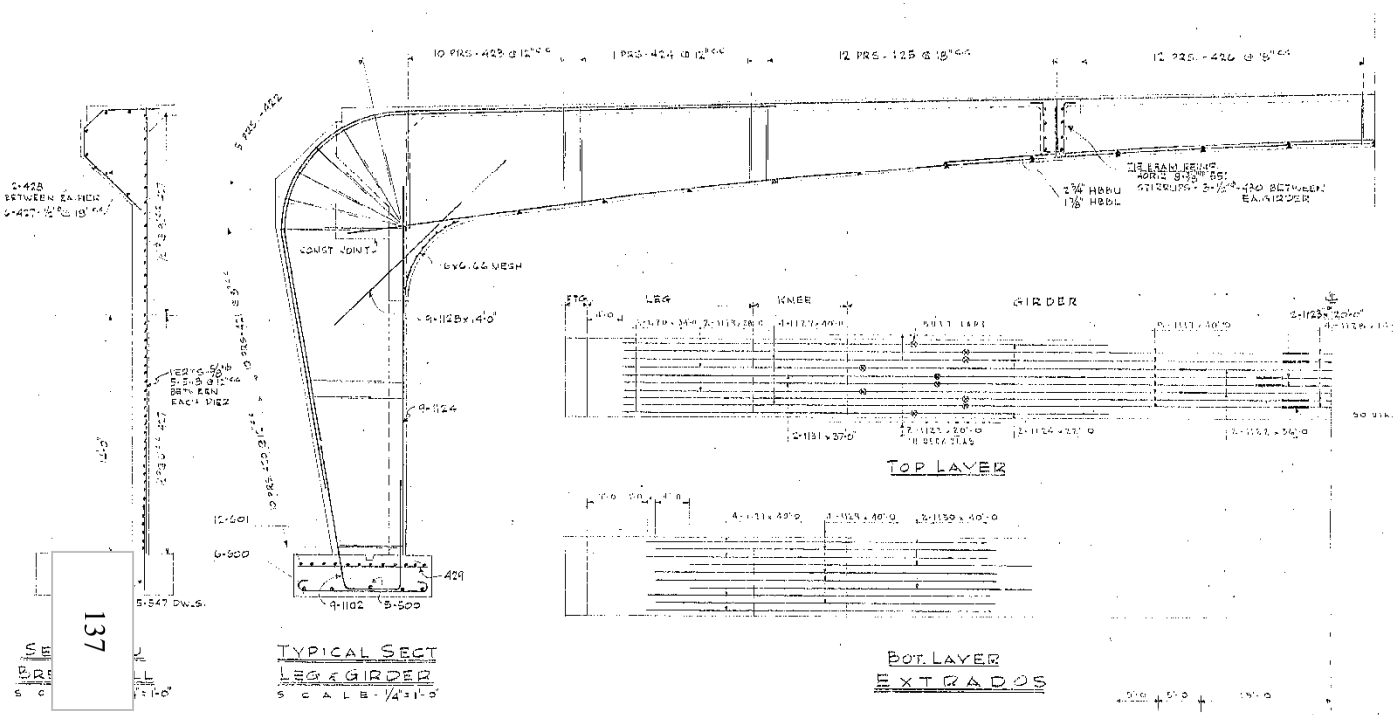

TYPICAL SECT. LEG & GIRDER
SCALE - 1/4" = 1'-0"

TYPICAL SECT. DECK & GIRDER
SCALE - 1/2" = 1'-0"

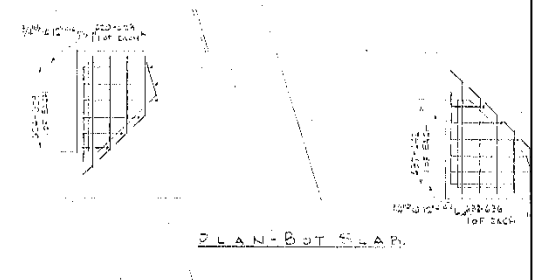

CATCH BASIN REINF.
SCALE - 1/4" = 1'-0"

DESIGN BASED ON
f'c CONC. 3000 P.S.I @ 28 DAYS
fs REINF. STEEL 20,000 P.S.I
ALL GIRDER STEEL TO BE "HI-STEEL"

REVISIONS:			
DATE	BY	DESCRIPTION	
21-5-54	RD	GIRDER STEEL REVISED	

OXFORD EAST BRIDGE
M. M. DILLON & CO. LTD.
CONSULTING ENGINEERS
LONDON, ONT. TORONTO
DEPARTMENT OF HIGHWAYS:-ONT.
BRIDGE OFFICE:-TORONTO

OXFORD EAST TOWNSHIP UNO
HIGHWAY No. 59

THE KING'S HIGHWAY No. 401
CO. OXFORD
TWP. OXFORD EAST LOT 18 & 19 CON.

REINF. PLACING - GIRDERS, DECK.

APPROVED
CHIEF BRIDGE ENGINEER CHIEF ENG.

R. M. DILLON
REGISTERED PROFESSIONAL ENGINEER
CIVIL
ENGINEER OF ONTARIO

DESIGN	R.A.C	CHECK	R.M.D	CONTRACT NUMBERS	
DRAWING	W.C.O	CHECK	A.R.		
TRACING	W.C.O	CHECK	A.R.	LOADING	STANDING NUMBER D-3439-4
DATE	MAY. 7. 1954			H20-S16	

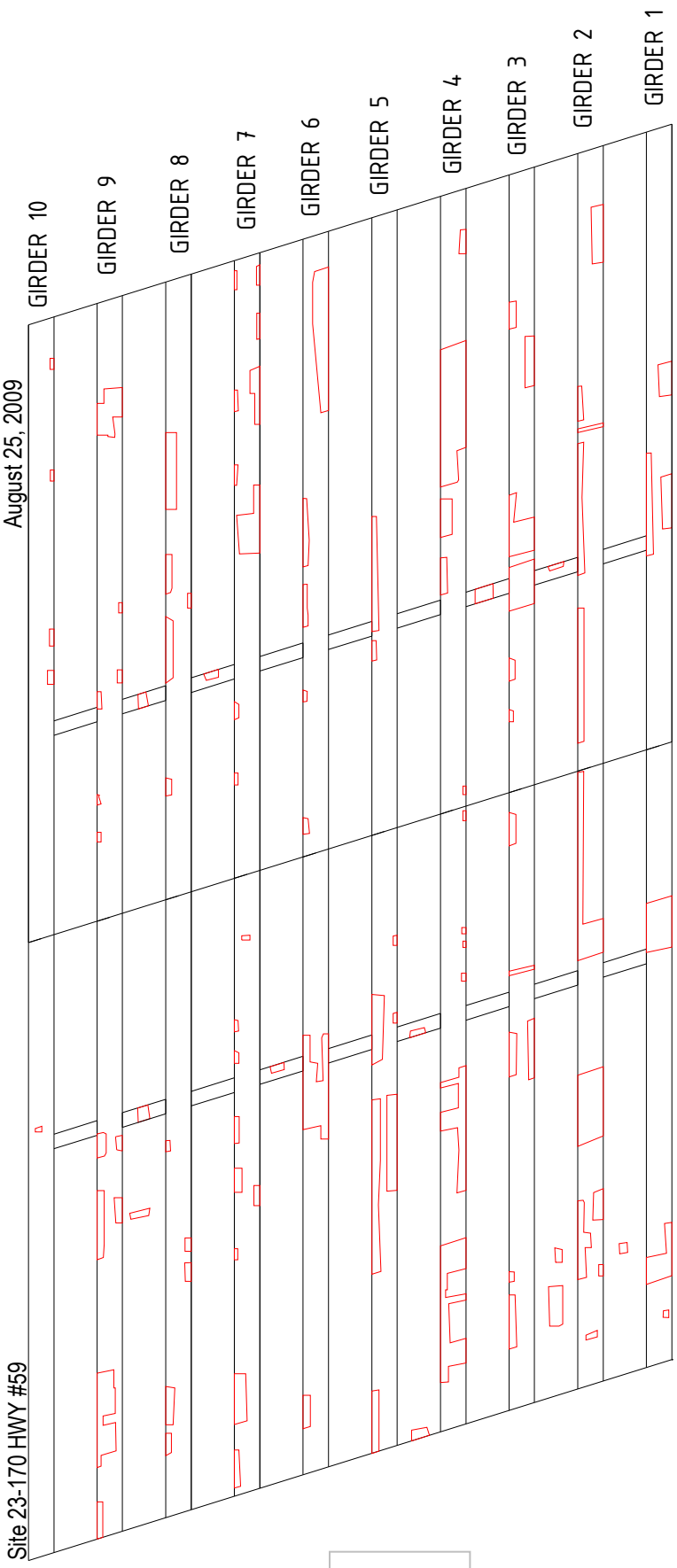

DRAWING #: 1

Aug. Spalling Survey

DRAWN BY: JL DATE: Sept. 2 2010

Site 23-170 HWY #59

July 28, 2009

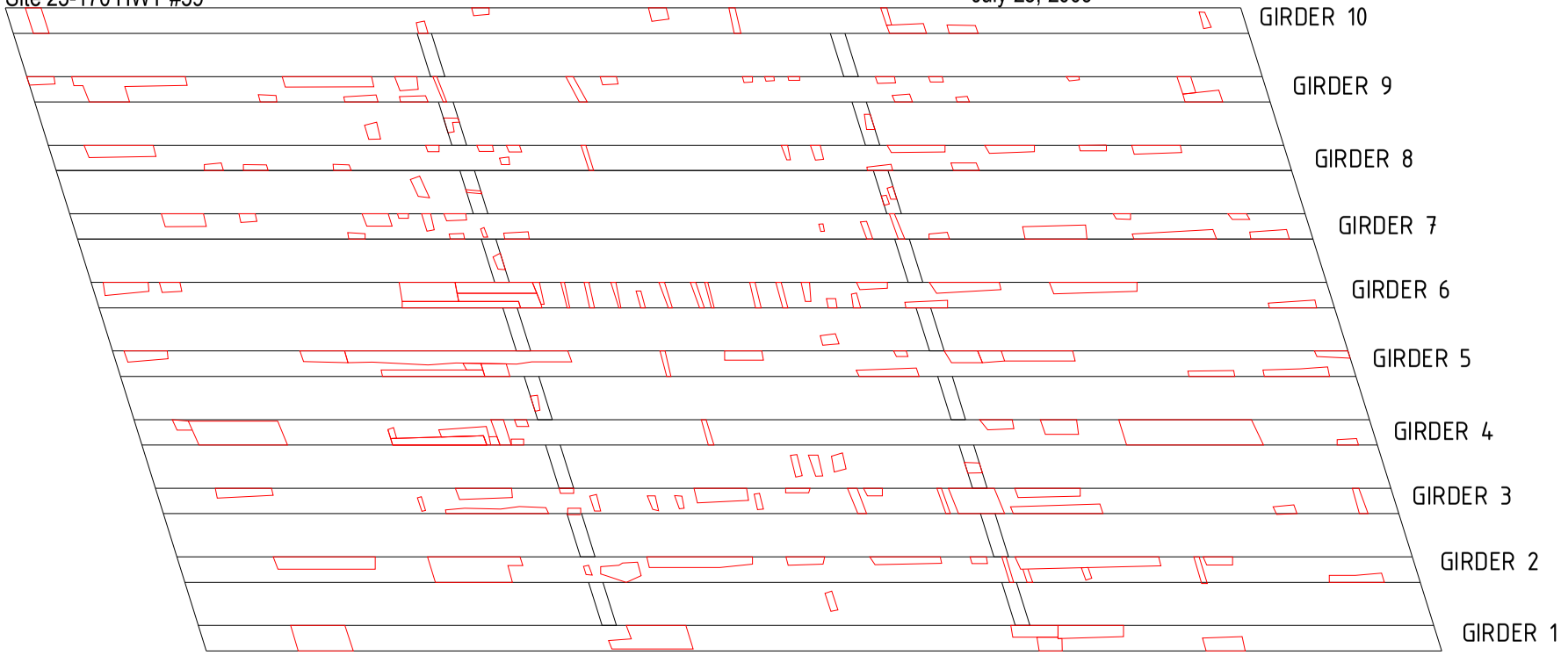

University of Waterloo

DRAWING #: 2

July Spalling Survey

DRAWN BY: JL DATE: Sept. 2 2010

METRIC

DIMENSIONS ARE IN METRES AND/OR MILLIMETRES UNLESS OTHERWISE SHOWN

CONT No 92-18
WP No 481-89-03

HIGHWAY 59 UNDERPASS STRUCTURE REHABILITATION
DECK & SOFFIT REPAIRS

SHEET 322

McCORMICK RANKIN
CONSULTING ENGINEERS

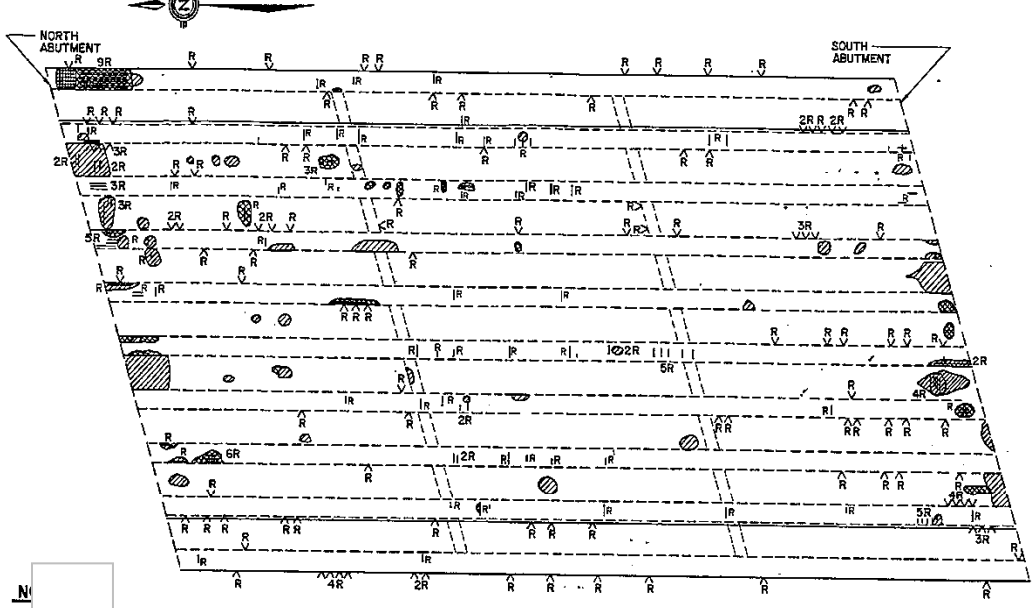

DECK SOFFIT DETERIORATION & REPAIR AREA
1:100

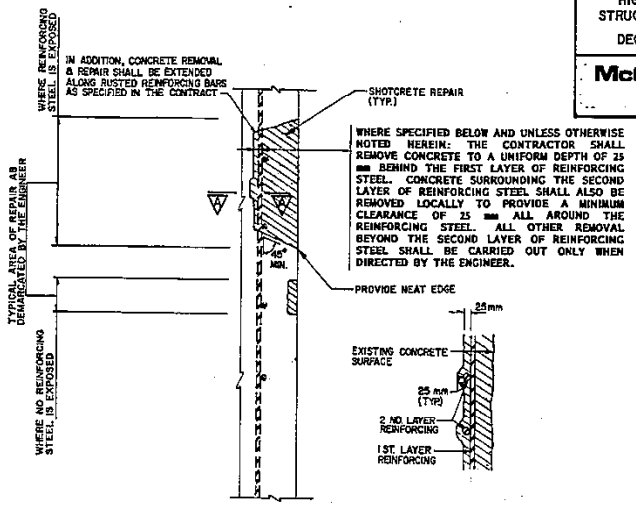

TYPICAL SHOTCRETE REPAIR DETAILS
N.T.S.

SECTION A-A
N.T.S.

140

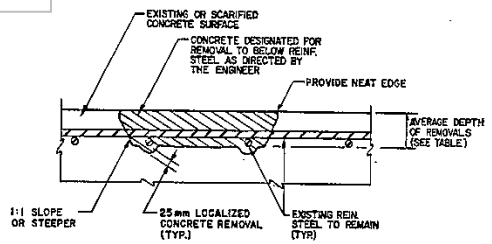

CONCRETE REMOVAL DETAIL
(DECK, SIDEWALK AND ENDPOST)
N.T.S.

NOTE:
THE MINIMUM DEPTH OF REMOVAL SHALL BE AS SHOWN IN THE DETAIL ABOVE OR AS FOLLOWS:
VERTICAL SURFACE 75mm
HORIZONTAL SURFACE (EXCLUDING DECK) 50 mm

LEGEND

- DELAMINATIONS
- SPALLS
- PATCHED AREA
- HONEYCOMBED AREA
- R EXPOSED REINFORCING STEEL (HORIZONTAL)
- R EXPOSED REINFORCING STEEL (VERTICAL)

CONCRETE REMOVAL TABLE

ITEM DESCRIPTION	COMPONENT	AREA OF REMOVAL (m^2)
CONCRETE REMOVAL — DECK SURFACE	DECK	16
	SIDEWALK	37
	END POST	7
CONCRETE REMOVAL — DECK SOFFIT	DECK/BEAMS	30
	BEAMS VERTICAL FACE	23
	ABUTMENT	15

DRAWING NOT TO BE SCALED
100 mm ON ORIGINAL DRAWING

REVISIONS

NO.	DATE	BY	DESCRIPTION

DESIGN D.G.D. | CHK R.S. | CODE OHBDC-83 | LOAD A-83 | DATE AUG. 1991
DRAWN S.F. | CHK D.G.D. | SITE 23-170 | STRUCT | SCHEME R1 | DWG. 4

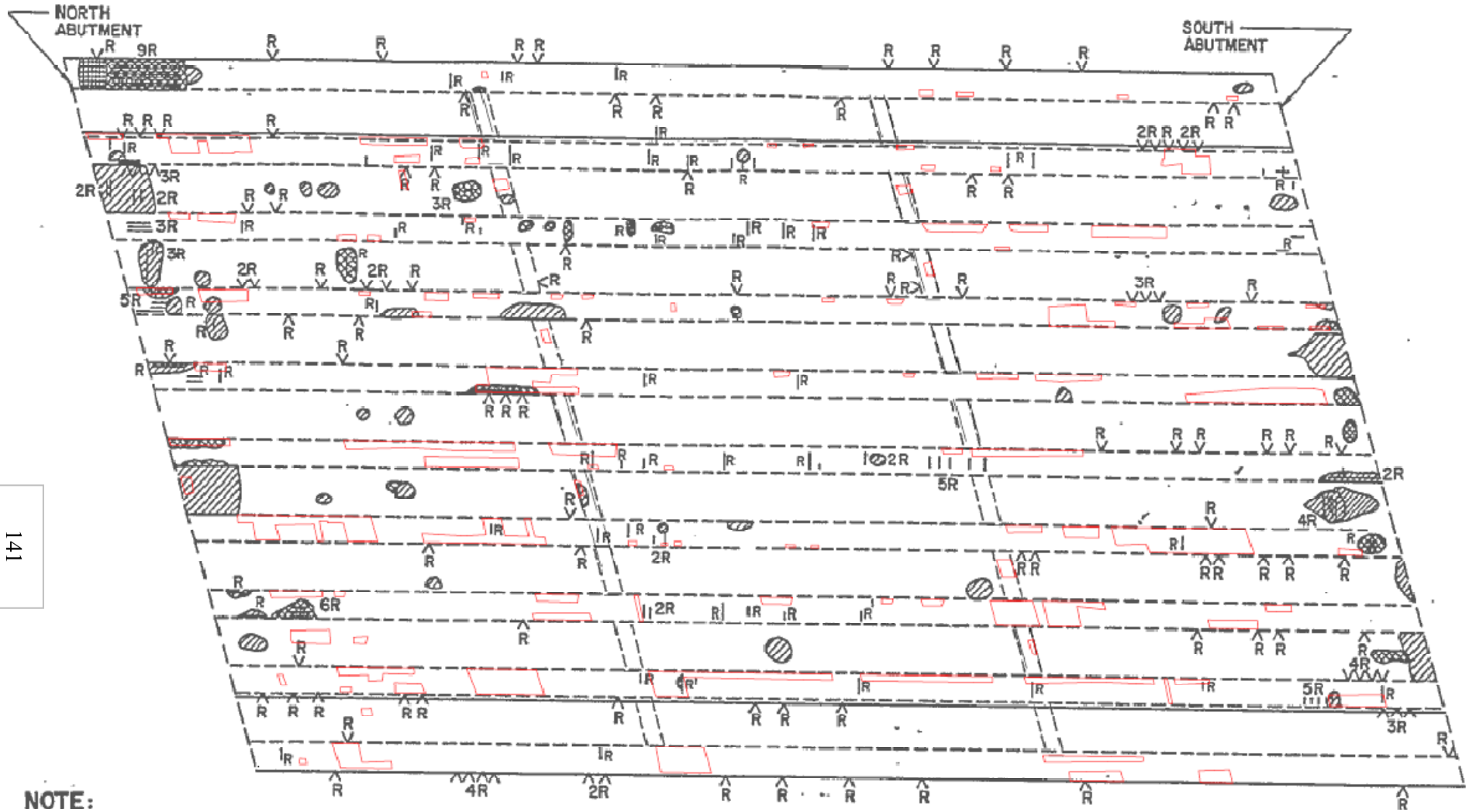

NOTE:

LEGEND

- DELAMINATIONS
- SPALLS
- PATCHED AREA
- HONEYCOMBED AREA
- R EXPOSED REINFORCING STEEL (HORIZONTAL)
- EXPOSED REINFORCING STEEL (VERTICAL)

University of Waterloo

DRAWING #: 3

'91 Repair and Current Spalling

DRAWN BY: JL DATE: Sept. 2 2010

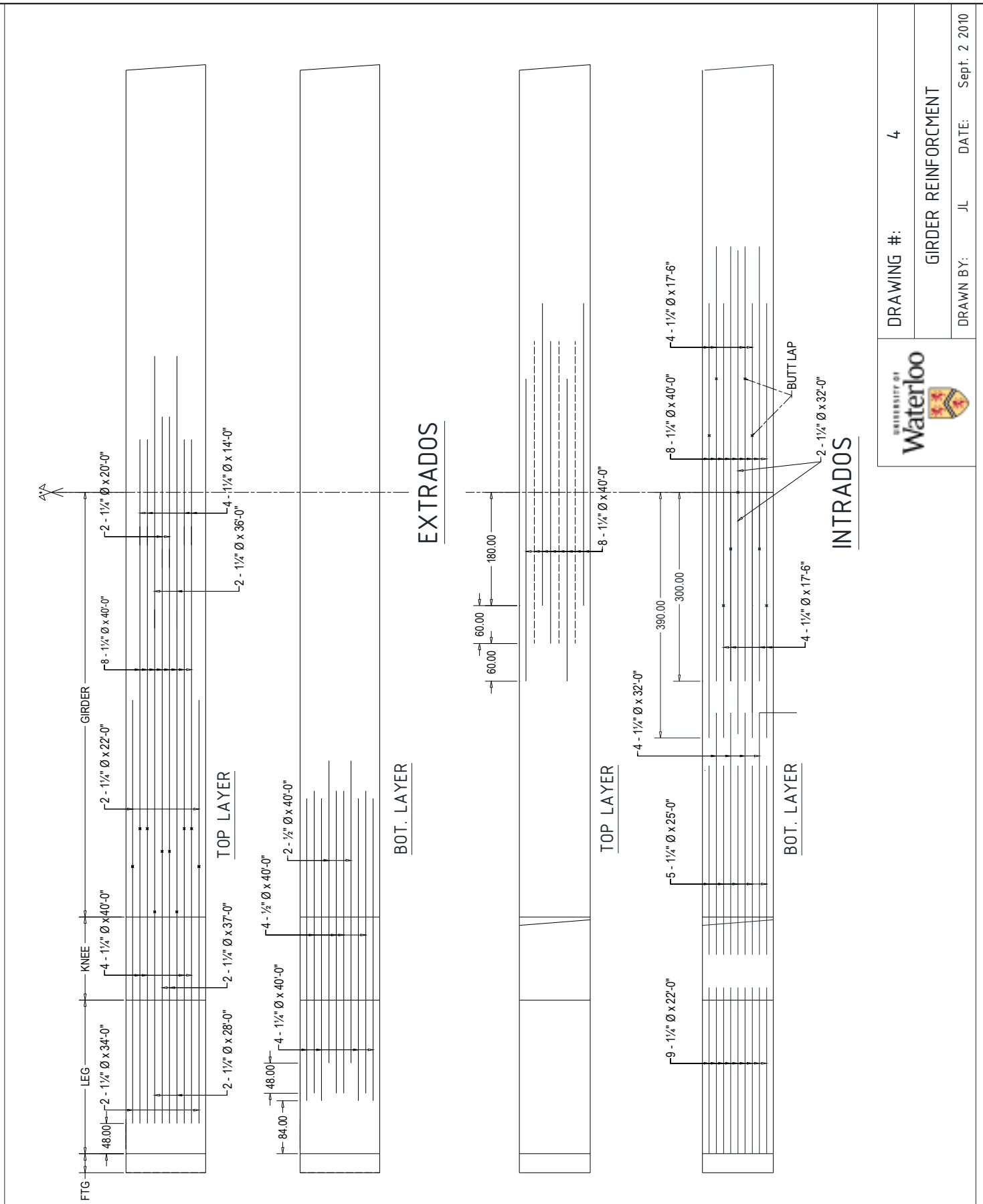
DRAWING #: 4
GIRDER REINFORCMENT
DRAWN BY: JL DATE: Sept. 2 2010
UNIVERSITY OF Waterloo
EXTRADOS
INTRADOS
TOP LAYER
BOT. LAYER
TOP LAYER
BOT. LAYER
GIRDER
LEG
KNEE
FTG
BUTT LAP
2 - 1¼" Ø x 20'-0"
4 - 1¼" Ø x 14'-0"
2 - 1¼" Ø x 36'-0"
8 - 1¼" Ø x 40'-0"
2 - 1¼" Ø x 22'-0"
4 - 1¼" Ø x 40'-0"
2 - 1¼" Ø x 37'-0"
2 - 1¼" Ø x 34'-0"
2 - 1¼" Ø x 28'-0"
2 - ½" Ø x 40'-0"
4 - ½" Ø x 40'-0"
4 - 1¼" Ø x 40'-0"
48.00
84.00
8 - 1¼" Ø x 40'-0"
180.00
60.00
60.00
4 - 1¼" Ø x 17'-6"
8 - 1¼" Ø x 40'-0"
2 - 1¼" Ø x 32'-0"
4 - 1¼" Ø x 17'-6"
390.00
300.00
4 - 1¼" Ø x 32'-0"
5 - 1¼" Ø x 25'-0"
9 - 1¼" Ø x 22'-0"

Site 23-170 HWY #59

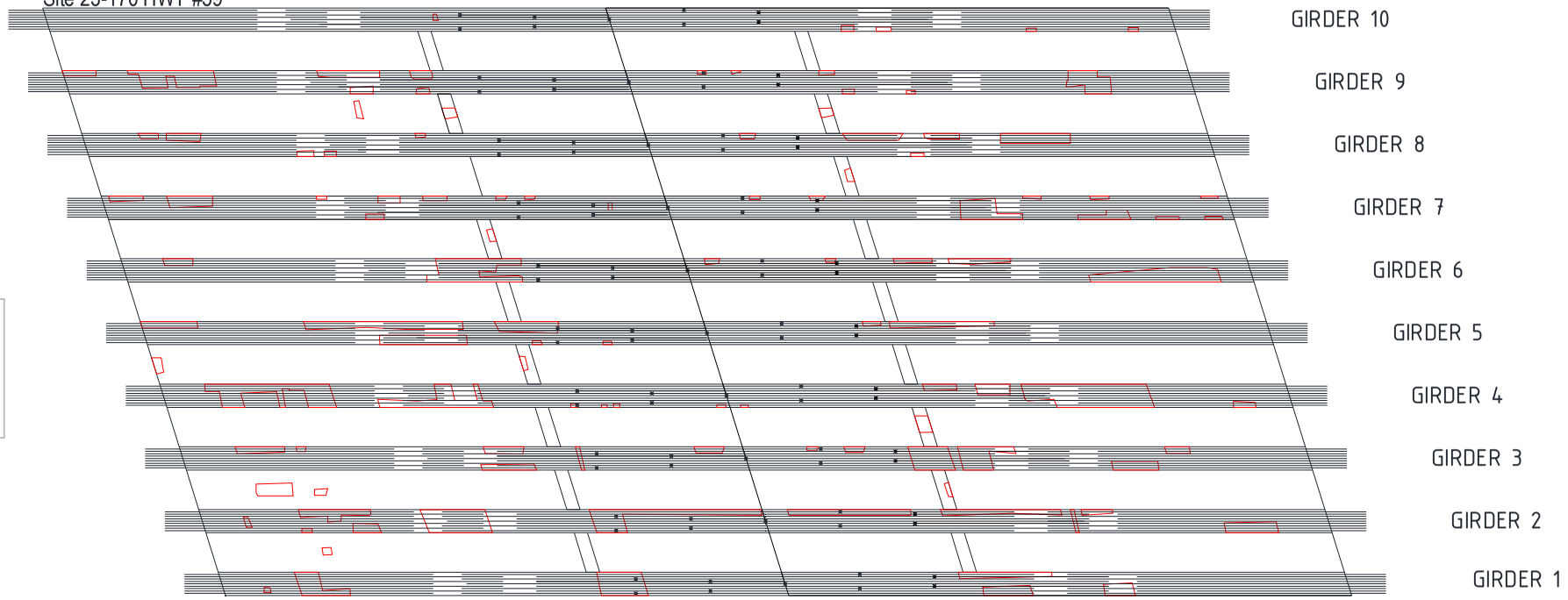

University of Waterloo

DRAWING #: 5

Reinforcement-Spalling Superposition

DRAWN BY: JL DATE: Sept. 2 2010

GIRDER 1

GIRDER 2

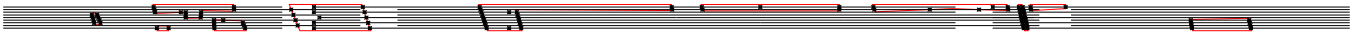

GIRDER 3

GIRDER 4

GIRDER 5

GIRDER 6

GIRDER 7

GIRDER 8

GIRDER 9

GIRDER 10

University of Waterloo	DRAWING #:	6
	Reinf.-Spalling Superposition for Analysis	
	DRAWN BY: JL	DATE: Sept. 2 2010

Appendix A-5 Bridge Loads

CLW Truck (Cl. 3.8.3.2 Fig 3.2)

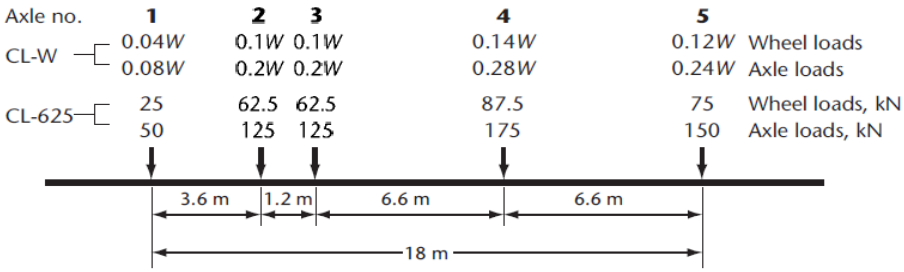

Station		Axel Load	
m	in.	KN	Kips
0	0	50	11.24
3.6	141.73	125	28.10
4.8	188.98	125	28.10
11.4	448.82	175	39.34
18	708.66	150	33.72

Component	Absolute Value
Maximum Positive Moment	7140.81 kip-in
Maximum Negative Moment	20028.4 kip-in
Maximum Shear	84.269 kip

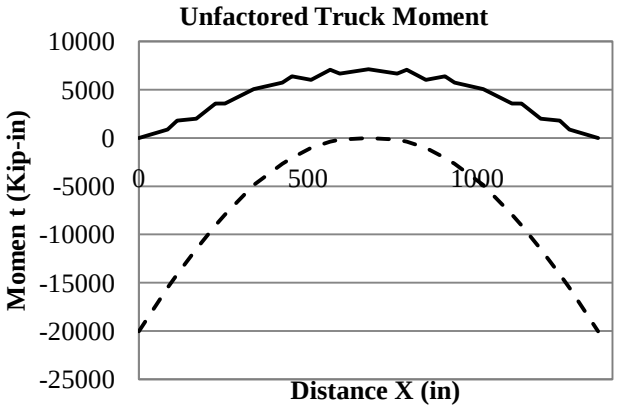

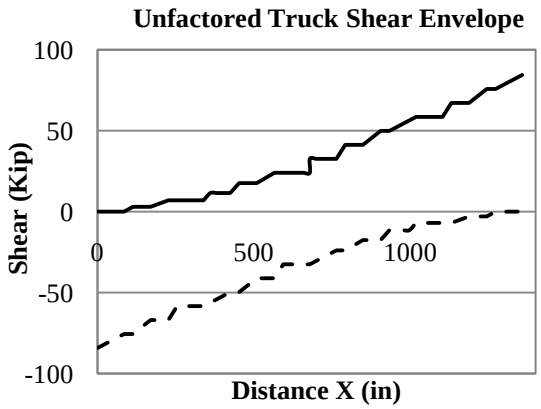

CLW Lane Load (Cl. 3.8.3.3 Fig 3.3)

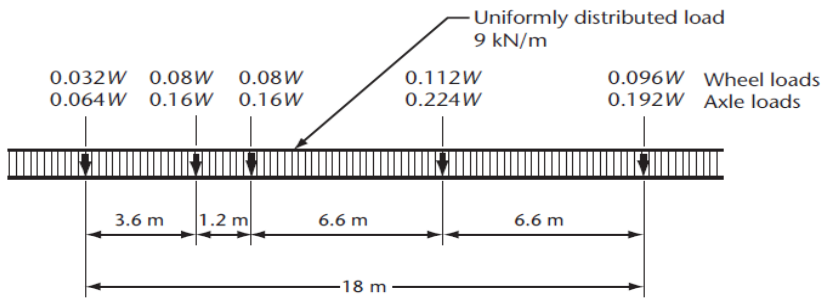

Station		Axel Load	
m	In.	KN	Kips
0	0	40	8.99
3.6	141.73	100	22.48
4.8	188.98	100	22.48
11.4	448.82	140	31.47
18	708.66	120	26.98
Lane Load		9 KN/m	0.051394 kip/in

0.8*Truck

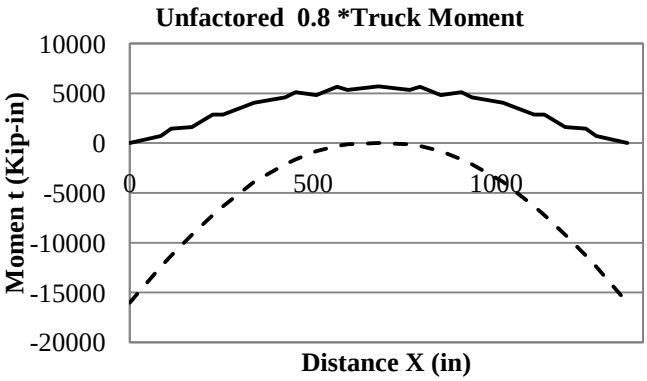

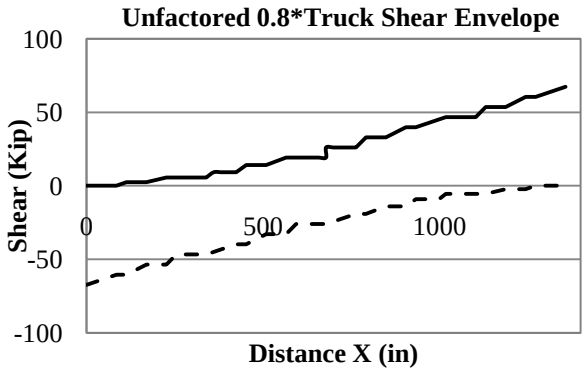

Lane Load

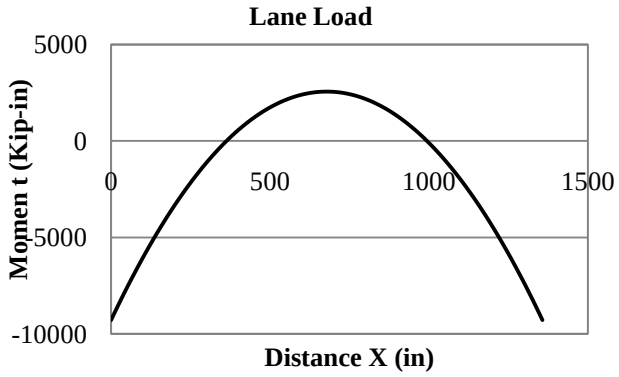

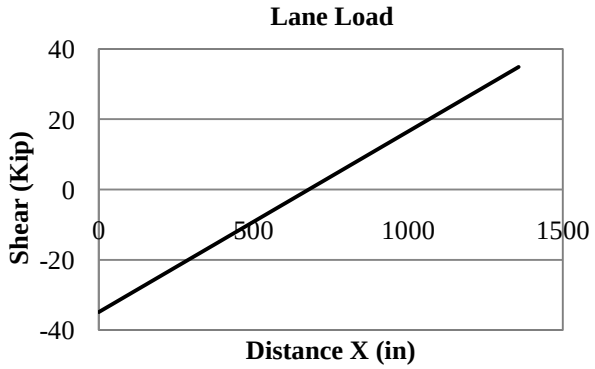

0.8Truck+Lane Load

Component	Absolute Value
Maximum Positive Moment	8269.912 kip-in
Maximum Negative Moment	25302.12 kip-in
Maximum Shear	102.298 kip-in

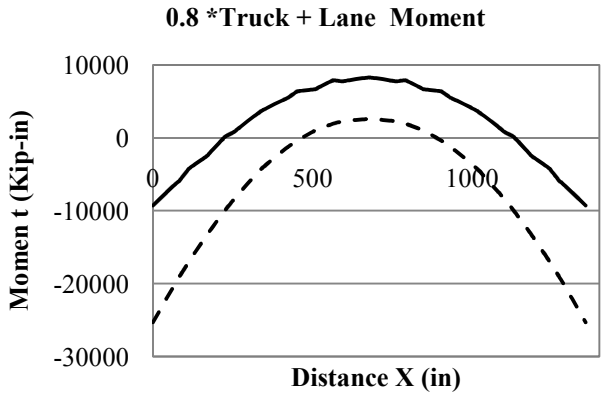

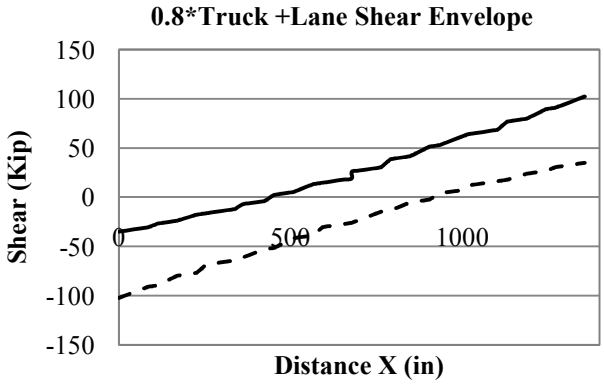

Girder Self Weight

Component	Absolute Value
Maximum Positive Moment	4181.326 kip-in
Maximum Negative Moment	16804.67 kip-in
Maximum Shear	72.907 kip

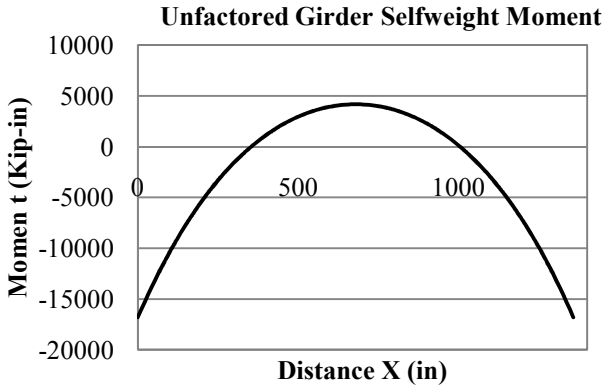

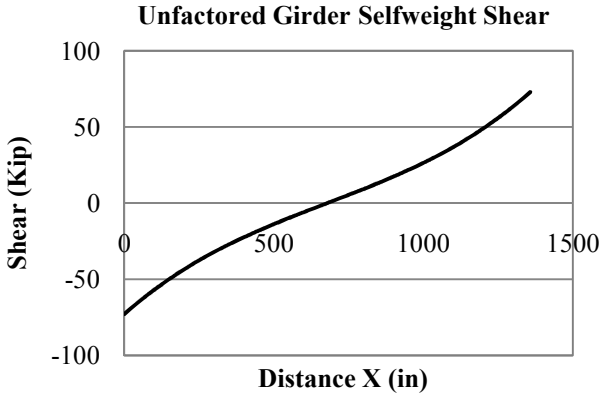

Slab Self Weight

Component	Absolute Value
Maximum Positive Moment	8412.203 kip-in
Maximum Negative Moment	2318.278 kip-in
Maximum Shear	31.622 kip

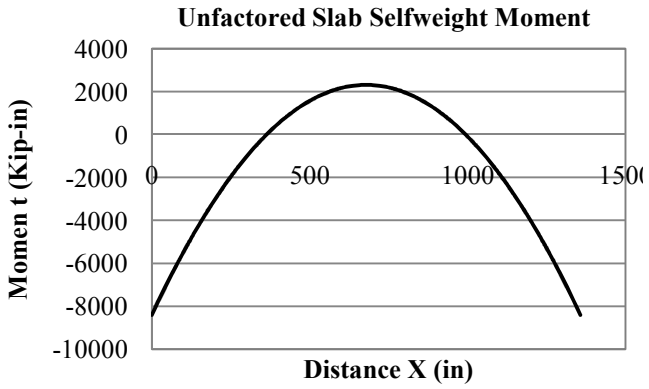

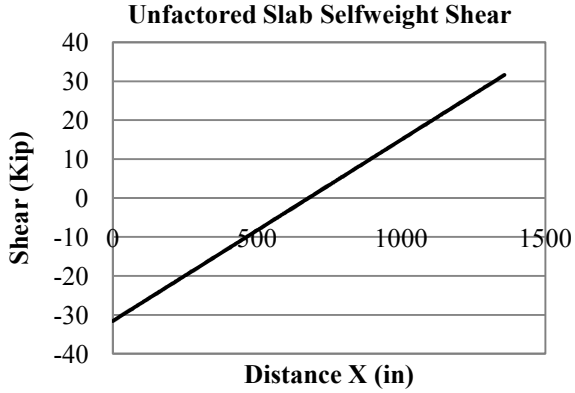

Appendix A-6 Structural Capacity

A-6-1 Known Information

Based on the original structure document the following information is known.

Material Property	Specified Value
Concrete Compressive Strength, f'_c	3000 psi (20.68 MPA)
Steel Yield Strength, f_y	275 MPA
Concrete Modulus of Rupture, f_r	2.729 MPA*2
Concrete Modulus of Elasticity, E_c	20463 MPA*1

$E_c = 4500\sqrt{f_c'} = 20463\ MPA$ *1

$f_r = 0.6\lambda\sqrt{f_c'} = 2.729\ MPA$ *2

Reinforcement	Diameter		X-Sectional Area	
	inches	mm	in^2	mm^2
Stirrups	½	12.7	0.1963	125.7
Bottom Lower	1 ¼	31.75	1.227	791.73

A-6-2 Required Development Length (CAN/CSA S6.06 Highway Bridge Code)

The following computes the required development length using Canadian standards.

Clear Cover= 2 5/8 in. – 1 ¼ (0.5) = 2" (25.4) = 50.8mm
Clear Spacing= 2.44" – 1 ¼" = 1.599" (25.4) = 40.49mm

K_1=1.0, K_2=1.0, K_3=1.0

Clear Cover= 50.8 > 31.75
Clear Spacing= 40.49 < (1.4*31.75) = 44.45mm

S = {12in , 18in} = {304.8mm , 457.2mm}, 304.8 is conservative for l_d .

$$K_{tr} = 0.45\frac{A_{tr}F_y}{10.5\ s\ n} = 0.45 * \frac{125.7 * 2 * 275}{10.5 * 304.8 * 9} = 0.72568$$

Dcs= 2/3 * 2.844" *25.4= 48.16 mm
(Ktr + dcs)= 0.72568 + 48.16 = 48.886 < 2.5 db =79.375

$$l_d = 0.45\frac{k_1k_2k_3}{(k_{tr} + d_{cs})}\left[\frac{f_y}{f_{cr}}\right]A_b$$

$$l_d = \frac{0.45}{48.886}\left[\frac{275}{0.4\sqrt{20.684}}\right]791.73 = 1109.86\ \text{mm} = 43.695\ \text{in}$$

A-6-3 Moment Resistance

In this section, the moment capacity of the girder is shown for a number of approximation of the section. Accuracy is increase with each successive section. Calculations are shown for the mid-span section.

Simplified Section #1

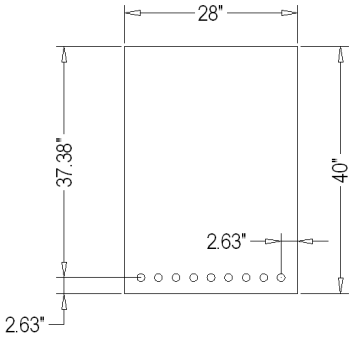

$$\rho_{bal} = \frac{\alpha_1\beta_1 f_c'}{f_y}\left[\frac{700}{700+f_y}\right] = \frac{0.82*0.918*20.7}{275}\left[\frac{700}{700+275}\right] = 4.07\%$$

$$\rho = \frac{A_s}{bd} = \frac{9*791.73mm^2}{28*25.4*37.38*25.4} = 1.055\%$$

Section is Under-Reinforced

$$I_g = \frac{1}{12}bh^3 = \frac{1}{12}(28*25.4)(40*25.4)^3 = 6.21x10^{10}mm^4$$

$$M_{cr} = \frac{f_r I_g}{y_t} = \frac{2.729*6.21x10^{10}mm^4}{[\frac{40*25.4}{2}]} = 333.6\ KN.m$$

$\alpha_1 = 0.85 - 0.0015f_c' = 0.85 - 0.0015*20.7 = 0.82$
$\beta_1 = 0.97 - 0.0025f_c' = 0.97 - 0.0025*20.7 = 0.918$

$$a = \frac{A_s f_y}{\alpha_1 f_c' b} = 9*791.73\ mm^2 * \frac{275\ MPA}{0.82*20.7MPA*711.2mm} = 162.32\ mm$$

$$M_r = A_s f_y\left(d - \frac{a}{2}\right) = 9*791.73mm^2*275\ MPA*\left((37.3*25.4) - \frac{162.32}{2}\right) = 1697\ KN.m$$

Simplified Section #2

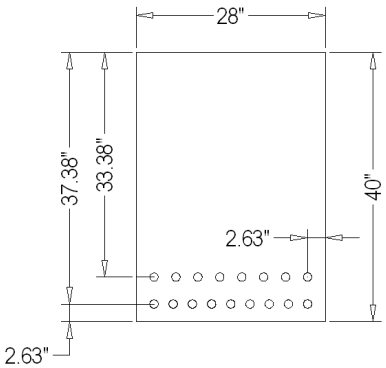

Simplified Section #3

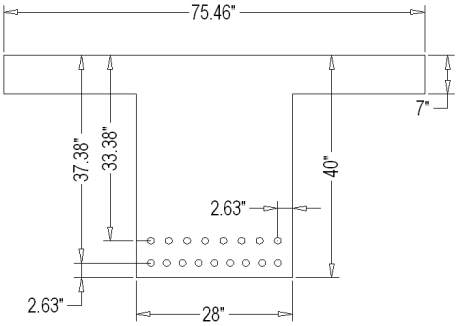

Each estimate is summarized in the following table.

Flexural Capacity	M_{cr} (KN.m)	Reinf. Ratio		M_r (KN.m)	
	Nominal	%	Failure	Nominal	Factored*
Section 1	333.6	1.055	Under-Reinf.	1697	1472.7
Section 2	333.6	2.106	Under-Reinf.	2765.9	2292.9
Section 3	414.63	0.781	Under-Reinf.	3184.7	2814.8

*$\phi_c = 0.65,\ \phi_s = 0.9\ (CSA\ S6.06)$

A-6-4 Shear Capacity

The shear capacity is computed using Simplified Section #1. The depth of the section is taken at the critical section in shear.

Simplified Method

$\beta = 0.18, \theta = 42°$

$d_V = \max\{0.9d, 0.72h\} = \max\{0.9 * (2219.2\text{mm}), 0.72 * 2286mm\} = 1997.3mm$

$V_c = 2.5\beta f_{cr}\, b_v d_v = 2.5 * 0.18 * 1.819 * 711.2mm * 1997.3mm = 1162.7KN$

$$V_s = \frac{A_v f_y d_v \cot\theta}{s} = \frac{251.4\ mm^2 * 275MPA * 1997.3\ mm \cot(42°)}{12" * 25.4} = 503.14\ KN$$

$V_r = V_s + V_c = 1162.7\ KN + 503.14\ KN = 1665.84\ KN$

Appendix A-7 Transverse Distribution

This section computes the transverse distribution of loads across the bridge in accordance with CAN/CSA S6-06.

A-7-1 Transverse distribution for vertical shear

For evaluation the number of design lanes were taken as the number of clearly designated traffic lanes as per (CAN/CSA S6-06 Cl.14.9.4.1).

# of design lanes=2

$$W_e = \frac{14.25m}{2} = 7.125m$$

S=1.9177m, S<2m

Type C bridge section (slab-on-girder) has been assumed

$$F = 6.10$$

$$F_v = \frac{SN}{F} = \frac{1.9177 * 10}{6.10} = 3.1438$$

$$V_{g,avg} = \frac{nV_T R_L}{N} = \frac{2V_T 0.9}{10}$$

$$V_g = F_v V_{g,avg} = 3.1438 * \frac{2 * 0.9}{10} V_T = 0.5659\, V_T$$

The factor is the same for both interior and exterior girders

A-7-2 Transverse distribution for moment

$$\mu = \frac{W_e - 3.3}{0.6} = \frac{7.125 - 3.3}{0.6} = 6.375 \leq 1.0 \;\; use\; 1.$$

From CSA S6-06 Table 5.3 Highway class A or B (Design of a new structure) has been assumed.

*Internal Girder L = 34.47m > 10m

Interior

$$F = 7.2 - [14/L] = \; 7.2 - [14/34.47\,] = 6.7938$$

$$C_f = 10 - [25/L] = 10\text{-}[25/34.47] = 9.2747\%$$

$$F_m = \frac{SN}{F\left[1 + \frac{\mu C_f}{100}\right]} \geq 1.05$$

$$F_m = \frac{1.9177 * 10}{6.7938 * \left[1 + \frac{1 * 9.2747}{100}\right]} = 2.5831$$

$$M_{g,avg} = \frac{nM_T R_L}{N} = \frac{2M_T 0.9}{10}$$

$$M_g = F_m M_{g,avg} = 2.5831 * \frac{2 * 0.9}{10} M_T = 0.46496 M_T$$

Exterior

$F = 6.8 - [3/L] = 6.8 - [3/34.47\ ] = 6.713$

$C_f = 10 - [25/L]$ =10-[25/34.47]=9.2747%

$$F_m = \frac{SN}{F\left[1 + \frac{\mu C_f}{100}\right]} \geq 1.05$$

$$F_m = \frac{1.9177 * 10}{6.713 * \left[1 + \frac{1 * 9.2747}{100}\right]} = 2.614$$

$$M_{g,avg} = \frac{nM_T R_L}{N} = \frac{2M_T 0.9}{10}$$

$$M_g = F_m M_{g,avg} = 2.614 * \frac{2 * 0.9}{10} M_T = 0.4706 M_T$$

Appendix A-8 Slab Strength

In this section the strength of the slab is computed to determine if the slab is capable of supporting load given a single girder fails. The slab is proportioned as follows.

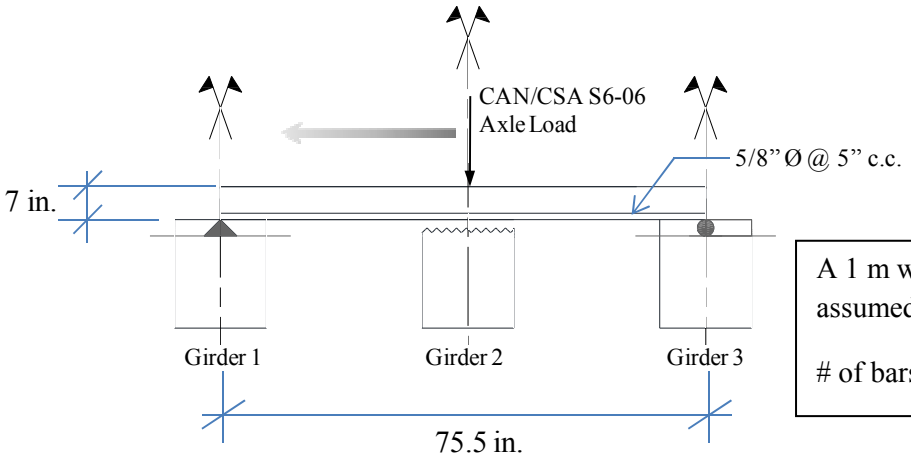

A 1 m wide slab strip has been assumed.

# of bars=39.37"/5" = 7.87 => 7 bars

A-8-1 Flexural Strength

Unfactored Capacity

$$\alpha = \frac{A_s f_y}{\alpha f_c^{'} b}$$

$f_c^{'} = 20.68\ MPA$

$\alpha_1 = 0.85 - 0.0015(20.68) = 0.819$

$$A_s = \pi\left(\frac{\frac{5}{8} * 25.4}{2}\right)^2 * 7 = 1385.53\ mm^2$$

$b = 1000\ mm$
$f_y = 274\ MPA$

$$\alpha = \frac{1385.53 * 275}{0.819 * 20.68 * 1000} = 22.5\ mm$$

$$M_r = 1385.53\ mm^2 * 275[(6.25 * 25.4) - \frac{22.5}{2})] = 56.2\ KN.m$$

Load

Worst case= 1 wheel applied at the mid-point

$$p = \frac{175}{2}(KN)$$

$$M = \frac{175}{4} * \frac{75.5}{2} * 25.4 = 41.95\ KN.m$$

Appendix B

Appendix B-1 Input File #1

Appendix B-2 Input File #2

Appendix B-3 Input File #3

Appendix B-4 Input File #4

Appendix B-5 Target Formation

Appendix B-6 Multi-Girder Code Input

Appendix B-7 Future Deterioration Sensitivity Study Results

Appendix B-8 Section Loss Results

Appendix B-9 Section Loss + Bond Deterioration Results

Appendix B-1 Input File #1

The following is a sample of the first input file required. The file describes the reinforcement as line data from AutoCad.

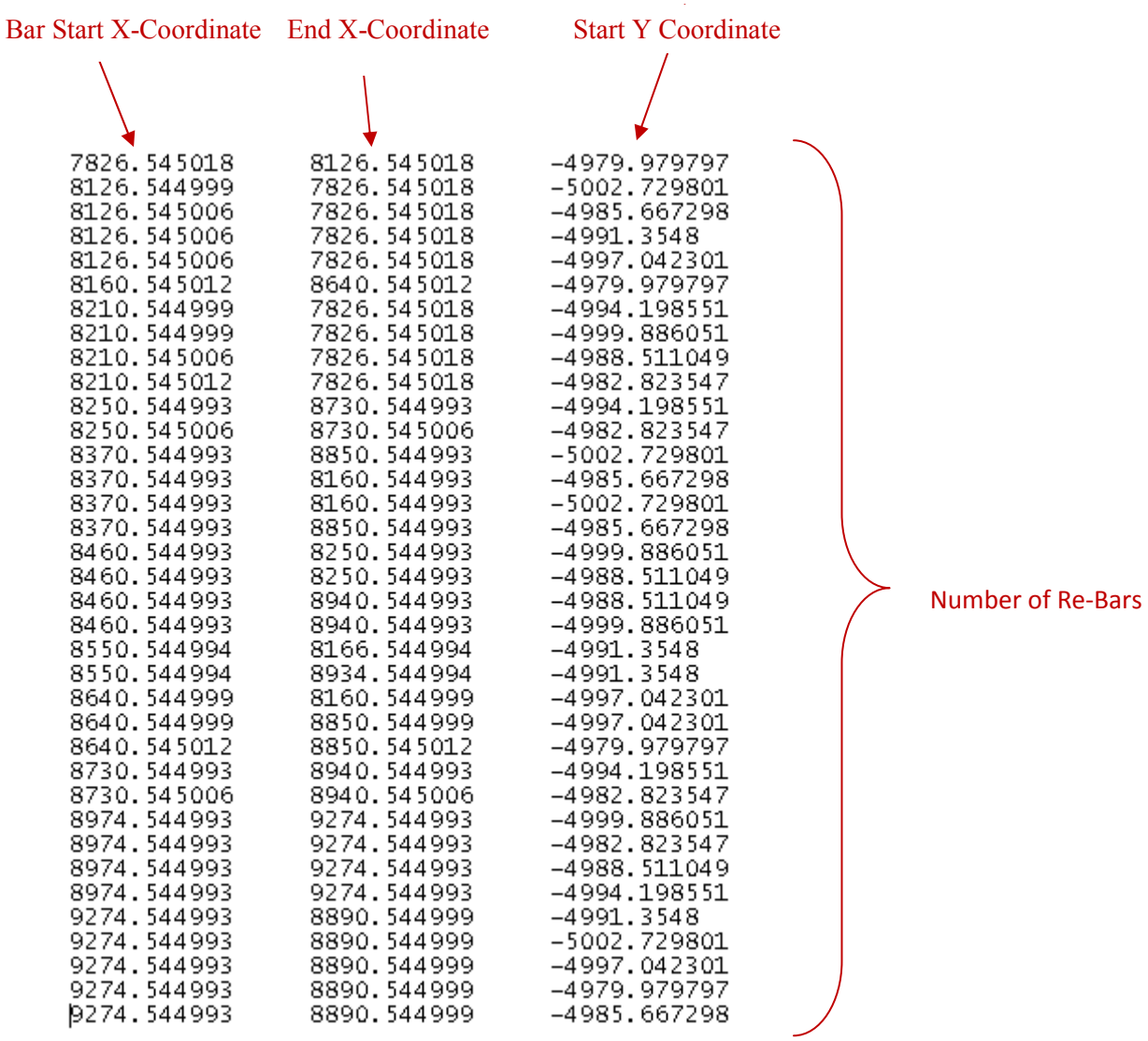

Appendix B-2 Input File #2

The following is a sample of the second required input file. The file describes the spalling as point data from AutoCad.

8351.78163075	-4999.88605128
8350.18772986	-4979.97979664
8351.78163075	-5002.72980128
8250.54500550	-4982.82354741
8247.19268298	-4979.97979664
8320.99295180	-4985.66729818
8300.08357706	-4997.04230050
8299.58365540	-4994.19855050
8320.40293686	-4988.51104896
8350.18772986	-4982.82354741
8319.81292193	-4991.35479973
8250.54499287	-4988.51104896
7919.85118513	-4982.82354741
7918.95141340	-4979.97979664
7954.62623876	-4982.82354741
7954.62623876	-4979.97979664
8236.27399339	-5002.72980128
8250.54499287	-4994.19855050
8248.40315778	-4985.66729818
8249.61363258	-4991.35479973
8250.54499287	-4999.88605128
8236.27399339	-4997.04230050
8588.21605544	-4982.82354741
9063.12531075	-4994.19855050
9126.29615797	-4988.51104896
9094.71073436	-4991.35479973
9034.90630270	-4999.88605128
9034.01919934	-4997.04230050
9180.44367738	-4988.51104896
9193.23340581	-5002.72980128
9192.34630270	-4999.88605128
9190.57209622	-4994.19855050
9189.68499287	-4991.35479973
9191.45919934	-4997.04230050
9035.79340581	-5002.72980128
8728.59456932	-4979.97979664
8716.82392798	-4979.97979664
8571.36145839	-4979.97979664
8588.75983760	-4979.97979664
8571.86614526	-4982.82354741
8845.52018911	-4979.97979664
8915.97417834	-4982.82354741
8866.01518160	-4982.82354741
8890.54499919	-4979.97979664
8799.08284421	-4979.97979664
8939.91590442	-4979.97979664

Appendix B-3 Input File #3

The third input file provides information regarding the bridge structure required for the strength evaluation and appears as follows.

```
<<INPUT DATA>>;
_____________________ANALYSIS_____________________________________
Are you evaluating known discrete sections or sections at even intervals along memeber?
0
How many cross sections do you want to evaluate?
300
_____________________BRIDGE_____________________________________
L
1357
_____________________RESISTANCE FACTOR_____________________________________
Steel   Conc.
0.9       0.75
_____________________MATERIAL PROPERTIES_____________________________________
fc     fy     Es    (psi)
3000   33359  29000
Nominal Aggregate size
0.8874
_____________________GEOMETRY_____________________________________
Section Width(b)     clear cover
28                   2.625
_____________________REINFORCEMENT_____________________________________
Stirrup Diameter       Longitudinal Bar Diameter;
     0.5                        1.25
Development Length
        36.15
-------------------- STIRRUP SPACING ------------------------
n# of Stirrups    @     a  Spacing of (FROM EITHER END OF GIRDER)
    10                          12
    11                          12
    12                          18
    12                          18
    12                          18
    12                          18
    11                          12
    10                          12

---------------ADDITIONAL LONGITUDINAL REINFORCMENT --------------------
BOTTOM LOWER REINFORCEMENT
Distance from bottom chord to CL of Bars
2.625

BOTTOM UPPER REINFORCEMENT
Distance from bottom chord to CL of Bars
6.625
Start Coord.     End Coord
424              904
484              964
544              1024
484              964
484              964
424              904
484              964
```

TOP UPPER REINFORCEMENT
Distance from top chord to CL of Bars
3

TOP LOWER REINFORCEMENT
Distance from Top chord to CL of Bars
7

Start Coord	End Coord
84	564
96	576
84	564
144	624
96	576
96	576
144	624
84	564
96	576
84	564
884	1364
874	1352
884	1364
824	1304
874	1352
874	1352
824	1304
884	1364
874	1352
884	1364

Appendix B-4 Input File #4

The last input file provides information regarding the load and load envelope as follows.

```
<<<<< LOAD DATA >>>>>>>
DLA
1.25
Live Load Factor
1.7
Dead Load Factor
1.2
Transverse Moment Distribution Factor
0.46496
Transverse SHEAR Distribution Factor
0.5659
_____________________ENVELOPES_____________________

******** DEAD LOAD ENVELOPES (UNFACTORED) ***********

****************** GIRDER ****************************

Dist X(in)  V(kips)     M(kips.in)
0           -72.907     -16804.67
21.208      -69.308     -15296.859
42.416      -65.83      -13864.09
```

```
1336.1          69.308      -15296.859
1357.308        72.907      -16804.67

****************** SLAB ****************************

Dist X(in)  V(kips)     M(kips.in)
0           -31.622     -8412.203
21.208      -30.634     -7752.028
```

```
1336.1          30.634      -7752.028
1357.308        31.622      -8412.203

*********** TRUCK ENVELOPE (UNFACTORED) ************

_______UPPER LIMIT_________
Dist X(in)  V(kips)             M(kips.in)
0               0                0
21.208          0                221.239
42.416          0                441.878
```

1293.684	77.807	662.517
1314.892	79.964	441.878
1336.1	82.122	221.239
1357.308	84.269	0

LOWER LIMIT

Dist X(in)	V(kips)	M(kips.in)
0	-84.269	-20028.387
21.208	-82.122	-18898.632
42.416	-79.964	-17769.123
63.624	-77.807	-16639.613
84.832	-75.649	-15510.104

Appendix B-5 Target Formation

The following sample array is the formulation created within the program before the strength evaluation begins.

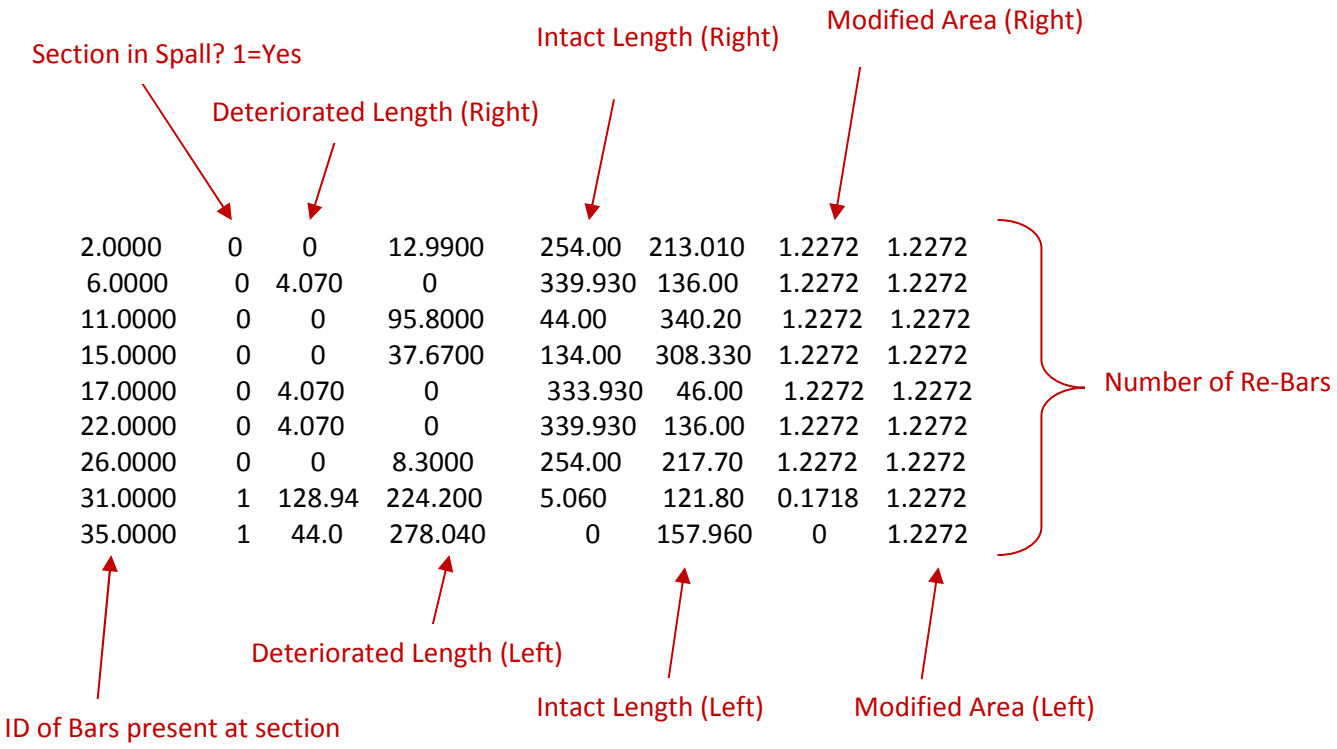

2.0000	0	0	12.9900	254.00	213.010	1.2272	1.2272
6.0000	0	4.070	0	339.930	136.00	1.2272	1.2272
11.0000	0	0	95.8000	44.00	340.20	1.2272	1.2272
15.0000	0	0	37.6700	134.00	308.330	1.2272	1.2272
17.0000	0	4.070	0	333.930	46.00	1.2272	1.2272
22.0000	0	4.070	0	339.930	136.00	1.2272	1.2272
26.0000	0	0	8.3000	254.00	217.70	1.2272	1.2272
31.0000	1	128.94	224.200	5.060	121.80	0.1718	1.2272
35.0000	1	44.0	278.040	0	157.960	0	1.2272

Appendix B-6 Multi-Girder Code Input

When completing the full bridge analysis, the following combined input file should be created for each girder instead of input file #1 an #2 for each.

```
line
8112.39957      8412.39957      -2259.115465
8412.399551     8112.39957      -2281.865469
8412.399558     8112.39957      -2264.802966
8412.399558     8112.39957      -2270.490468
8412.399558     8112.39957      -2276.177968
8446.399564     8926.399564     -2259.115465
8496.399551     8112.39957      -2273.334218
8496.399551     8112.39957      -2279.021719
8496.399558     8112.39957      -2267.646717
8496.399564     8112.39957      -2261.959215
8536.399545     9016.399545     -2273.334218
8536.399558     9016.399558     -2261.959215
8656.399545     9136.399545     -2281.865469
8656.399545     8446.399545     -2264.802966
8656.399545     8446.399545     -2281.865469
8656.399545     9136.399545     -2264.802966
8746.399545     8536.399545     -2279.021719
8746.399545     8536.399545     -2267.646717
8746.399545     9226.399545     -2267.646717
8746.399545     9226.399545     -2279.021719
8836.399547     8452.399547     -2270.490468
8836.399547     9220.399547     -2270.490468
8926.399551     8446.399551     -2276.177968
8926.399551     9136.399551     -2276.177968
8926.399564     9136.399564     -2259.115465
9016.399545     9226.399545     -2273.334218
9016.399558     9226.399558     -2261.959215
9260.399545     9560.399545     -2279.021719
9260.399545     9560.399545     -2261.959215
```

```
point
8348.94567638   -2273.33421844
8370.12052183   -2276.17796844
8339.38109522   -2281.86546921
8324.88299793   -2267.64671689
8360.38924004   -2259.11546457
8360.71832158   -2261.95921535
8339.26952465   -2279.02171921
8372.47108774   -2281.86546921
8424.41624325   -2267.64671689
8422.10785206   -2261.95921535
8339.15795404   -2276.17796844
8339.04638347   -2273.33421844
8371.29580495   -2279.02171921
8215.79163931   -2273.33421844
8214.58169194   -2270.49046767
8217.00158635   -2276.17796844
9011.33898047   -2259.11546457
9048.04996275   -2259.11546457
8213.37174457   -2267.64671689
8277.65941115   -2281.86546921
8308.59479192   -2267.64671689
8324.56811585   -2270.49046767
8325.19788001   -2264.80296612
8290.16353939   -2281.86546921
8274.15595053   -2259.11546457
8274.90190771   -2261.95921535
8426.72463444   -2273.33421844
```

Appendix B-7 Future Deterioration Sensitivity Study Results

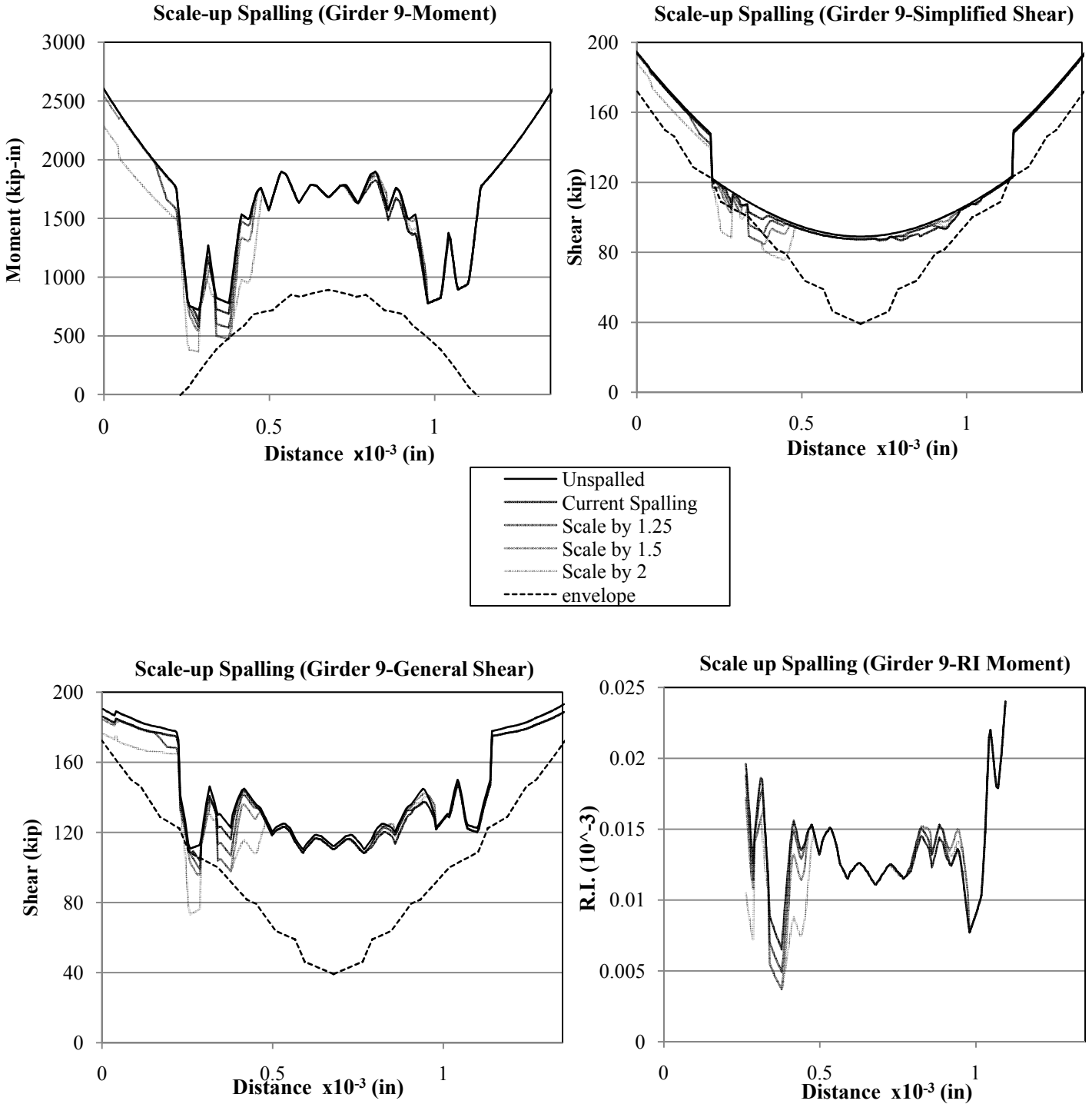

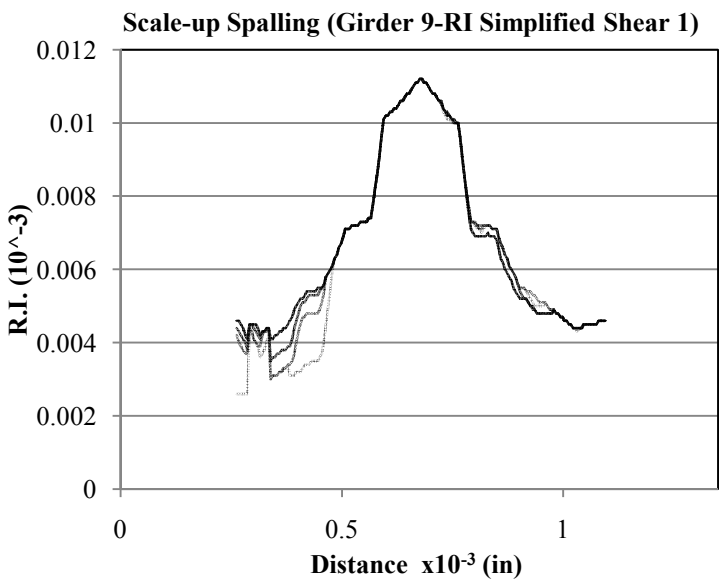
Scale-up Spalling (Girder 9-RI Simplified Shear 1)
0.012
0.01
0.008
0.006
0.004
0.002
0
R.I. (10^-3)
0
0.5
1
Distance x10-3 (in)

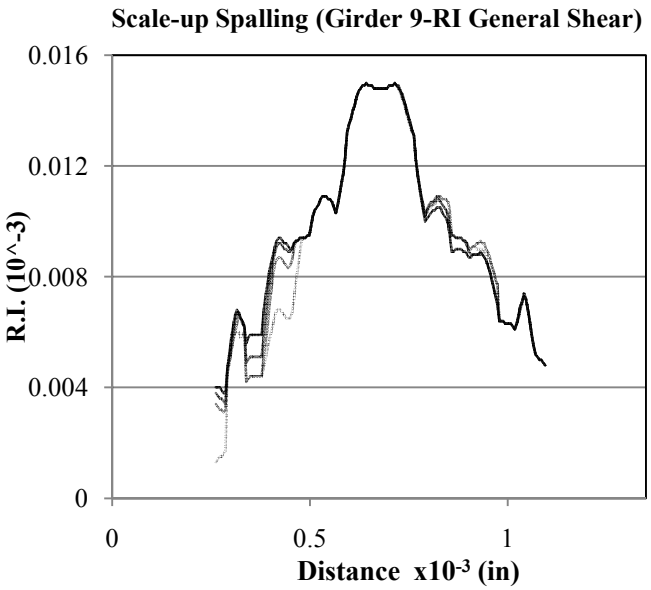
Scale-up Spalling (Girder 9-RI General Shear)
0.016
0.012
0.008
0.004
0
R.I. (10^-3)
0
0.5
1
Distance x10-3 (in)

Appendix B-8 Section Loss Results

Girder	Intact Section Corrosion, Q_i	Spalled Section Corrosion, Q_s
2	6%	15%

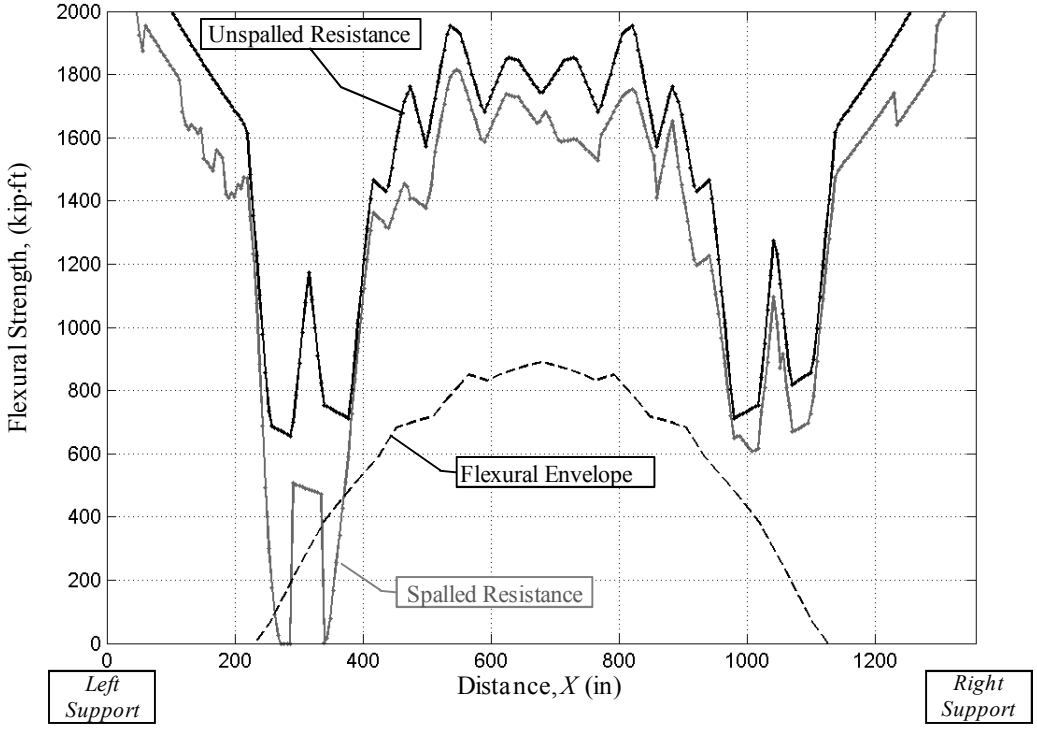

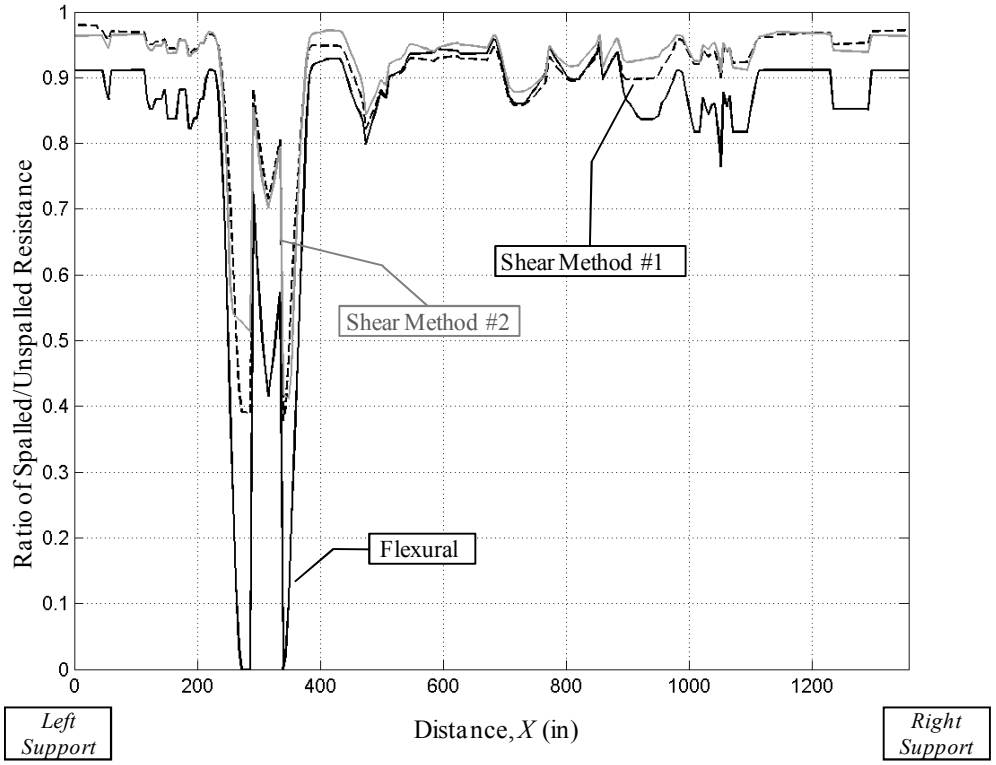

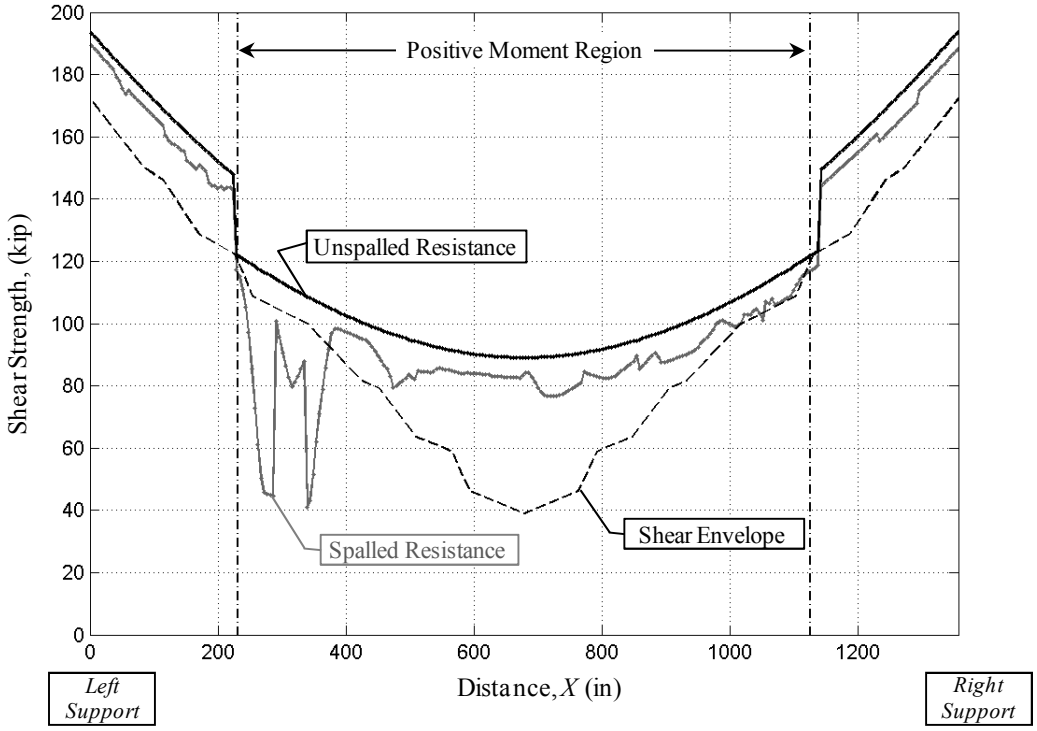
Positive Moment Region
Unspalled Resistance
Spalled Resistance
Shear Envelope
Shear Strength, (kip)
Distance, X (in)
Left Support
Right Support

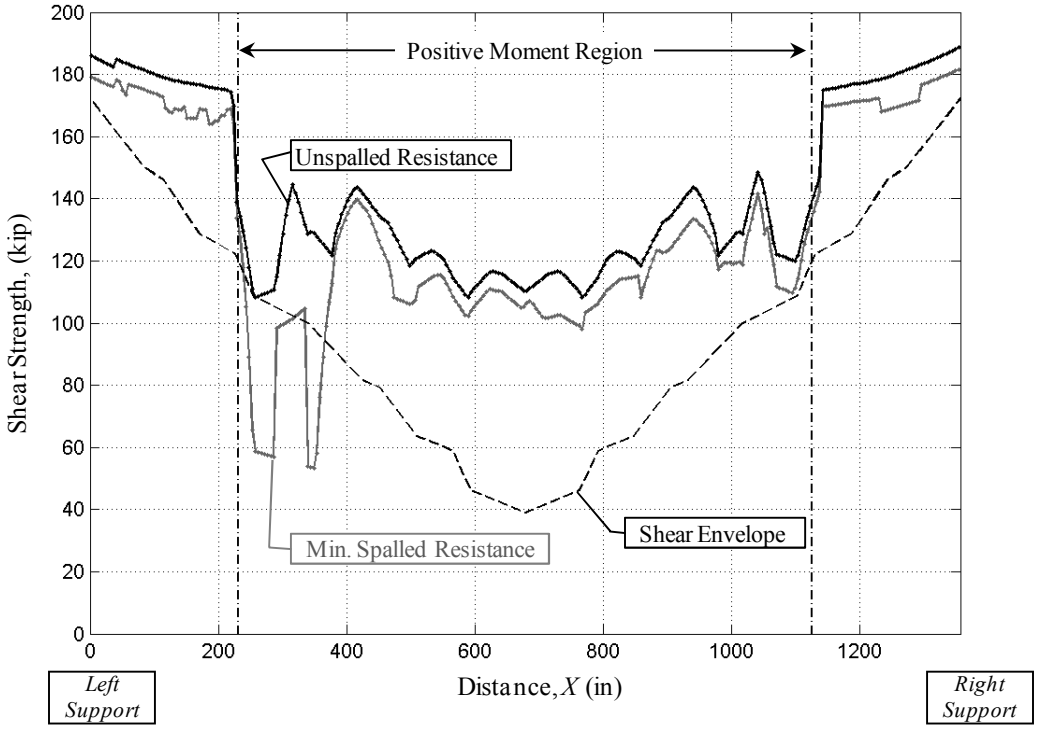
Positive Moment Region
Unspalled Resistance
Min. Spalled Resistance
Shear Envelope
Shear Strength, (kip)
Distance, X (in)
Left Support
Right Support

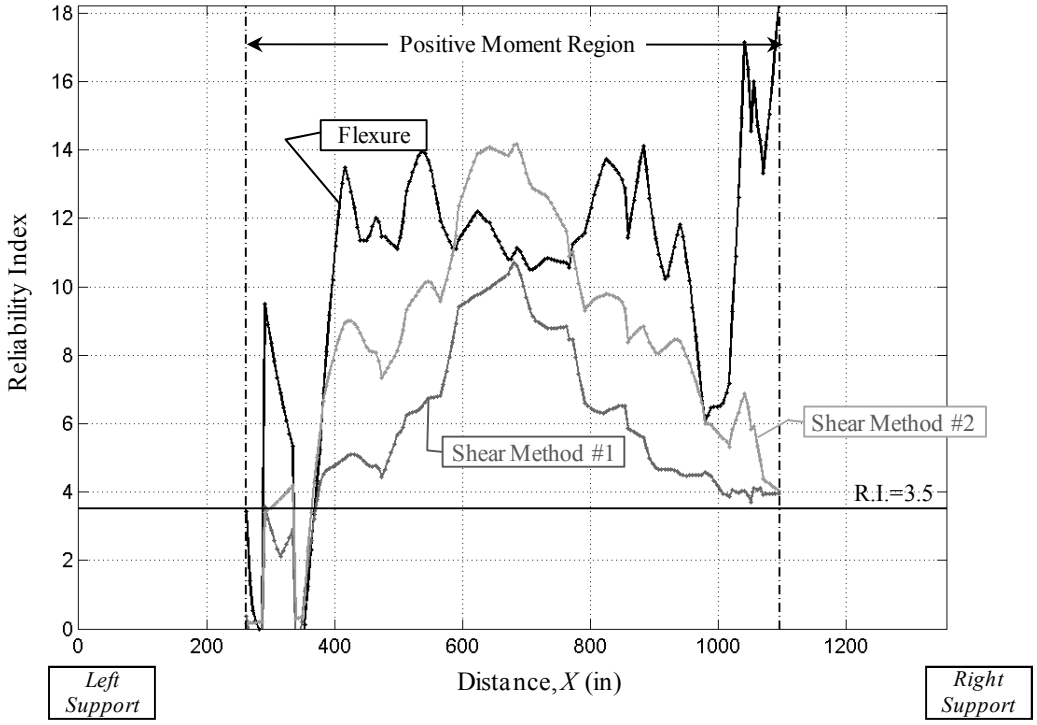
Positive Moment Region
Flexure
Shear Method #2
Shear Method #1
R.I.=3.5
Reliability Index
Distance, X (in)
Left Support
Right Support
0
2
4
6
8
10
12
14
16
18
0
200
400
600
800
1000
1200

Appendix B-9 Section Loss + Bond Deterioration Results

Girder	Intact Section Corrosion, Q_i	Spalled Section Corrosion, Q_s
2	6%	15%

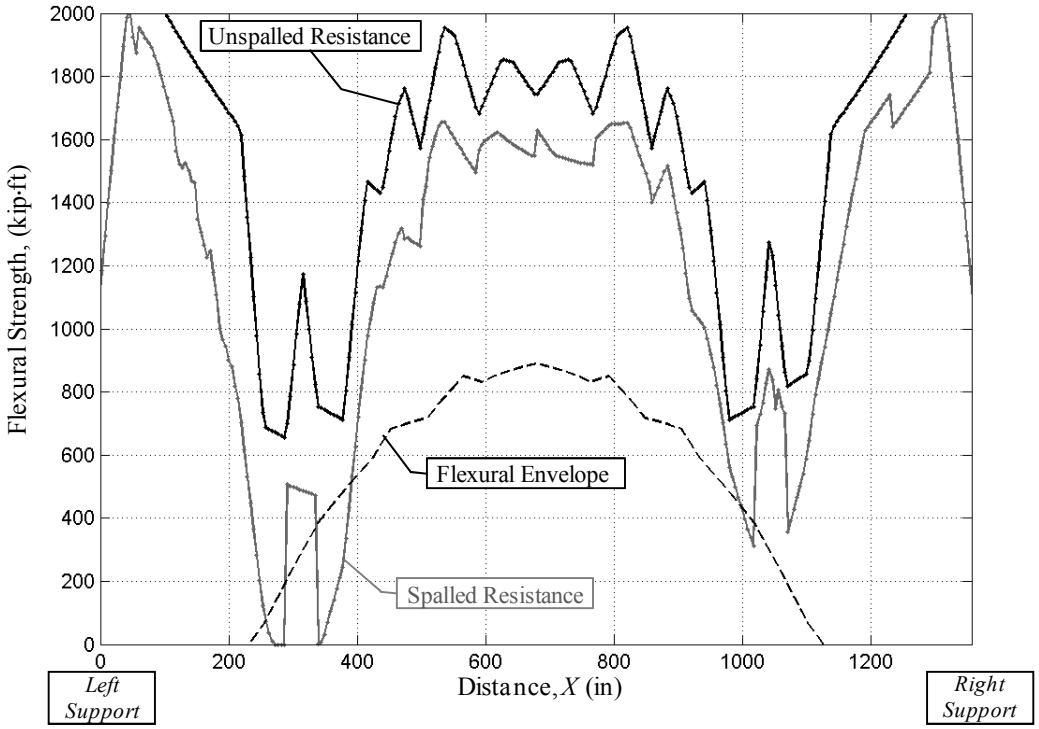

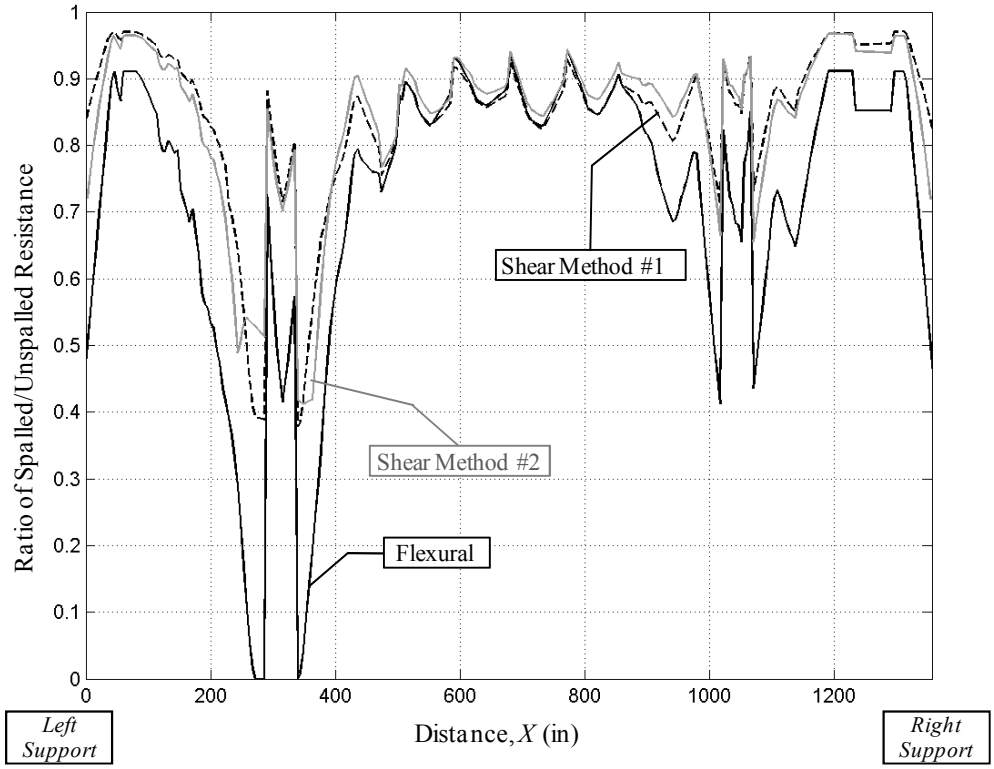

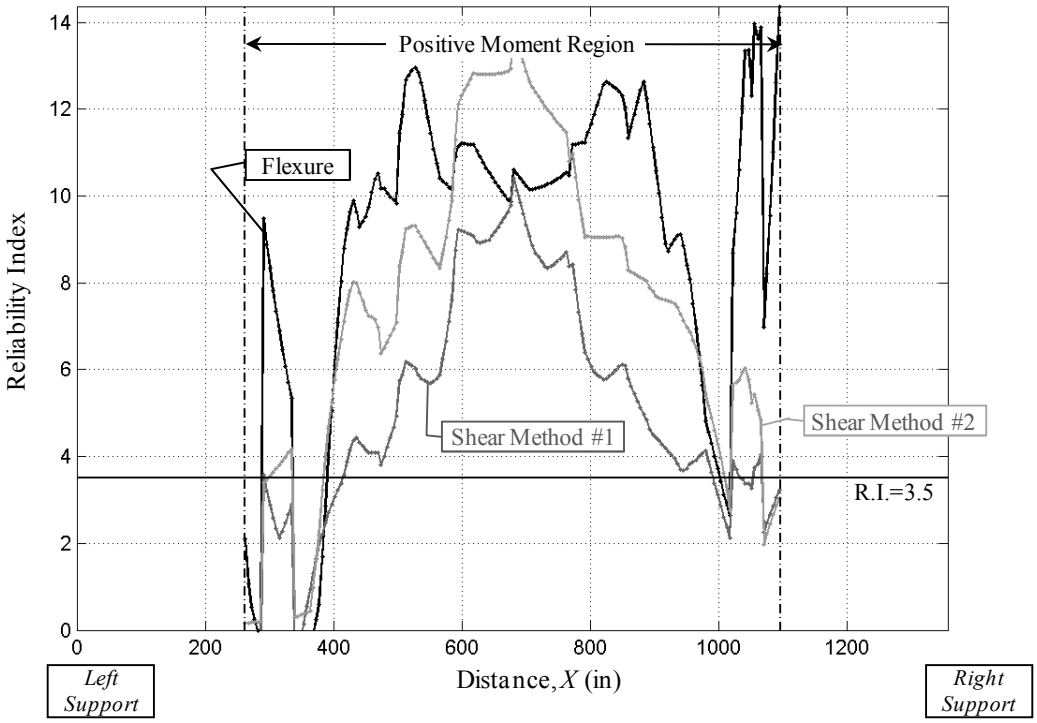
Positive Moment Region
Flexure
Shear Method #1
Shear Method #2
R.I.=3.5
Reliability Index
Distance, X (in)
Left Support
Right Support

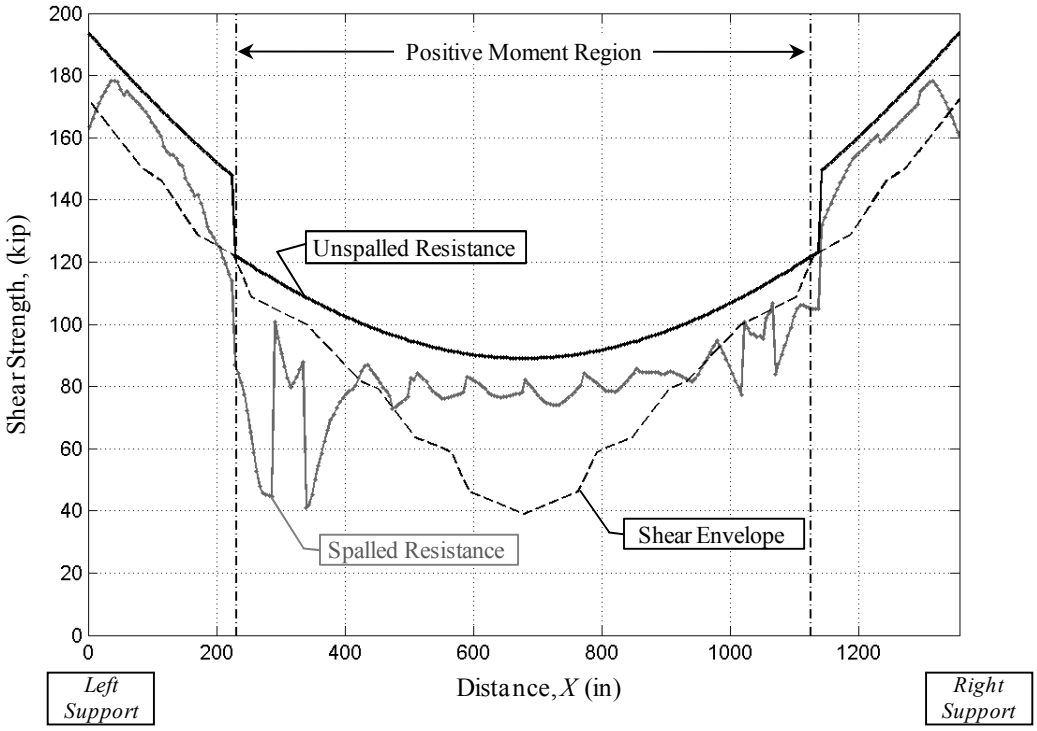
Positive Moment Region
Unspalled Resistance
Spalled Resistance
Shear Envelope
Shear Strength, (kip)
Distance, X (in)
Left Support
Right Support

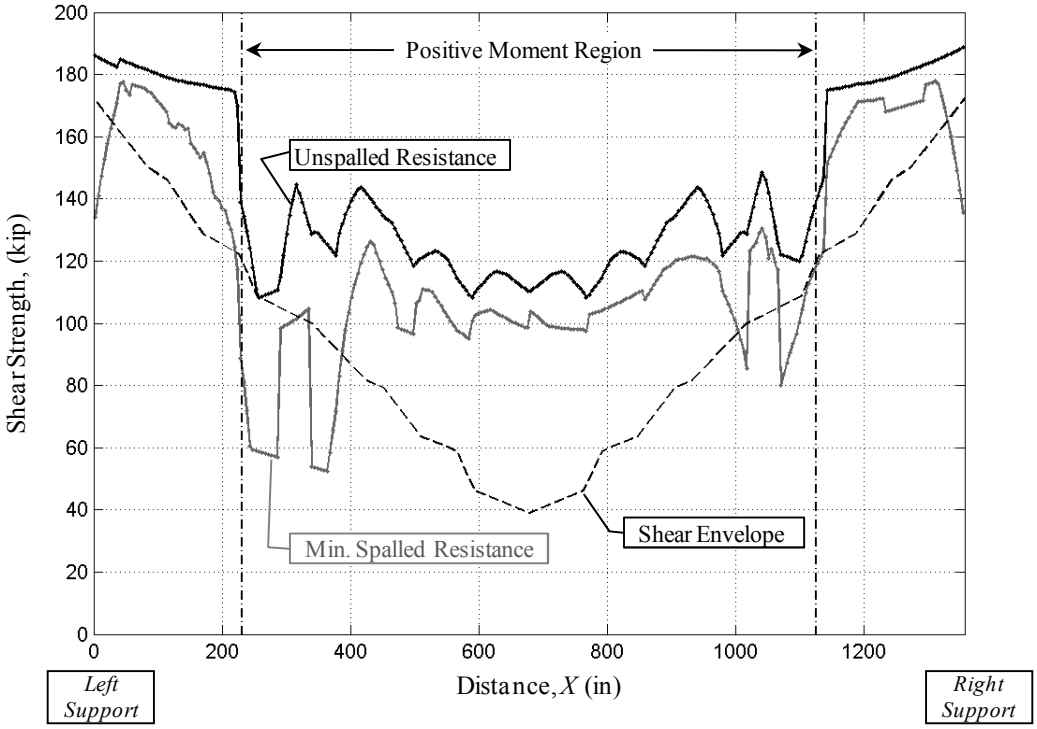
Positive Moment Region
Unspalled Resistance
Min. Spalled Resistance
Shear Envelope
Shear Strength, (kip)
Distance, X (in)
Left Support
Right Support
0
20
40
60
80
100
120
140
160
180
200
0
200
400
600
800
1000
1200

Appendix C

Appendix C-1 Test Specimen Detail

Appendix C-2 Test Specimen Design

Beam #1

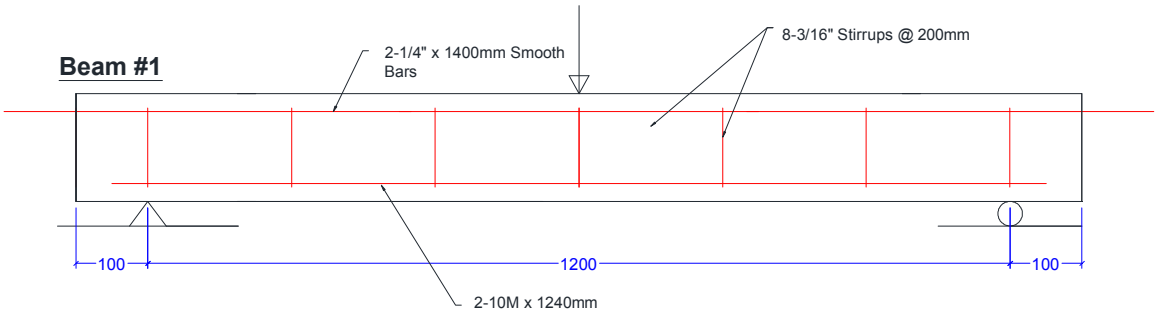

Beam #2

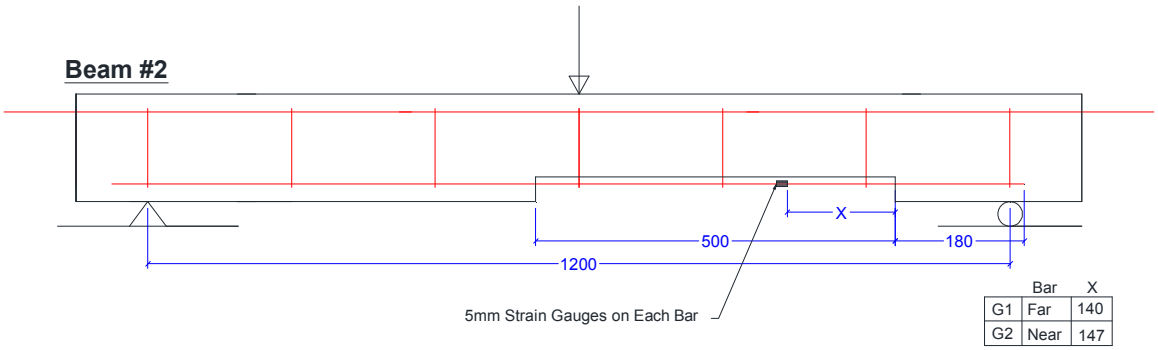

	Bar	X
G1	Far	140
G2	Near	147

Beam #3

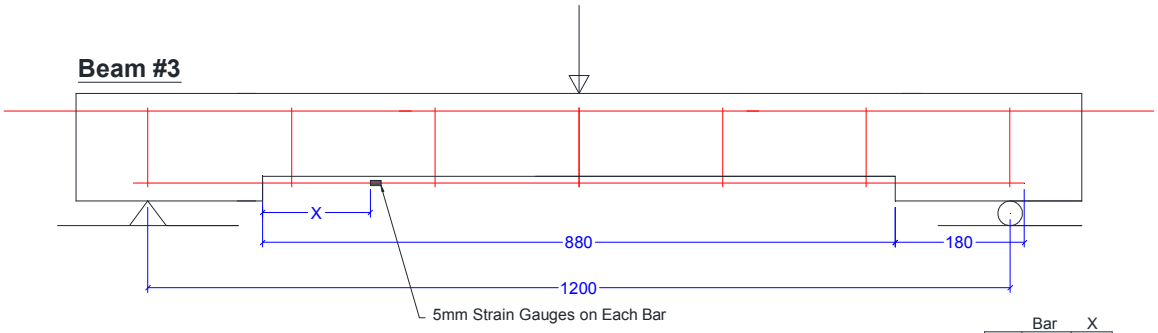

	Bar	X
G1	Far	150
G2	Near	149

Beam #4

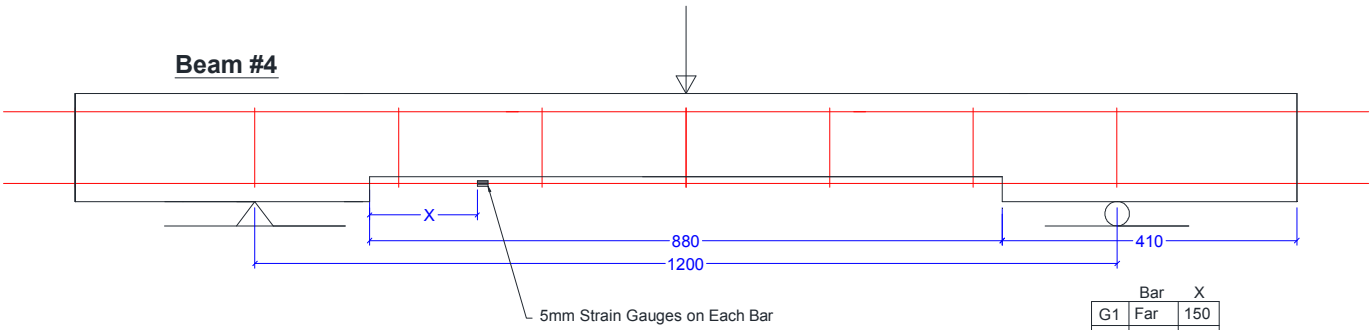

	Bar	X
G1	Far	150
G2	Near	153

University of Waterloo	DRAWING #:	6
	Test Specimen Detail	
	DRAWN BY: JL	DATE: Mar. 28 2011

Beam #5

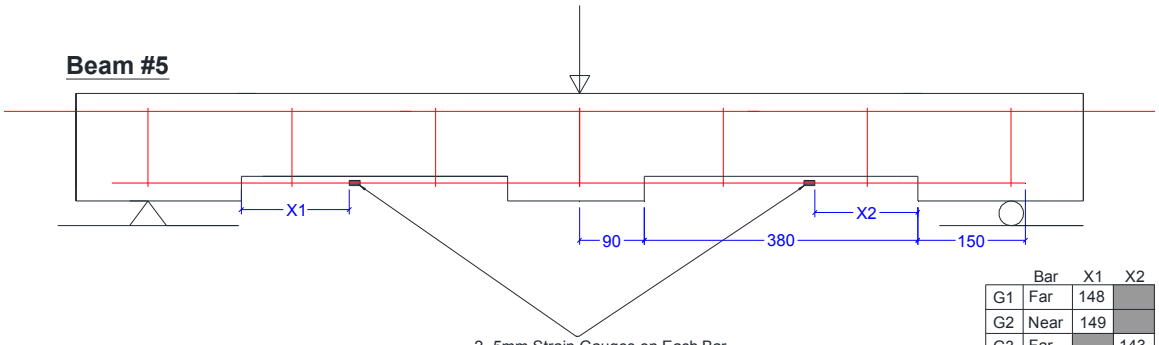

	Bar	X1	X2
G1	Far	148	
G2	Near	149	
G3	Far		143
G4	Near		144

Beam #6

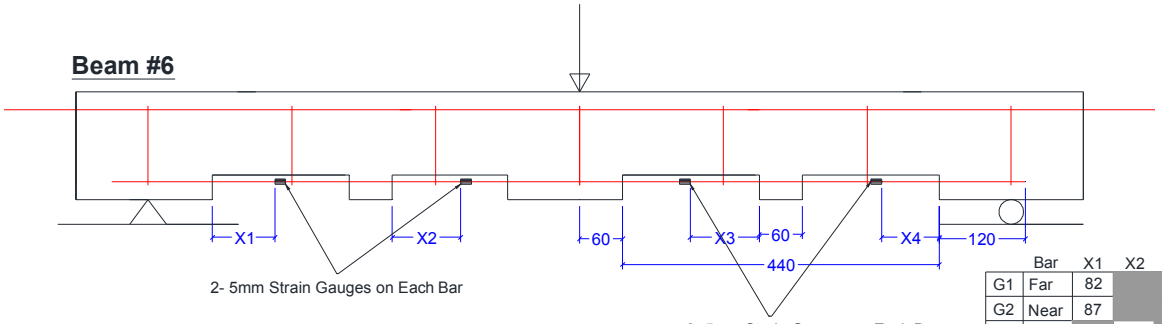

	Bar	X1	X2	X3	X4
G1	Far	82			
G2	Near	87			
G3	Far		95		
G4	Near		97		
G5	Far			93	
G6	Near			96	
G7	Far				78
G8	Near				80

Beam #7

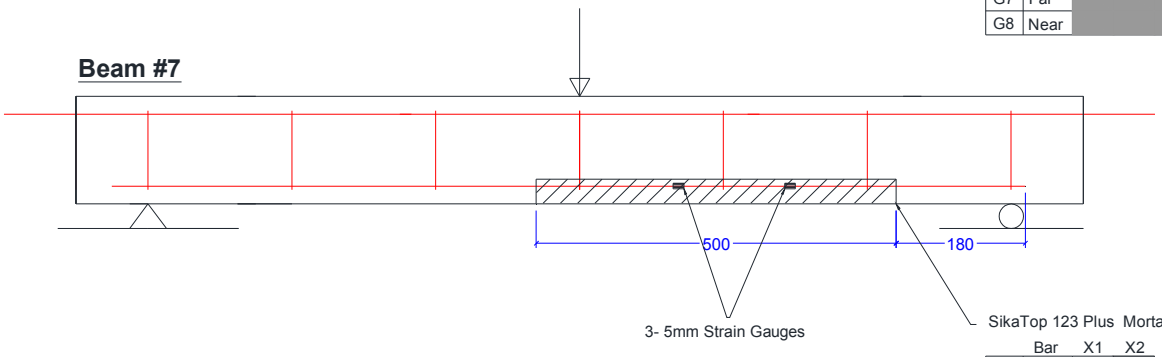

	Bar	X1	X2
G1	Far	140	
G2	Far		295
G3	Near	140	

Beam #8

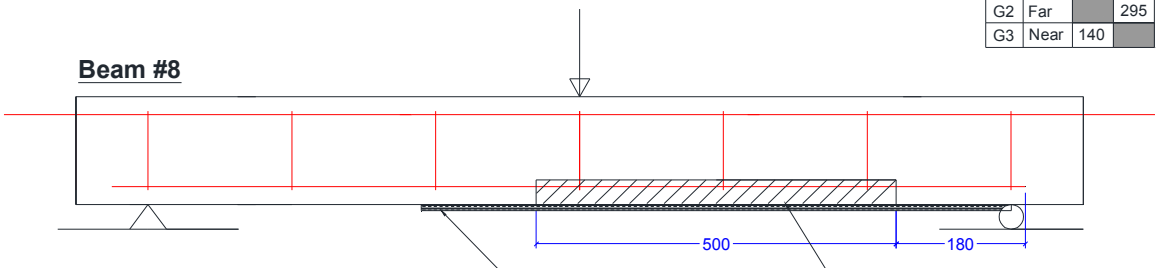

	Bar	X
G1	Far	140

University of Waterloo

DRAWING #: 7

Test Specimen Detail

DRAWN BY: JL DATE: Sept. 2 2010

Beam #9

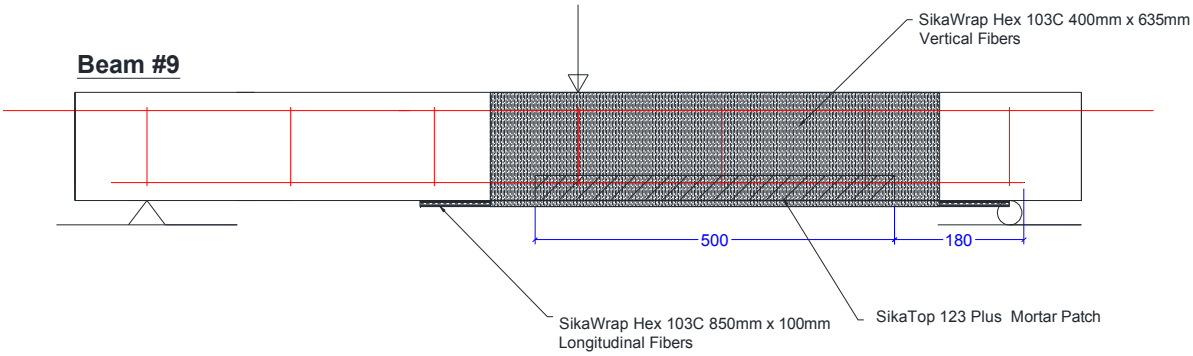

Beam #10

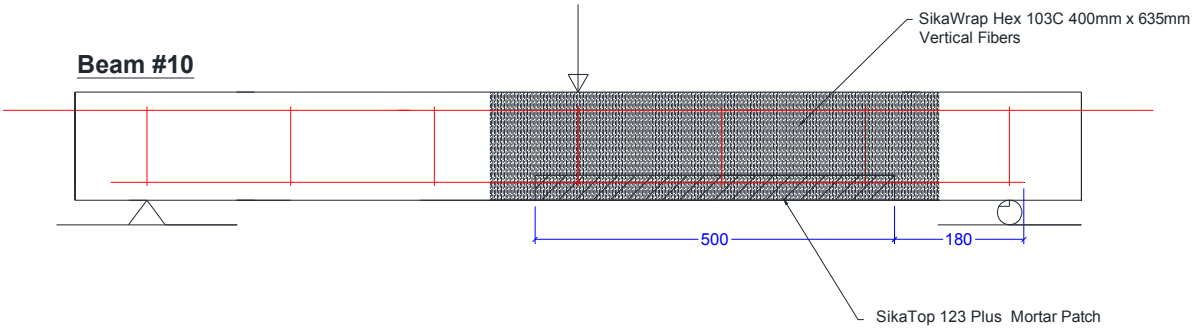

Beam #11

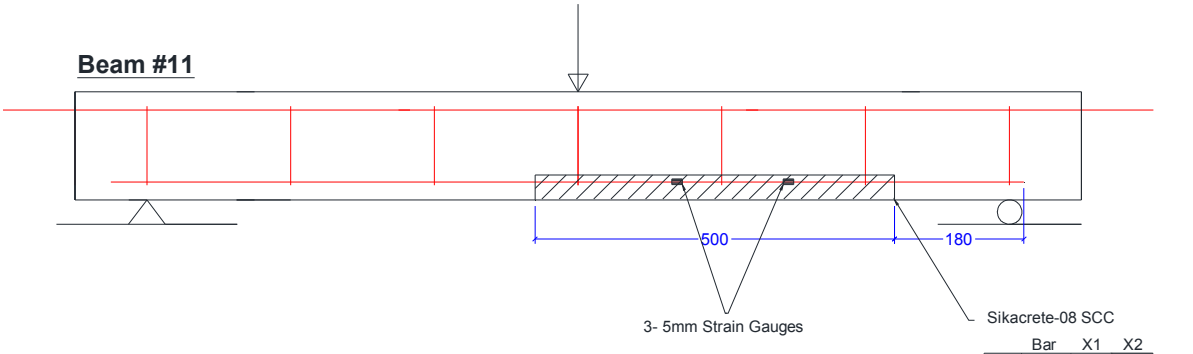

	Bar	X1	X2
G1	Far	140	
G2	Far		300
G3	Near	145	

Beam #12

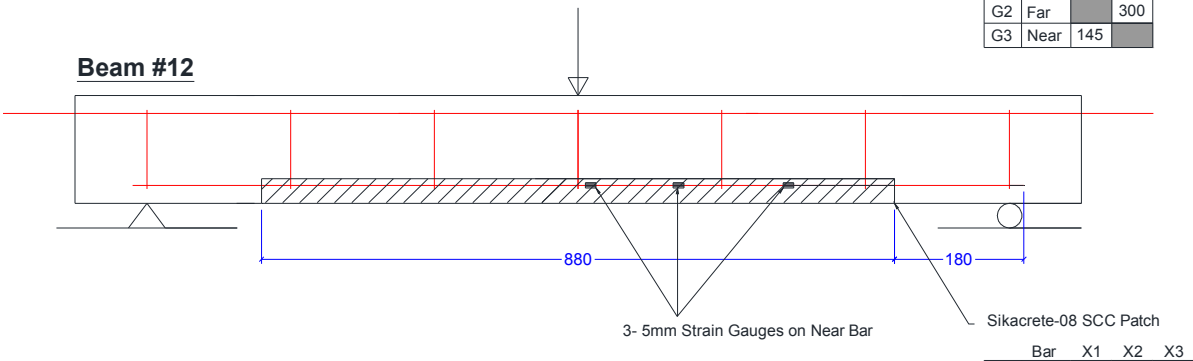

	Bar	X1	X2	X3
G1	Far	140		
G2	Far		293	
G3	Far			415

University of Waterloo

DRAWING #: 8

Test Specimen Detail

DRAWN BY: JL DATE: Sept. 2 2010

Appendix C-2 Test Specimen Design

The following shows sample calculation for the design and evaluation of the lab specimens. Only case (b) material strength calculations are shown here.

C-2-1 Development Length

$k_1 = 1.0,\ k_2 = 1.0,\ k_3 = 1.0,\ k_4 = 0.8$

$Clear\ Cover = 25\ mm > d_b = 11.3\ mm$
$Clear\ Spacing = 37.78\ mm > 1.4d_b = 15.82\ mm$

Minimum Stirrups provided

$$l_d = 0.45\ k_1k_2k_3k_4 \frac{f_y}{\sqrt{f_c'}}\ d_b$$

$$l_d = 0.45 * 0.8 * \frac{450}{\sqrt{18.1}} * 11.3\ = 430\ mm$$

C-2-2 Moment Resistance (Unspalled)

$$\alpha_1 = 0.85 - 0.0015f_c' = 0.85 - 0.0015 * 18.1 = 0.8229$$

$$a = \frac{A_s f_y}{\alpha_1 f_c' b} = 200mm^2 * \frac{450MPA}{0.8229 * 18.1MPA * 100mm} = 60.43\ mm$$

$$M_r = A_s f_y \left(d - \frac{a}{2}\right) = 200mm^2 * 450MPA * \left(150 - 25 - \frac{11.3}{2} - \frac{60.43}{2}\right) = 8.022\ KN.m$$

$$M_{max} = \frac{Pl}{4}, \quad P = \frac{4*M_{max}}{l} = 8022(KN.mm) * \frac{4}{1200mm} = 26.74\ KN$$

Check Steel Strain

$$\frac{d-c}{x} = \frac{c}{0.0035}$$

$$x = (119.35 - 73.43) * \frac{0.0035}{73.43} = 0.00219 > 0.002\ (Underreinforced)$$

C-2-3 Shear Resistance (Unspalled)

$$d_V = \max\{0.9d, 0.72h\} = \max\left\{0.9 * \left(150 - 25 - \frac{11.3}{2}\right), 0.72 * 150\right\} = 108mm$$
$$A_v = \pi(3/16" * 25.4/2)^2 = 17.8mm^2 * 2 = \ 35.63mm^2$$

Check Minimum shear reinforcement

$$A_{Vmin} = 0.06\sqrt{f_c'}\frac{b_w s}{f_y} = \frac{0.06 * \sqrt{18.1\ MPA} * 100 * 200mm}{450} = 11.34\ mm^2 < A_v \quad (ok)$$

Simplified Method

Assumed stirrups do not contribute to strength

$$S_{ze} = \frac{35 * S_z}{15 + A_g} = \frac{35 * 108}{15 + 9mm} = 157.5mm$$

$$\beta = \frac{230}{(1000 + S_{ze})} = 0.199, \ \theta = 35°$$

$$V_c = \lambda\beta\sqrt{f_c'}\, b_w d_v = 1.0 * 0.199 * \sqrt{18.1MPA} * 100mm * 108mm = 9.144\ KN$$

$V_r = V_s + V_c$= 0+9.144 = 9.144 KN
$P = V_r * 2 = 18.28\ KN$

General Method

Iterative spreadsheet created. $V_r = 31.8\ KN$

C-2-4 Moment Resistance (Spalled)

Spalled calculations shown for Beam #2 only.

$$A' = A_d\left[\frac{l_i}{l_d}\right] = 200mm^2\left[\frac{180}{430}\right] = 83.72mm^2$$

$$a = \frac{A_s f_y}{\alpha_1 f_c' b} = \frac{83.72mm^2 * 450MPA}{0.8229 * 18.1MPA * 100mm} = 25.29\ mm$$

$$M_r = A_s f_y\left(d - \frac{a}{2}\right) = 83.73mm^2 * 450MPA * \left(150 - 25 - \frac{11.3}{2} - \frac{25.29}{2}\right) = 4.02\ KN.m$$

$$M_{max} = \frac{Pl}{4}, \quad P = \frac{4 * M_{max}}{l} = 4020(KN.mm) * \frac{4}{1200mm} = 13.4KN$$

C-2-5 Shear Resistance (Spalled)

Simplified Method

$$\varepsilon_x{}' = \frac{A_s}{A_s'} * \varepsilon_x = \frac{200}{83.72} * \ 0.00085 = 0.00203$$

$$\beta = \frac{0.4}{(1 + 1500\varepsilon_x{}')} \frac{1300}{(1000 + S_{ze})} = \frac{0.4}{(1 + 1500 * 0.00203)} \frac{1300}{(1000 + 157.5)} = 0.1111$$

$$\theta = 29 + 7000\ \varepsilon_x{}' = 29 + 7000 * 0.00203 = 43.21°$$

$$V_c = \lambda\beta\sqrt{f_c'}\ b_w d_v = 1.0 * 0.1111 * \sqrt{18.1\ MPA} * 100mm * 108mm = 5.105\ KN$$

$V_r = V_c$= 5.10 *KN*

$P = V_r * 2 = 10.2\ KN$

General Method

Iterative spreadsheet created

Appendix D

Appendix D-1 Reliability Analysis Input File

Appendix D-1 Reliability Analysis Input File

```
<<RELIABILITY DATA>>;
# Rand Variables
1000000
```

Resistance Variables

	Mean Bias	COV Bias	Distribution
MAT'L STRENGTHS			
Concrete_Compressive_Strength	1.25	0.131	Normal
Rebar_Yield_Strength	1.115	0.1	lognormal
ANALYSIS			
Moment_Strength_Approx_(Mr)	1.14	0.13	Normal
Shear_Strength_Approx_(Vr)	1.34	0.176	Normal
DEVELOPMENT			
CSA_dev_length	0.785	0.161	Normal
DETERIORATION			

Solicitiation Variables

	Mean Bias	COV Bias	Distribution
DEAD LOAD			
DL_Self_weight(CIP)	1.050	0.1	Normal
DL_Analysis*	0.93	0.12	Normal
LIVE LOAD			
Extreme_Event	1.247	0.058	Gumbel
LL_Analysis	0.93	0.12	Normal
DLA	1.1	0.072	Normal